THE UNIVERSITY OF ALBERTA

DIGITAL BIAS MODULATION OF IMPATT DIODE OSCILLATORS

by

Ⓒ Anthony M. Rybczynski

A THESIS

SUBMITTED TO THE FACULTY OF GRADUATE STUDIES AND RESEARCH IN PARTIAL FULFILMENT OF THE REQUIREMENTS FOR THE DEGREE OF MASTER OF SCIENCE

DEPARTMENT OF ELECTRICAL ENGINEERING

EDMONTON, ALBERTA

FALL, 1972

[illegible]

[illegible]

[illegible]

[illegible]

[illegible] ③

[illegible]

[illegible]

[illegible]

[illegible]

[illegible]

[illegible]

[illegible]

THE UNIVERSITY OF ALBERTA

THE FACULTY OF GRADUATE STUDIES AND RESEARCH

The undersigned certify that they have read, and recommend to the Faculty of Graduate Studies and Research, for acceptance, a thesis entitled "Digital Bias Modulation of IMPATT Diode Oscillators" submitted by Anthony M. Rybczynski in partial fulfilment of the requirements for the degree of Master of Science.

ABSTRACT

A systematic study has been carried out of the properties of bias-modulated IMPATT oscillators. In theory, this form of Amplitude Shift Keying exhibits an error performance comparable to, or better than, most other modulation schemes.

During the course of this research, the thermal properties of avalanche diodes have been studied. The effects of the bias and RF circuits of bias-modulated oscillators on system performance have been evaluated. RF spectra and injection properties of pulsed IMPATT oscillators have also been investigated.

It has been found that, due to the heating and cooling of the diode junction occurring with each pulse, there is substantial evidence of frequency pushing in the output spectrum of bias-modulated oscillators. As a result of this undesired FM component, nonsymmetrical broadening of the RF spectra of pulsed oscillators results. Due also to frequency pushing, the use of injection to lock the frequency of the pulsed oscillator is somewhat limited. It has also been found, from an analysis of the RF circuit, that maximizing the loaded Q of the oscillator circuit maximizes the attainable bit rate.

ACKNOWLEDGEMENTS

The author wishes to express his appreciation to the following:

Dr. P.A.Goud, his supervisor, for suggesting this project, for his advice and encouragement during the course of this work.

Dr. J. Nigrin for the many hours of useful discussions.

Members of the Microwave Electronics Laboratory for their helpful suggestions and criticisms.

The author wishes to thank his wife, Galina, whose patience and understanding too often remained unanswered, and his daughter, Natasha, whose smiles were always welcome.

The author is also indebted to the following organizations:

To the Communications Research Center for its support of this research under DSS Contract OGR2-0195.

To the National Research Council for the provision of an NRC Scholarship.

To the University of Alberta for an Intersession Bursary and for two Graduate Teaching Assistantships.

Table of Contents

LIST OF TABLES

LIST OF FIGURES

CHAPTER I

INTRODUCTION

1-1 Digital Modulation Techniques

There are three fundamental methods of modulating a Pulse Code Modulated (PCM) baseband signal onto a radio frequency carrier[1]. These are: Phase Shift Keying (PSK), Frequency Shift Keying (FSK), and Amplitude Shift Keying (ASK). These methods are not mutually exclusive as various combinations are possible; for example, Bell Labs are presently evaluating a combination of ASK and PSK for improved system performance[2]. PSK, FSK and ASK are now discussed in turn.

1-1-1 Phase Shift Keying

In PSK, the phase of the carrier is switched between various discrete, equispaced values. For binary PSK, the angles are normally chosen 180° apart; for ternary PSK, the phase angles are normally chosen 120° apart; in general, the modulated wave may thus be represented as

$$x(t) = A\cos(2\pi ft + \Theta_j) \qquad (1.1)$$

where: A is the carrier amplitude

f is the carrier frequency

Θ_j is K x 360/n

n is the number of discrete phases

K is the integer from 1 to n.

As far as noise performance is concerned, PSK requires at least 3 dB less power than FSK or ASK, for the same probability of error[1]. For PSK, the required transmitter bandwidth is approximately twice the pulse repetition frequency of the baseband signal.

Since this elementary form of PSK requires an absolute phase reference (and hence will not tolerate phase fluctuations in the transmission channel), a slightly different type of PSK called Differential Phase Shift Keying is normally used in practice. This system maintains a phase reference only between successive symbols (as opposed to a phase reference between a particular symbol and the start of transmission) and so it is relatively insensitive to phase fluctuations in the channel. Relative to conventional PSK, DPSK requires about 1 dB more power for the same probability of error. For either system, the transmitted bandwidth is approximately equal to twice the pulse repetition frequency.

1-1-2 Frequency Shift Keying

FSK signals consist of a constant amplitude RF waveform having different frequencies, one frequency for each of the possible message signals. In general, the modulated wave may be represented as;

$$x(t) = A \cos(2\pi f_j t) \qquad (1.2)$$

where A is the carrier amplitude

f_j is the frequency for the j^{th} symbol

Such a system is less optimal than PSK (or DPSK) on an error performance basis, though it is better than ASK in this regard. The bandwidth requirement of FSK is twice that of either ASK or PSK. FSK does have one significant advantage over the other modulation methods in that it exhibits a very low threshold of detection (the level below which the received signal carries no information). This property makes FSK quite suitable for low signal-to-noise applications. However, because of the restricting bandwidth, the discussion is henceforth restricted to ASK and PSK systems.

1-1-3 Amplitude Shift Keying

The simplest modulation technique is ASK; the carrier's amplitude is switched between two or more levels (i.e., ON and OFF for binary signals). In general, the modulating signal is given by:

$$x(t) = A_j \cos(2\pi ft) \qquad (1.3)$$

where A_j is the amplitude of the carrier corresponding to the j^{th} symbol.

The bandwidth of an ASK signal is comparable to that obtained with PSK (twice the pulse repetition frequency), though the error performance is about 3 dB lower.

There are two possible methods of detecting an ASK signal: synchronous detection and envelope detection. The former technique consists of multiplying the incoming signal by a local oscillator signal (synchronized to the carrier) and passing the resulting signal through a low-pass filter. The latter technique requires passing the signal through an envelope detector. Envelope or noncoherent detection, though simpler, is more susceptible to noise than synchronous or coherent detection. In fact, coherent ASK requires about 1 dB less power than noncoherent ASK for the same error performance.

1-1-4 Summary

The significant facts to be retained from the above discussion of digital modulation systems are the following:

1. PSK and ASK have the same bandwidth requirements.
2. PSK requires 3 dB less power for a given error performance as compared to ASK.
3. Implementation of a noncoherent ASK system is the simplest form of digital modulation and hence is the least expensive to realize. This will be discussed further in the next section.

4. The error performance for various binary systems is shown in Figure 1.1[3].

1-2 Digital Modulation at Microwave Frequencies Utilizing Solid State Devices

1-2-1 PSK: Path Length Modulation

Because of its overall performance, PSK has received relatively the most attention, compared to the other digital modulation systems. The required phase shift is commonly achieved by direct switching of a low-loss diode connected between a short-circuited transmission line and a circulator (Fig. 1.2).

In 1967, Nakamura and Inoue[4] investigated the relationship between diode charcteristics and modulation loss, generation of AM components and power limitations. They in fact designed a 4-phase modulator at 2 GHz with a 7.7 Mbit modulating signal. Previously, in 1964, Hines[5] published his theoretical work on the limitations in phase shifting using semiconductor diodes. He considered at some length the impedance characteristics, switching times and power limitations of semiconductor diodes. He also developed a model for a diode in its ON and OFF states.

More recently, in 1971, Kurokawa *et al.*[6] at Bell Labs have developed a Path Length Modulator operating at 50 to 60 GHz with a

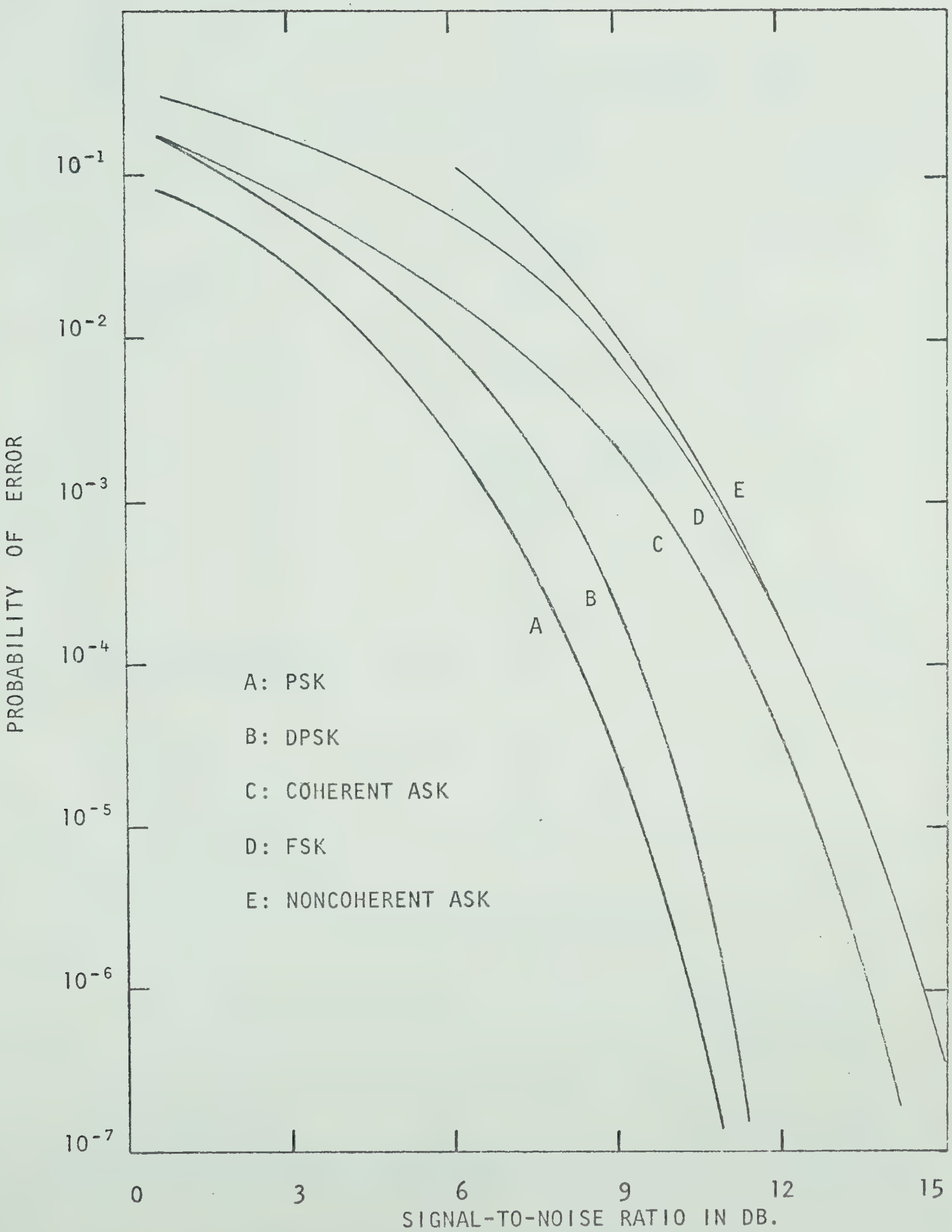

FIG. 1.1 ERROR PROBABILITIES FOR VARIOUS BINARY MODULATION SYSTEMS [3]

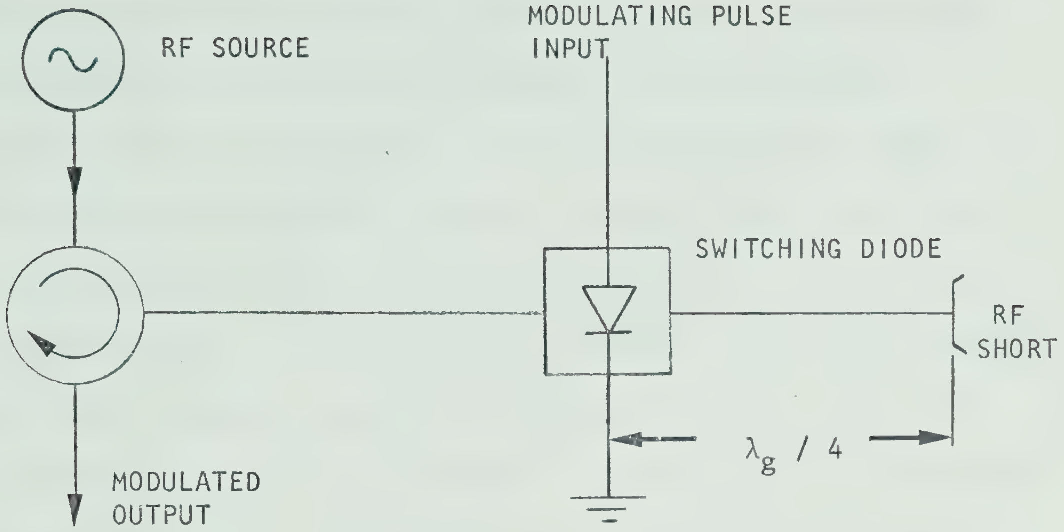

FIG. 1.2 PATH LENGTH MODULATOR

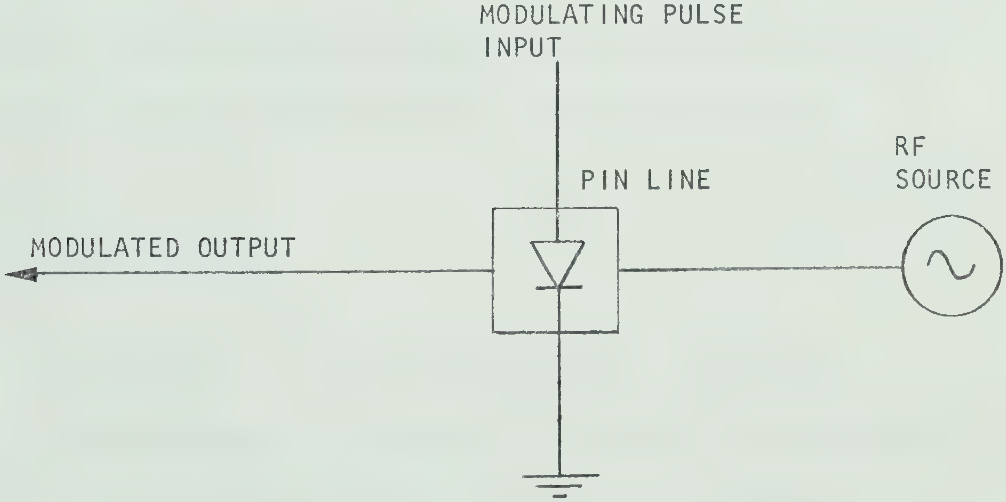

FIG. 1.3 PIN LINE MODULATOR

FIG. 1.4 BIAS MODULATED OSCILLATOR

baseband signal of 300 Mbits per second. They used a 100 mW IMPATT diode oscillator and a specially designed PIN diode switch. A PIN diode was chosen, in preference to Schottky barrier or p-n junction diodes, because the impedance level of the switching circuit can be made quite high and because the switching characteristic is relatively independent of bias voltage. A special circulator was also designed to handle the broadband signals. In addition, a drive circuit had to be designed to switch the PIN diode between its ON and OFF states in minimum time. It is thus apparent that the equipment requirements for Path Length Modulators (and PSK systems in general) are very stringent. In some cases (e.g. private data communication systems), the above-mentioned hardware requirements could be prohibitively costly in comparison with other alternatives.

1-2-2 ASK: PIN Modulator

A PIN Modulator is a high speed, current-controlled absorption type attenuator. Commercially available PIN Modulators[7] consist of a low-pass filter in the bias port, two high-pass filters in the two RF ports and a given number of PIN diodes. Operation of this device is based on the fact that, above a certain frequency (dependent on the minority carrier lifetime and on the thickness of the intrinsic region), the PIN diode ceases to rectify the signal any longer; this effect is due to the stored charge in the "I" layer.If the amount of stored charge is increased (by

increasing the forward bias current), the equivalent resistance of the diode is decreased. In the pulse mode, the attenuation is switched between its maximum and minimum values. A general configuration is shown in Figure 1.3.

Such a system (as does the Path Length Modulator discussed in the previous section) permits the separate optimization of the modulator and of the oscillator. A high Q oscillator can be used for low noise operation and for short-term frequency stability.

As was pointed out in Section 1.1, an ASK modulator suffers a 3 dB power disadvantage compared to a PSK modulator at the same power level. For solid state sources, there is an upper limit on the output power dictated by the maximum diode temperature. Therefore, by running the oscillator at twice the rated power for an average of half the time at pulse rates in excess of the thermal time constant, this disadvantage can be largely overcome. This possibility is discussed in the next section.

1-2-3 ASK: Bias-Modulated Oscillator

A bias-modulated oscillator combines the modulation and oscillator functions into a single unit. It is an oscillator with a PCM source in the bias circuit so that it pulses ON and OFF in accordance with the modulating signal. Such an oscillator is, on the average, ON only 50% of the time and therefore dissipates half as much heat as under continuous operation. Therefore, it can be

run at twice the cw power level,thus cancelling the 3 dB advantage of PSK systems. It is also recalled that the bandwidth requirements are identical for the two systems. In addition, the hardware required for a Bias-Modulated Oscillator is minimal as compared to that for a Path Length Modulator, or even for a PIN Modulator, since only an oscillator and bias circuit are required. (cf. Fig. 1.4)

The performance of a Bias-Modulated Oscillator is substantially similar to that of a Path Length Modulator in regard to probability of error and transmitted bandwidth. There are also significant cost advantages in using Bias-Modulated Oscillators, a fact which makes them suitable for private data links (e.g. intercity computer-to-computer links where cost of laying cables might be prohibitively high.)

1-3 Synopsis

This thesis discusses the feasibility of a Bias-Modulated Oscillator as a practical means of Amplitude Shift Keying a binary PCM signal. Emphasis is always placed on the most important system parameters (power,error rate and bandwidth) as these are the determining factors whether any modulation system is useful. The experimental circuit is first discussed (Chapter II), recognizing that there are three distinct circuits involved: the RF, bias and triggering circuits.

As the temperature of the diode junction increases, the breakdown voltage increases,resulting in a decrease of the diode current. Since the diode is pulse operated, the instantaneous junction temperature varies with time, which results in an undesirable change in the diode current. The effects of the junction thermal properties on the performance of the Bias-Modulated Oscillator are discussed in Chapter III.

Next, a theoretical study is presented (Chapter IV) dealing with the tradeoff between the build-up and decay times of the oscillator and the loaded Q of the circuit. The optimum Q is determined (a high Q results in a large decay time and a low Q results in a large build-up time) and consequently a maximum usable bit rate is determined.

Since the electronic susceptance is a function of the diode current, whenever the current changes, the frequency changes. As a result, the RF and the baseband spectra are no longer the same, which would be the case if the carrier frequency remained constant. In Chapter V, experimental results are presented and discussed and a computer program is developed to calculate the spectra of varying-frequency pulses. The effects of injecting a cw signal into a pulsed IMPATT oscillator are then discussed (Chapter VI).

Finally, Chapter VII concludes the study with a discussion of the results and of possible future avenues of research.

CHAPTER II

THE EXPERIMENTAL CIRCUIT

2-1 Preliminary Remarks

The work reported on the following pages has been carried out on IMPATT (IMPact ionization and Avalanche Transit Time) diodes, oscillating in the 4 to 6 GHz range. (Haddad's recently published book[8] discusses the characteristics of IMPATT diodes with many recent references.) IMPATT diodes were chosen because of their favourable characteristics (the only solid state sources with 1 Watt output power at 50 GHz) and because work was concurrently being done on the transient response of IMPATTs[9]. Though the particular diodes used operated over a considerably wider range (cf. Table 2.1), this

Table 2.1 SPECIFICATIONS OF HP 5082-0437 IMPATT DIODE USED IN EXPERIMENTAL WORK [10]

frequency range	5 to 9 GHz
typical operating voltage	110 V.
typical operating current	25 mA.
efficiency	3.5%
output power	100 mW.
thermal resistance	35°C/W.
package capacitance	0.2 pF.
package inductance	0.5 nH.

particular frequency was chosen according to the availability of equipment. For a discussion of microwave oscillators, the reader is referred to a paper by Kurokawa[11].

The ultimate aim of the research reported here was to study the feasibility and limitations of bias modulating an IMPATT oscillator, possibly up to bit rates of 46 Mbps . This bit rate was chosen as it coincides with that of the Bell System T-3 carrier equipment[12]. In the experimental work, a pulse generator was used instead of a more realistic PCM source. For a unipolar signal, as is in fact used in the T-3 system, the output of the pulse generator with a 50% duty cycle corresponds to the following bit stream: 1,1,1,1,1... . In this case, the pulse repetition rate corresponds to the bit rate of the PCM signal. This is not true in all cases: for a unipolar synchronous PCM signal (i.e. equal duration pulses with no separation between them), the pulse repetition rate corresponds to exactly half the bit rate of the PCM signal. In this case, the output of the pulse generator with a 50% duty cycle is equivalent to the following bit stream: 1,0,1,0,1,0... .

2-2 Experimental Circuit and Model

The circuit of Figure 2.1 was used in much of the experimental work reported here. The bias circuit will be characterized

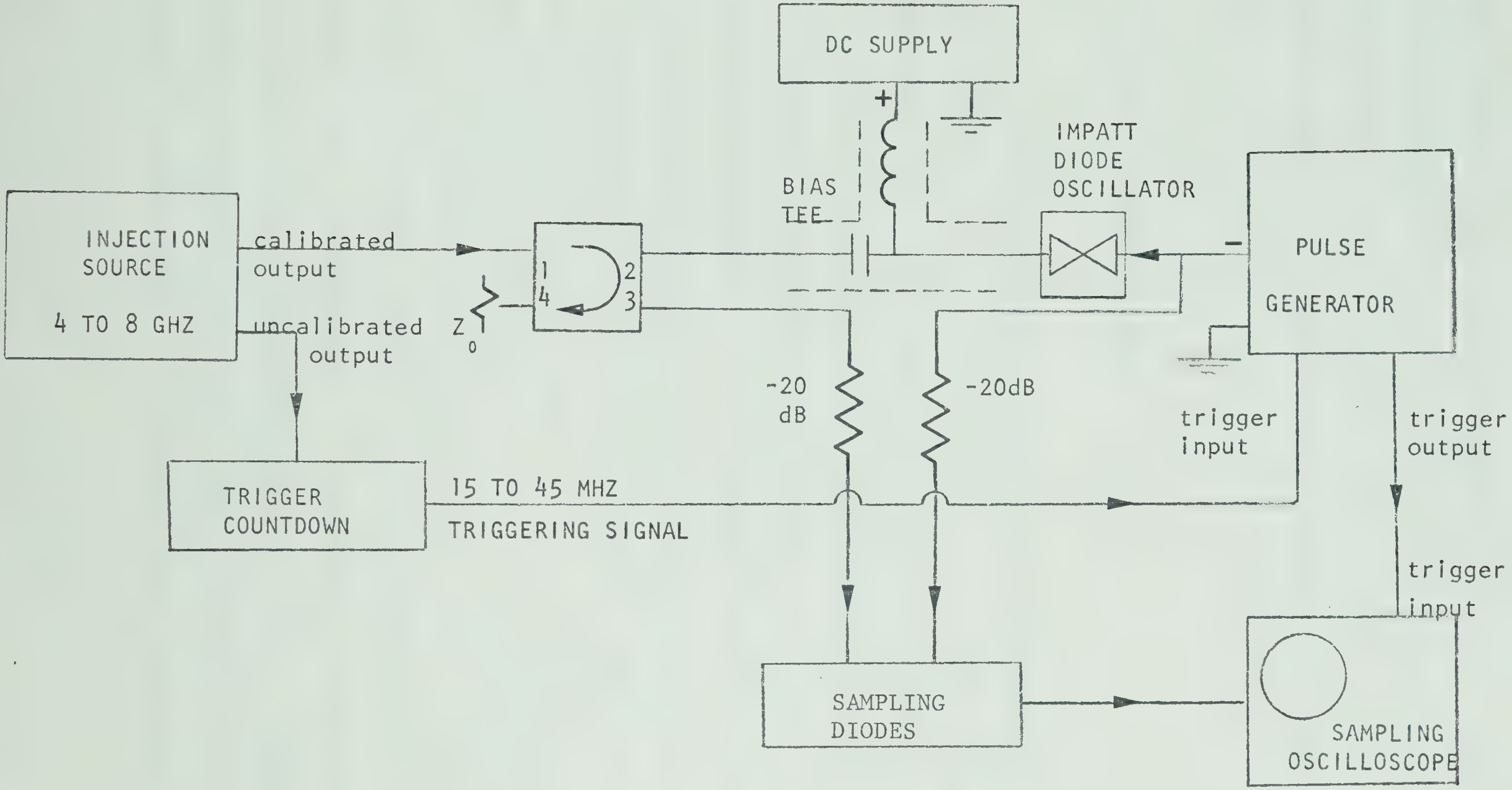

FIG. 2.1 EXPERIMENTAL CIRCUIT USED IN EVALUATION OF BIAS MODULATED OSCILLATOR

by a lumped circuit using experimentally measured values for the lumped elements. The analysis of this circuit will furnish information on how quickly the circuit can respond to a fast rise-time voltage pulse. The triggering circuit and the RF circuit will also be discussed.

2-2-1 The Resonator Circuit

The IMPATT diode (cf. Table 2.1) was end-mounted in a double-slug 14 mm. coaxial cavity (Fig. 2.2). The two slugs were adjustable and the load impedance could be transformed to the diode as required. The cavity circuit can be modelled by five lossless transmission line sections[13] in cascade, two of which represent the slug sections and the last three the transmission line sections. In addition, the discontinuities due to the slugs can be included as appropriate discontinuity capacitances[14]. These cascaded transmission lines can be put in parallel with the diode (i.e. wafer and package) to obtain a complete model of the circuit.

It should be noted that,if planes A and B (cf.Fig. 2.2) contacted each other, then one side of the diode would be effectively grounded. This configuration is suitable for cw operation or for pulsed operation with the pulse generator across the GROUND-NEGATIVE terminals of the DC power supply. This last case is not acceptable because the pulse generator is loaded by the capacitance of the

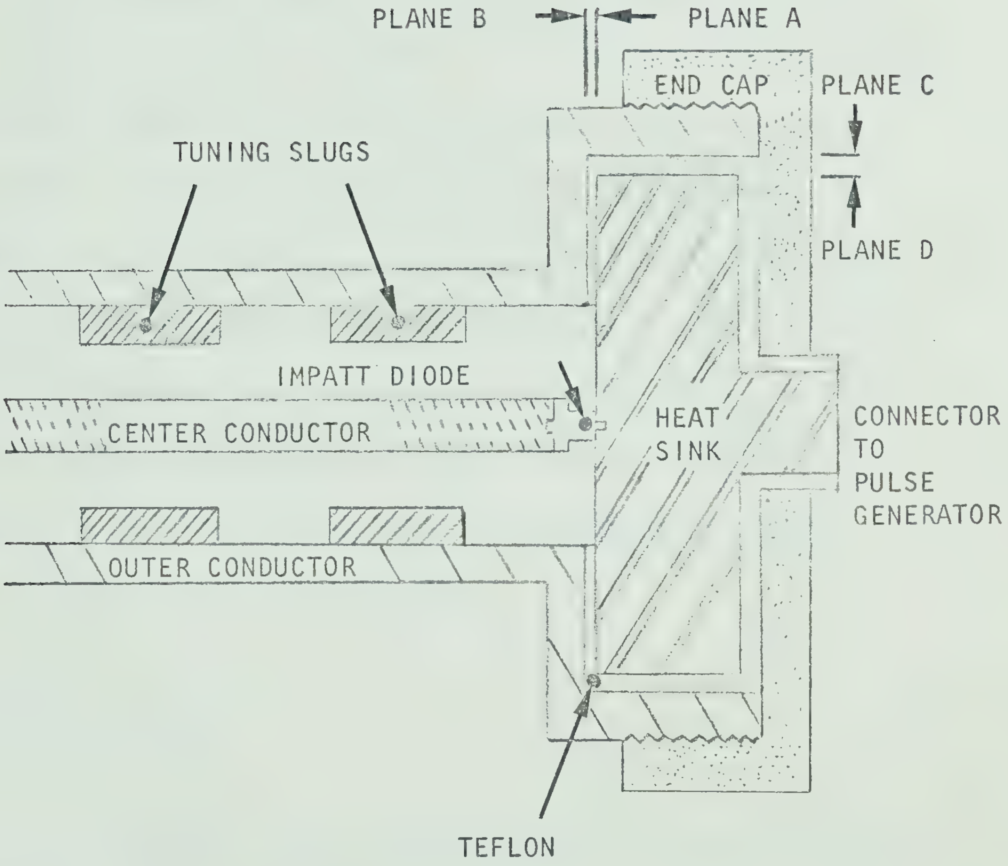

FIG. 2.2 CROSS-SECTION OF 14 MM. COAXIAL CAVITY WITH END-MOUNTED IMPATT DIODE.

power supply negative terminal to ground, which for the HP6207B DC power supply is about 1500 pF. Therefore, for pulsed operation, planes A and B are separated by a 15 mil thick Teflon sheet and the pulse generator reapplied between the heat sink and ground. In addition, there is a capacitance between planes C and D and so the total capacitance for the heat sink to ground is 100 pF. (as measured on a #71A Boonton meter). At 5GHz, this capacitance is equivalent to an impedance of $1/\pi$ ohms. The penalty for decreasing the RF impedance further is a prohibitively high time constant as seen by the pulse generator. Noting that the output impedance of the pulse generator is 50 ohms and without including any other capacitances, the time constant of the circuit is 5 nsecs. There is a distinct tradeoff between the value of the RF short and the time constant associated with the circuit. The value chosen for the RF blocking capacitance (heat sink to ground) is considered to be near optimum for the circuit used.

2-2-2 The Bias Circuit

The bias circuit as seen from the pulse generator terminals can be modelled as shown in Figure 2.3. This circuit is analyzed in Appendix A and the theoretically calculated diode current is shown graphically in Figure 2.4 for a unit-step input voltage. It is seen that the risetime is approximately 8.2 nsecs. With a

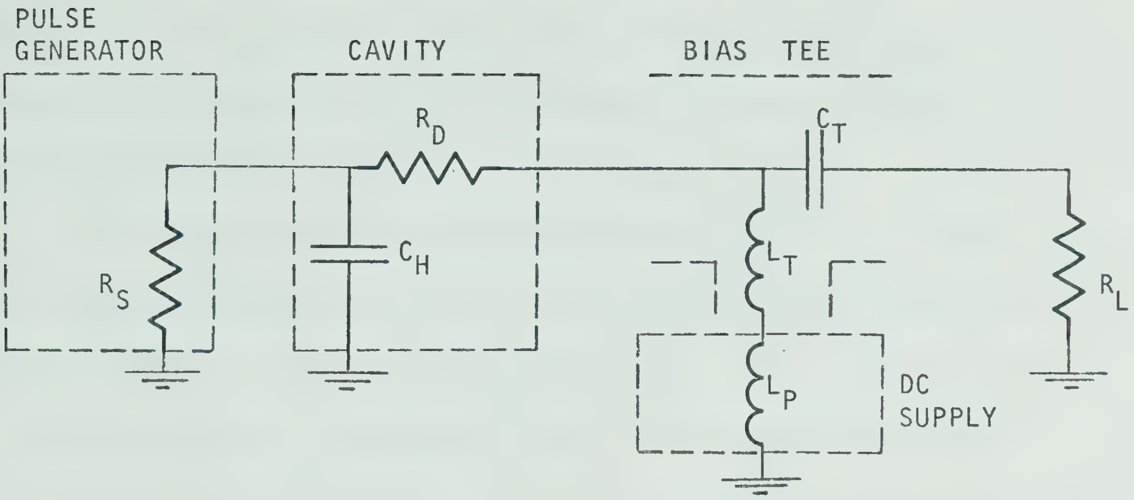

where

R_D = diode resistance = 150Ω
C_H = heat sink capacitance to ground = 100 pF.*
C_T = bias tee capacitance in RF arm = 12 pF.*
L_T = bias tee inductance in DC arm = 20 nH. @50MHz**
L_P = DC supply input inductance = 160 nH. @50 MHz**
R_S = pulse generator source resistance = 50Ω
R_L = load resistance = 50Ω

* measured with Boonton 71A Inductance-Capacitance Meter.
** measured with Hewlett Packard HP8405A Vector Voltmeter.

Fig. 2.3 BIAS CIRCUIT AS SEEN FROM PULSE GENERATOR TERMINALS

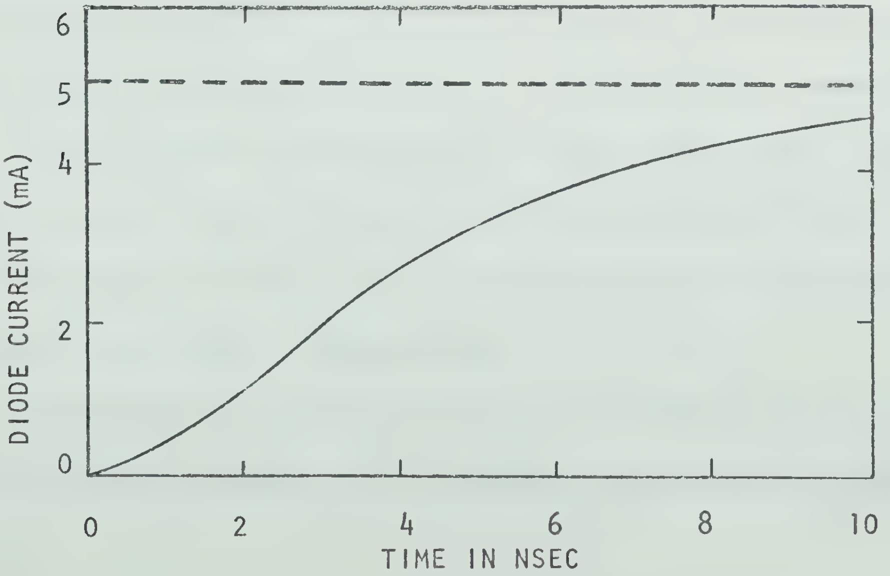

FIG. 2.4 DIODE CURRENT IN RESPONSE TO UNIT-STEP APPLIED VOLTAGE

2 nsec.-risetime applied voltage pulse, the minimum risetime for the current through the diode is increased to about 10 nsecs.; the decay time for the current is about 10 nsecs. as well.

The major contributing factor to the length of the risetime and decay time of the diode current is the time constant of the parallel R-C circuit at the output of the pulse generator (i.e. R_s in parallel with C_h in Figure 2.3). For a unit-step voltage input, the risetime of this R-C circuit is 10.9 nsecs. This quantity can be decreased in one of three ways:

1. by decreasing the value of C_h.
2. by decreasing the value of R_s.
3. by both 1. and 2.

C_h is the heat sink capacitance to ground and acts as an RF short as seen by the cavity*.Decreasing this capacitance below about 100 pF. results in an excessive amount of RF radiation losses through the back of the cavity. Decreasing the value of R_s (i.e. by further loading the pulse generator) results in too low a voltage pulse across the diode. There is a tradeoff for high-prf pulse generators between short transients and high amplitudes. With these considerations, the near optimum values of R_s and C_h are those given in Figure 2.3. It is stressed that these results are restricted to the circuit used in the experiments reported here.

These rise- and decay times are not prohibitively long for high bit rate ASK systems. In the commonly considered $\sin^2 x$ pulse,

---

* Care must be taken that the planar capacitor does not act as a radial-mode cavity.

the risetime is 30% of the total pulse length. As the RF pulse is of the same general shape as the current pulse, the transients place a lower limit on the length of the pulse at about 25 nsecs. For the T-3 system, this would correspond to a maximum bit rate of 20 Mbits. This is the maximum bit rate the experimental bias circuit can handle.

It has been assumed in the above discussion that the RF oscillations start as soon as the pulsed current starts to flow and that they follow the current waveform closely. The second assumption is almost never true as will be seen in Chapter 4. (The single exception is the case where the oscillator is pulsed between two similar levels of oscillation.) The first assumption is also in general not true; however, it is valid when the diode is biased above the breakdown voltage (i.e. avalanching)such that any further increase in the bias voltage (i.e. increase in the DC current) will result in RF oscillations. The following discussion will explain this point.

In order for the diode to oscillate, the magnitude of the electronic conductance must be equal to or greater than the circuit conductance. As the current increases, the magnitude of the electronic conductance increases until oscillations are possible. Once oscillations commence, the magnitude of the electronic conductance decreases as the RF amplitude increases until equilibrium is reached; under steady state conditions, the magnitudes of the electronic and circuit conductances

are equal.

There are various possibilities for biasing the diode under pulsed operation; that is,

1. biasing at 0V DC (i.e., no DC bias voltage).
2. biasing at the breakdown voltage.
3. biasing below the oscillation threshold but above the breakdown voltage.
4. biasing at the oscillation threshold.

A tradeoff exists in high-prf pulse generators between fast risetimes and high pulse amplitudes; for the required risetimes (i.e., in the order of a couple of nsecs), only 10V pulse generators were found to be commercially available. In addition, biasing below the breakdown voltage and pulsing the diode into avalanche breakdown results in fluctuations at the front edge of the diode current pulse; this is due to the statistical nature of the avalanche process. These two considerations preclude biasing the diode below the breakdown voltage. Biasing below the oscillation threshold introduces some finite time delay (i.e., a fraction of the current risetime) before the current has reached the threshold level and oscillations are possible. Therefore, the optimal biasing point for bias-modulation applications is at the oscillation threshold. This biasing point has the added advantage that the diode is already dissipating one or two Watts; hence the temperature fluctuations under pulsed conditions are minimized.

2-2-3 Trigger Circuit

In order to exhibit a stable display of the RF pulse envelope, it is necessary to trigger the oscilloscope from the pulse generator. However, a coherent display of the actual RF oscillations is not possible because the oscillations start with random phase during each pulse. By injecting a low power signal, close in frequency to the small-signal free-running oscillator frequency, the oscillations will have phase coherence between pulses. However, some technique must be used to synchronize the applied pulses with the phase of the injected signal (and hence the phase at the start of oscillation). This is achieved by triggering the pulse generator by a signal which is harmonically related to the injected signal. Experimentally, the uncalibrated output from the injection source was fed into a trigger countdown unit, the output of which triggers the pulser (Fig. 2.1).

2-3 Summary

The experimental RF, bias and trigger circuits have been discussed. The experiments were conducted in the 4 to 6 GHz range. The IMPATT diode oscillator was biased near the threshold of oscillation and pulsed into oscillation by a pulse generator in the bias circuit.The pulse repetition frequency was varied from

1 to 25 Mbit/sec. An analysis of the bias circuit showed that for a step input voltage, the resultant current pulse through the diode had an 8 nsec risetime. This placed a limit on the minimum pulse length that the bias circuit can handle. The various possibilities of biasing the diode were discussed. The optimum bias point was found to be the oscillation threshold level.

CHAPTER III

EFFECTS OF TEMPERATURE ON THE OPERATION OF BIAS-MODULATED IMPATT DIODE OSCILLATORS

3-1 Introduction

In order to understand the properties of bias-modulated IMPATT diode oscillators, it is important to study how the junction temperature affects the properties of avalanche diodes. The breakdown voltage of an avalanche diode increases with increasing junction temperature. Since the instantaneous diode current is a very sensitive function of the difference between the voltage across the diode and the instantaneous breakdown voltage, increasing the junction temperature (e.g. by increasing the bias pulse length) increases the breakdown voltage, which reduces the instantaneous bias current. Consequently, the output power,as well as the oscillation frequency, changes. When dealing with the junction temperature, two auxiliary parameters, i.e. a junction thermal resistance and, in the simplest case, a single junction thermal time constant, are used. In cw operation, the junction thermal resistance is the most important thermal parameter; in pulsed operation, both thermal parameters are equally important. These thermal parameters and their effects on pulsed IMPATT diode oscillators are now discussed.

3-2 Temperature Dependence of Diode Breakdown Voltage

The circuit shown in Figure 3.1 was used to measure the variation of diode breakdown voltage (V_b) with temperature. DC supply "A" was put in series with the constant current supply because the latter had a maximum output voltage of 100 Volts while the diode breakdown voltage was over 110 Volts. DC supply "B" was included in the circuit to increase the sensitivity of the digital voltmeter. The IMPATT diode was mounted in a special holder in an oven, the temperature of which was variable from room temperature to 200°C.

Initially, the reverse bias I-V characteristic of the diode was measured at 160°C to determine the current at which avalanche breakdown might be considered to occur. The measured I-V characteristic is given in Figure 3.2. It is seen that for a current of 80μA, the breakdown voltage is suitably well-defined. Next, the temperature was changed to a lower value and the breakdown voltage (i.e. the voltage at which the DC current was 80μA) was measured again. The diode breakdown voltage was remeasured at progressively lower temperatures; the results are shown graphically in Figure 3.3. From this graph, it is seen that the temperature coefficient of the diode breakdown voltage ranges from 105 to 118 mV/°C over the temperature range of interest. This suggests that the instantaneous junction temperature could be measured indirectly by measuring the instantaneous breakdown voltage. This technique is,in fact, used in the determination

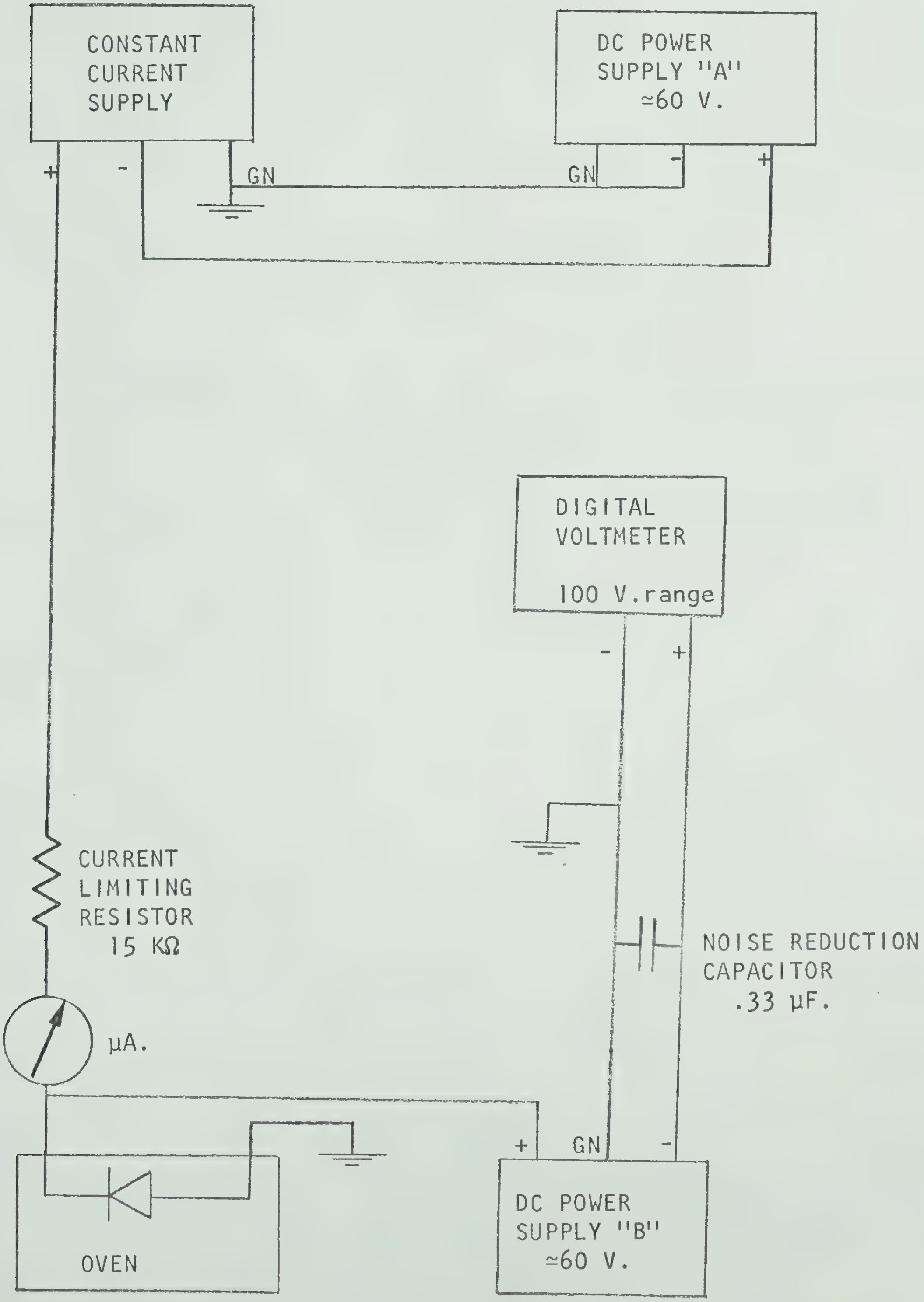

FIG. 3.1 CIRCUIT USED TO MEASURE TEMPERATURE VARIATION OF DIODE BREAKDOWN VOLTAGE

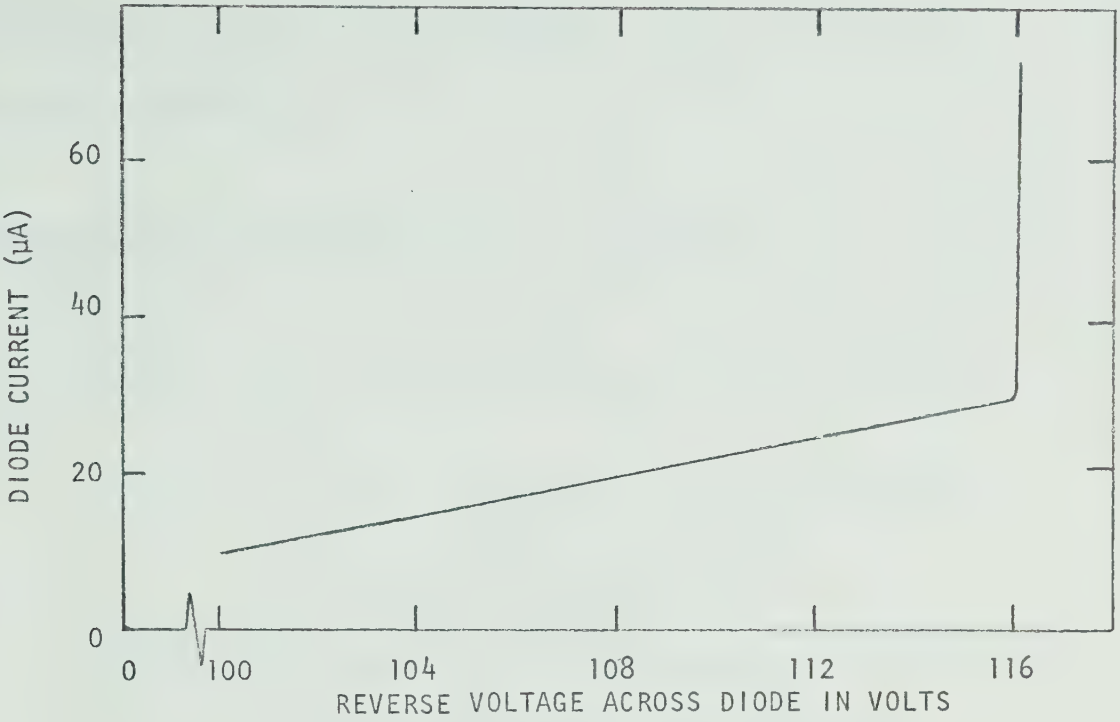

FIG. 3.2 REVERSE BIAS I-V CHARACTERISTIC OF IMPATT DIODE AT 160°C

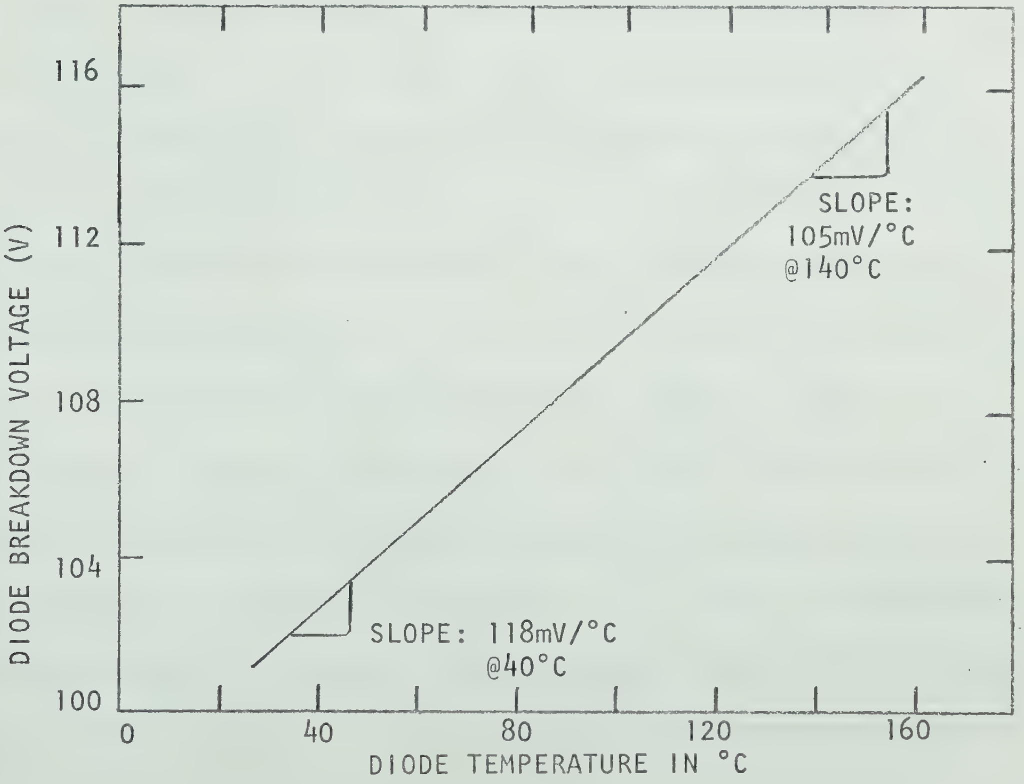

FIG. 3.3 TEMPERATURE VARIATION OF DIODE BREAKDOWN VOLTAGE

of the thermal parameters of the avalanche diode as is discussed in Sections 3-3 and 3-4.

3-3 Determination of the Diode Thermal Resistance

The diode thermal resistance (R_θ) may be written as[15]:

$$R_\theta = (T_j - T_o) / P \quad °C/W \qquad (3.1)$$

where:

T_j is the junction temperature

T_o is the heat sink temperature

P is the power dissipation in the diode

R_θ is equal to the temperature rise in the diode produced by a power dissipation of 1 Watt. The diode thermal resistance was measured by biasing the diode well into avalanche breakdown (i.e. the power dissipation region) and pulsing the diode with a narrow,low duty-cycle pulse back to breakdown[16]. The point of breakdown was determined by monitoring the current and by noting when avalanching has just ceased. The instantaneous diode breakdown voltage was then measured by means of an oscilloscope. Using this technique, the graph given in Figure 3.4 was obtained. From the graph, it is seen that,under steady-state conditions, the diode temperature is a linear function of the power being dissipated in the diode. From the slope of this line, the thermal resistance is found to be 25°C/W.

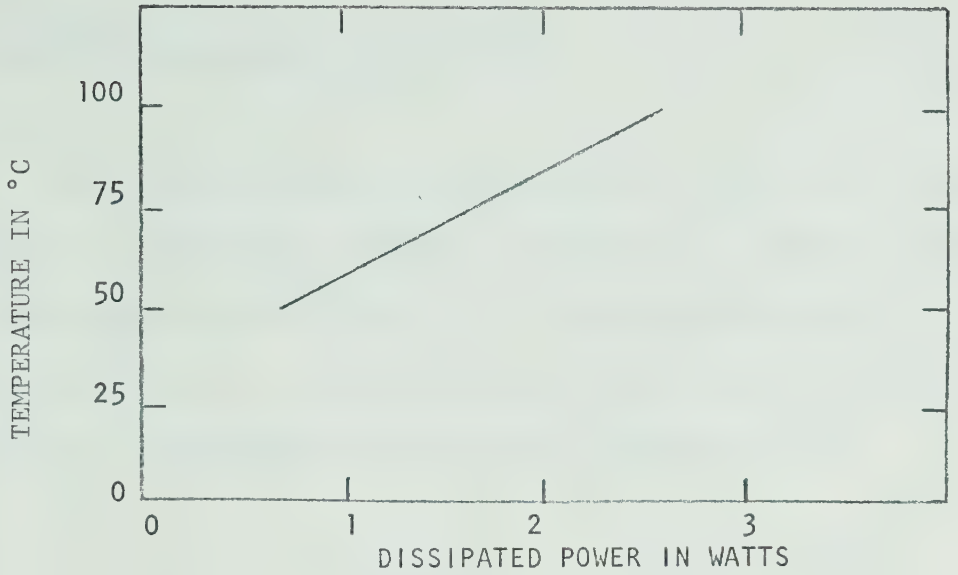

FIG. 3.4 DIODE TEMPERATURE AS A FUNCTION OF DISSIPATED POWER UNDER STEADY-STATE CONDITIONS

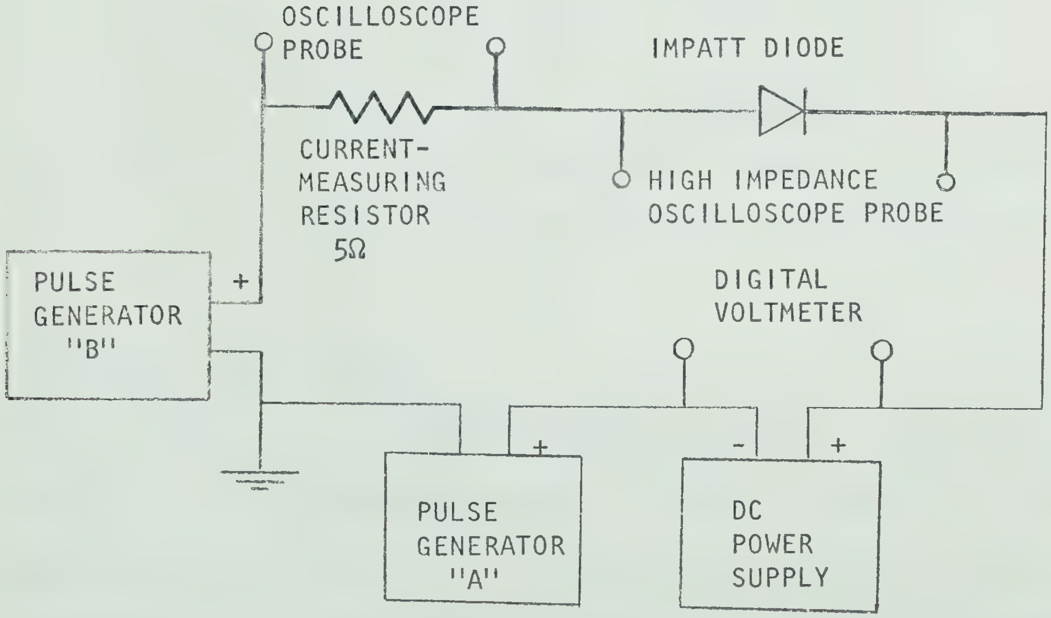

FIG. 3.5 DOUBLE PULSE GENERATOR CIRCUIT TO MEASURE THERMAL TIME CONSTANT OF THE DIODE

3-4 Thermal Time Constant Measurement

In general, the thermal response of a diode can be described by means of an equivalent circuit consisting of a parallel combination of lumped-constant R-C circuits. As a first approximation, the model can be simplified to a single parallel R-C circuit. The junction temperature during power dissipation is then given by[17]:

$$T_f = T_i + (P_d R_\theta + T_h - T_i)(1 - e^{-t/\tau}) \qquad (3.2)$$

where:

T_f is the junction temperature at time t

T_i is the initial junction temperature

P_d is the power dissipated in the diode

R_θ is the thermal resistance

T_h is the heat sink temperature

τ is the thermal time constant (i.e. $R_\theta C_h$)

C_h is the heat capacity of the semiconductor

The thermal time constant, τ, can be evaluated from the transient thermal response of an avalanching diode by using a double-pulse technique[18]. The measurement circuit is shown in Figure 3.5. Pulse generator "A" is used to pulse the diode into breakdown and thus the temperature of the diode increases due to the power dissipation in the diode. When the pulse ends, the temperature decreases and, as a first approximation, has a single time constant equal to τ.

The temperature is monitored by using a second pulse to measure the breakdown voltage in much the same way as was discussed in Section 3-3. It is noted that the power dissipation, P_d, is zero when the main pulse ends. Maximum resolution is obtained by apllying as short a monitoring pulse as possible (experimentally, a 500 nsec. pulse was used). An experimental plot of the diode temperature as a function of time (time origin is taken as the instant the main pulse ends) is shown in Figure 3.6. From the graph, it is seen that the temperature decreases to 1/e of its original value in 20 μsecs. Thus, assuming a single time constant as a first approximation, the theoretical exponential curve is also included in Figure 3.6.

From equation 3.2, the diode junction temperature can be crudely approximated as a function of time for an arbitrary pulse repetition rate or duty cycle. The temperatures predicted by equation 3.2 are generally lower than the experimentally observed temperatures, because this equation assumes that the thermal behaviour of the diode can be modelled as a lumped-constant parallel R-C circuit (where R is R_θ and C is C_h). Nevertheless, this model proves to be useful in understanding the thermal properties of pulsed IMPATT diode oscillators.

3-5 Effects of Temperature on the Operation of Bias-Modulated IMPATT Oscillators

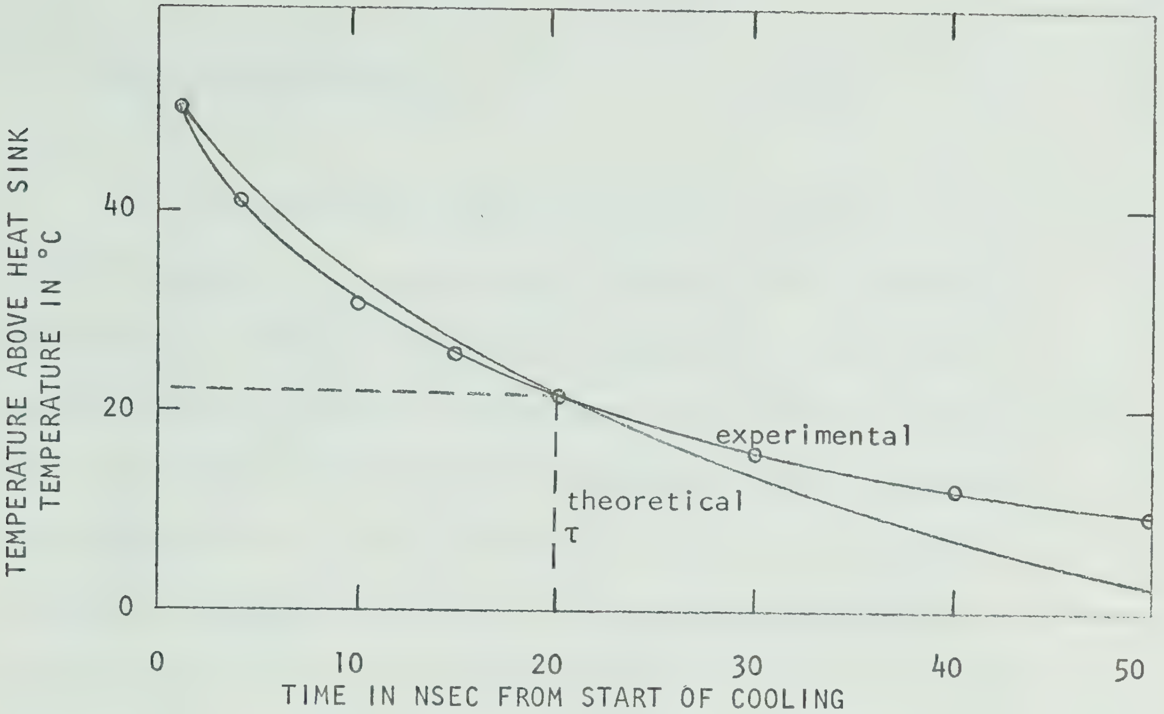

FIG. 3.6 THEORETICAL AND EXPERIMENTAL COOLING CURVES FOR IMPATT DIODE USED

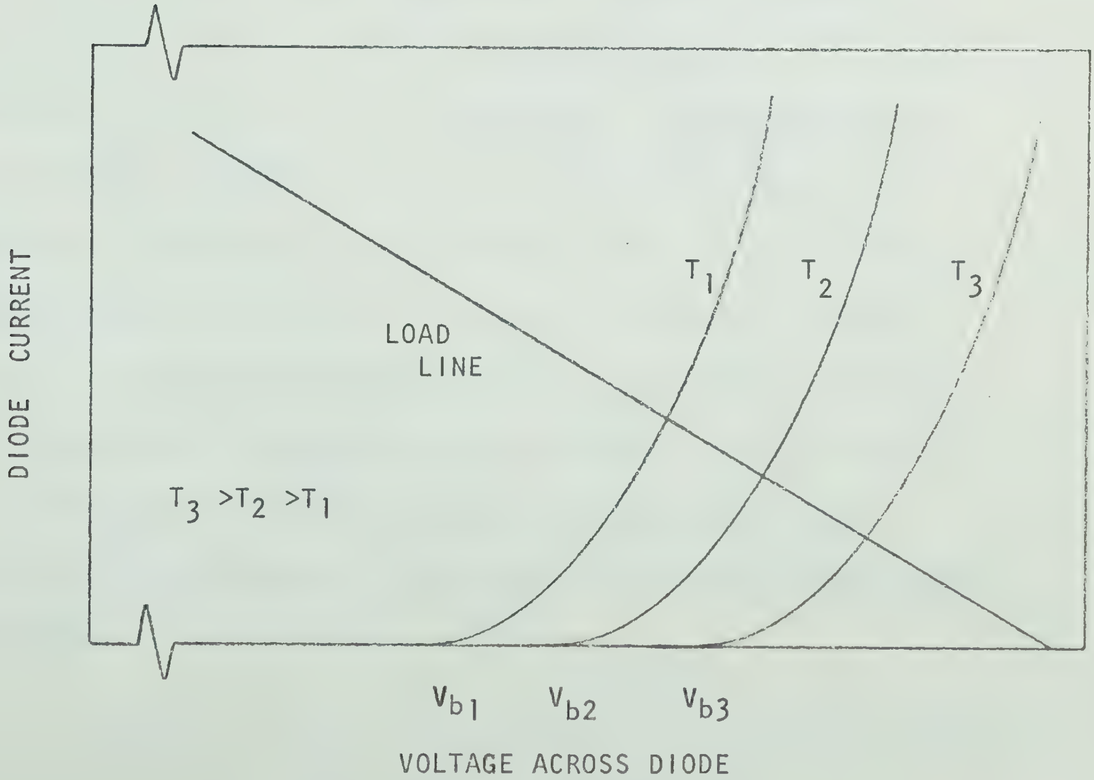

FIG. 3.7 REVERSE BIAS I-V CHARACTERISTIC OF DIODE FOR DIFFERENT TEMPERATURES

3-5-1 Choice of Bias Point

If the temperature of the diode remains constant, then the bias voltage can be chosen to be simply at the threshold of oscillation. In this case, the actual sequence of modulating pulses would not affect the operation of the modulator. However, due to the continuous increase and decrease of diode temperature, the breakdown voltage (see section 3-2) (and hence the bias current) is continually changing. This point is illustrated in Figure 3.7, where the I-V characteristic of the diode under reverse bias at various temperatures is shown. A hypothetical load line is also included. As the temperature increases, the breakdown voltage increases and the bias current decreases. Hence, for a 50% duty cycle square wave, the bias voltage is chosen to be at the oscillation threshold, where the ON pulse is applied. After the ON has terminated, the temperature is at its maximum value and the bias current is well below the threshold of oscillation. As the diode cools, the bias current increases until it reaches the threshold level at the instant the next ON pulse is applied. A plot of the voltage, current and temperature as a function of time is shown in Figure 3.8a. It is assumed that the pulse sequence has been on for some time so that the temperature oscillates around some "equilibrium" temperature.

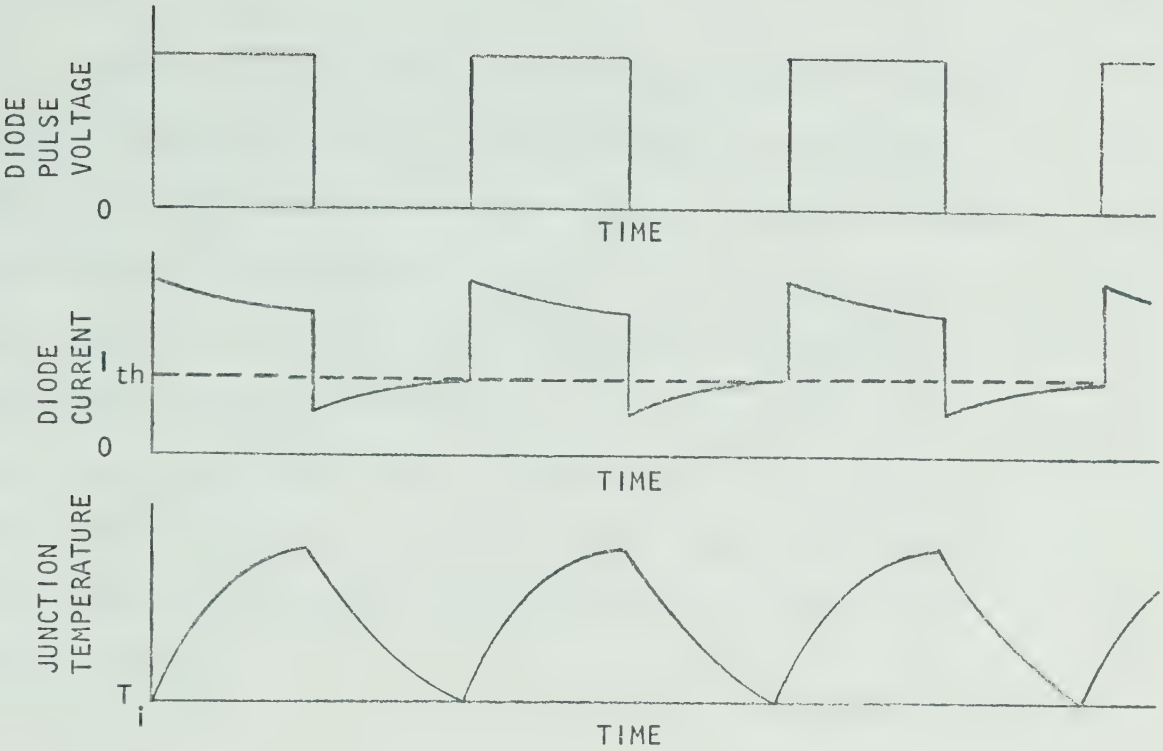

FIG. 3.8a VOLTAGE, CURRENT AND TEMPERATURE WAVEFORMS FOR ON-OFF-ON-OFF-ON-OFF-ON PULSE SEQUENCE

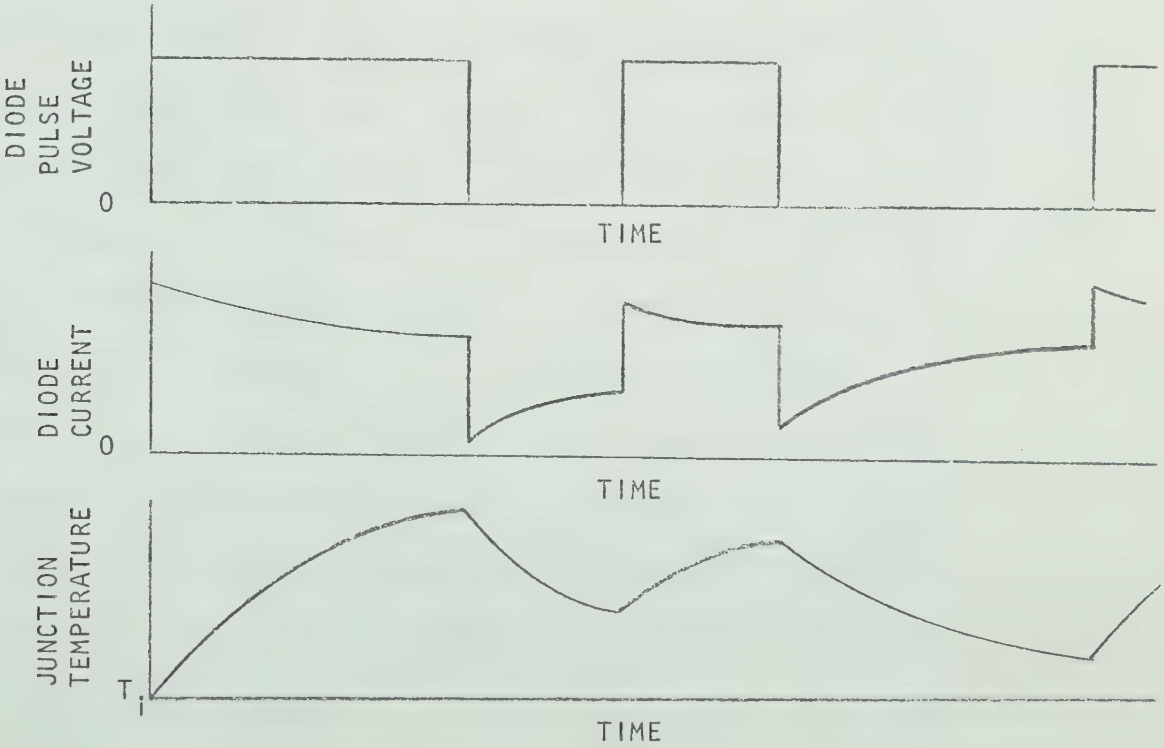

FIG. 3.8b VOLTAGE, CURRENT AND TEMPERATURE WAVEFORMS FOR ON-ON-OFF-ON-OFF-OFF-ON PULSE SEQUENCE

For a realistic pulse train, biasing becomes a serious problem. The reason for this is that the manner in which the temperature varies depends on which sequence of pulses is being transmitted. An illustration is given in Figure 3.8.b. Under these conditions, no "equilibrium" temperature exists.The major constraint in choosing the "optimal" bias point is that the bias current must never exceed the threshold value during an OFF pulse. In practice, the bias voltage should be chosen well below the bias level required for an ON, OFF, ON, OFF... pulse train.

3-5-2 Effect of Temperature on System Performance

The change of breakdown voltage with temperature also affects frequency and power output of the oscillator. As has been explained, the current decreases during the ON pulse due to heating of the diode. This decrease in current results in an undesired AM noise component in the output power (i.e. the RF power is changing). This is of minor consequence for high bit rates,since this power change is generally only in the order of a few percent of the total power. The amount of undesired AM increases as the length of the pulse increases and hence is only a serious problem for lower bit rates (i.e. less than about 500 KHz).

A much more important effect is the change in frequency when the bias current changes during heating and cooling of the diode. This change is due to the current dependence of electronic susceptance of the diode. In fact, during a 100 nsec pulse, a 14 MHz change in the carrier frequency has been observed (cf. Chapter 5). This is a substantial portion of the bandwidth of the signal and results in a significant spreading of the RF spectrum (and a subsequent loss of power from the main RF lobe). In addition, for a realistic pulse sequence, the average carrier frequency of any given pulse also depends on the temperature at the beginning of the pulse. These important points are discussed at greater length in Chapter 5.

3-6 Summary

The effect of temperature on the properties of IMPATT diodes has been discussed in order to gain insight into how the diode temperature affects the dynamic characteristics of IMPATTs. The temperature dependence of diode breakdown voltage has been measured. The thermal resistance has been found to be 25° C/w. An expression for junction temperature during power dissipation has been given, under the assumption that the thermal response of the diode can be approximated by the response of a lumped-constant parallel R-C circuit. This is true only as a first approximation; for greater accuracy, a cascade of R-C circuits must be considered.

The choice of bias point was discussed for the bias modulator.It was seen that the "optimal" bias point should be chosen so that the bias current must never exceed the threshold value during an OFF pulse. Problems arise because the bias current is a function of the temperature (through the temperature dependence of the diode breakdown voltage).

Undesired AM and FM were shown to be the two major effects of the junction temperature on the system performance of the bias-modulated IMPATT oscillator. Heating of the diode causes the bias current to decrease. This decrease results in a proportional decrease in RF power. This change in the power is negligible for short pulses, though it may be excessive when longer pulses are used. Due to the current dependence of the diode electronic susceptance, the frequency of oscillation changes appreciably for a small change in temperature. This latter point is discussed in Chapter 5.

CHAPTER IV

Q-FACTOR DEPENDENCE OF BUILD-UP AND DECAY TRANSIENTS

4-1 Introduction

The transient response of an IMPATT diode oscillator is described by means of an equivalent R-L-C circuit. The differential equation describing this circuit is analyzed. The bias current and RF voltage dependence of the electronic conductance is assumed such that a satisfactory correlation exists between the theoretical and experimental results. Thus, the build-up and decay transients of the RF oscillations have been calculated for various values of loaded Q. In this way, it is found that the maximum bit rate can be obtained by maximizing the loaded Q of the circuit.

The various constants in the analysis have been measured for the experimental RF circuit. The bias circuit has not been included to keep the discussion as general as possible.

4-2 Transient Analysis

The transient response of an avalanche diode oscillator can be modelled by means of an equivalent R-L-C circuit (Fig. 4.1) The variable active part of the diode is modelled by a bias-current and RF-voltage dependent electronic conductance, $G_e[A(t),I(t)]$.

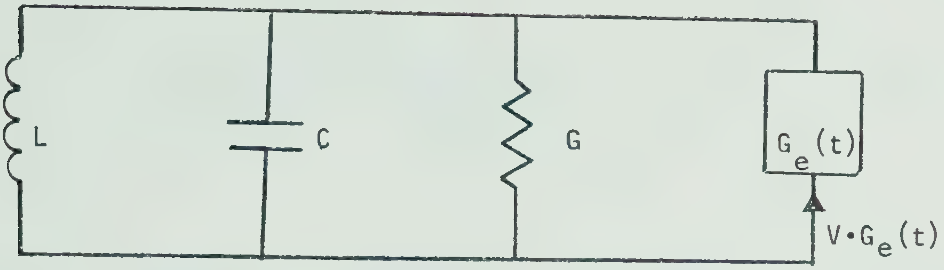

$$G_e(t) = G_e[A(t), I(t)]$$

FIG. 4.1 ASSUMED EQUIVALENT R-L-C CIRCUIT FOR TRANSIENT ANALYSIS OF IMPATT DIODE OSCILLATOR

The electronic susceptance is assumed to be constant for this transient analysis and is lumped into "C" in Figure 4.1; the passive part of the diode conductance is lumped in with the other losses of the circuit (i.e. G). The following equation results from applying Kirchoff's Current Law to the circuit shown in Figure 4.1:

$$V \{ G + G_e(A,I) \} + \int \frac{V}{L} dt + C \frac{dV}{dt} = 0 \tag{4.1}$$

Differentiating equation 4.1, a second order differential equation is obtained:

$$C \frac{d^2V}{dt^2} + \{G + G_e(A,I)\} \frac{dV}{dt} + \{ \frac{1}{L} + \frac{\partial G_e}{\partial A} \frac{dA}{dt} + \frac{\partial G_e}{\partial I} \frac{dI}{dt} \} V = 0 \tag{4.2}$$

The solution of equation 4.2 is assumed to be expressed in the functional form:

$$V(t) = A(t) \sin \Phi(t) \tag{4.3}$$

and hence:

$$\frac{dV}{dt} = \left(\frac{dA}{dt}\right)\sin\Phi + A\left(\frac{d\Phi}{dt}\right)\cos\Phi \qquad (4.4)$$

and

$$\frac{d^2V}{dt^2} = \left(\frac{d^2A}{dt^2}\right)\sin\Phi + 2\,\frac{dA}{dt}\left(\frac{d\Phi}{dt}\right)\cos\Phi + A\left(\frac{d^2\Phi}{dt^2}\right)\cos\Phi - A\,\frac{d\Phi^2}{dt}\sin\Phi \qquad (4.5)$$

Substituting equations 4.3, 4.4 and 4.5 into equation 4.2 and grouping the cosine and sine terms together, the following equation results:

$$D(t)\,\cos\Phi + F(t)\,\sin\Phi = 0 \qquad (4.6)$$

where:

$$D(t) = A\,\frac{d^2\Phi}{dt^2} + 2\,\frac{dA}{dt}\,\frac{d\Phi}{dt} + A\,\frac{d\Phi}{dt}\,\frac{G + G_e(A,I)}{C} \qquad (4.7)$$

$$F(t) = \frac{d^2A}{dt^2} - A\,\frac{d\Phi^2}{dt} + \frac{dA}{dt}\,\frac{G + G_e(A,I)}{C} + A\left\{\frac{1}{LC} + \frac{1}{C}\,\frac{\partial G_e}{\partial A}\,\frac{dA}{dt} + \frac{1}{C}\,\frac{\partial G_e}{\partial I}\,\frac{dI}{dt}\right\} \qquad (4.8)$$

If equation 4.6 is to hold for all time, then the time-varying coefficients of the cosine and sine terms (i.e. D(t) and F(t) respectively) must be both identically equal to zero*.The first of these two equations may be written as follows:

$$2\,\frac{dA}{dt} + A\left\{\frac{G + G_e(A,I)}{C} + \frac{d^2\Phi}{dt^2}\Big/\frac{d\Phi}{dt}\right\} = 0 \qquad (4.9)$$

* It is assumed that D(t) and F(t) vary much slower than Φ(t).

It has been seen that equation 4.6 can be separated into two coupled second order differential equations. Under certain conditions, equation 4.9 can be solved independently to yield the envelope of the RF oscillations at any instant of time. Since $d\Phi/dt$ is equal to the instantaneous frequency of the RF oscillations, during the transient state, therefore,

$$\left| \frac{d^2\Phi}{dt^2} \Big/ \frac{d\Phi}{dt} \right| << \left| \frac{G + G_e(A,I)}{C} \right|$$

except in the case when the magnitude of the electronic conductance approaches the value of the passive conductance in the circuit. This latter case generally only occurs near equilibrium. Therefore, using the above approximation, equation 4.9 can be simplified as follows:

$$\frac{dA}{dt} = - \frac{G + G_e(A,I)}{2C} A \qquad (4.10)$$

$$= \alpha(A,I) A$$

where $\alpha(A,I)$ is the growth factor

Equation 4.10 should describe satisfactorily the build-up and decay transients of the RF voltage, assuming that $G_e(A,I)$ is chosen properly. For a complete solution of the amplitude and phase at any time, the original differential equation (4.2)

must be solved.

Kramer[19] has suggested that the RF voltage dependence of the electronic conductance, $G_e(V)$, may be approximated by a symmetrical nonlinear function of V; that is,

$$G_e(V) = G_{ess}(I) + a\,V^2 \tag{4.11}$$

where $G_{ess}(I)$ is the small-signal electronic conductance (function of bias current)

In order to evaluate the constant "a", it is noted that when the RF voltage has reached its steady-state value in a given oscillator

$$G_e(V_{max}) = -G \tag{4.12}$$

and

$$a = -\frac{G_{esm} + G}{{V_{max}}^2} \tag{4.13}$$

where G_{esm} = maximum small-signal electronic conductance

V_{max} = maximum RF voltage

Normalizing the maximum RF voltage to unity and assuming that the voltage dependence of the electronic conductance is given by equation 4.11, equation 4.10 may be written as follows:

$$\frac{dV}{dt} = \frac{-1}{2C}\{ G\ (1 - V^2) + G_{ess}(I) - G_{esm}\ V^2 \}\ V \qquad (4.14)$$

where the initial condition is that the voltage at the time origin is equal to the preoscillation noise level, normalized to the maximum RF voltage. From the measurements recorded in Chapter 6, it was found that the noise power was equal to -35 dBm; the peak output power of the pulsed oscillator was 15 dBm. Thus, the normalized noise voltage was taken to be 0.003.

Scharfetter and Gummel[20] have done a large-signal analysis of a Read diode oscillator. Figure 4 of their paper demonstrated the calculated RF voltage dependence of the electronic conductance; their results are repeated here in Figure 4.2. For lower amplitudes, a strong linear dependence of conductance and RF amplitude is evident. Therefore, a second expression for the electronic conductance as a function of V can be assumed as follows:

$$G_e(V) = G_{ess}(I) + bV \qquad (4.15)$$

Once again, equation 4.12 is used to evaluate the constant, "b", and it is found to be of the same form as equation 4.13:

$$b = - \frac{G_{esm} + G}{V_{max}}$$

Normalizing the maximum RF voltage to unity and assuming equation

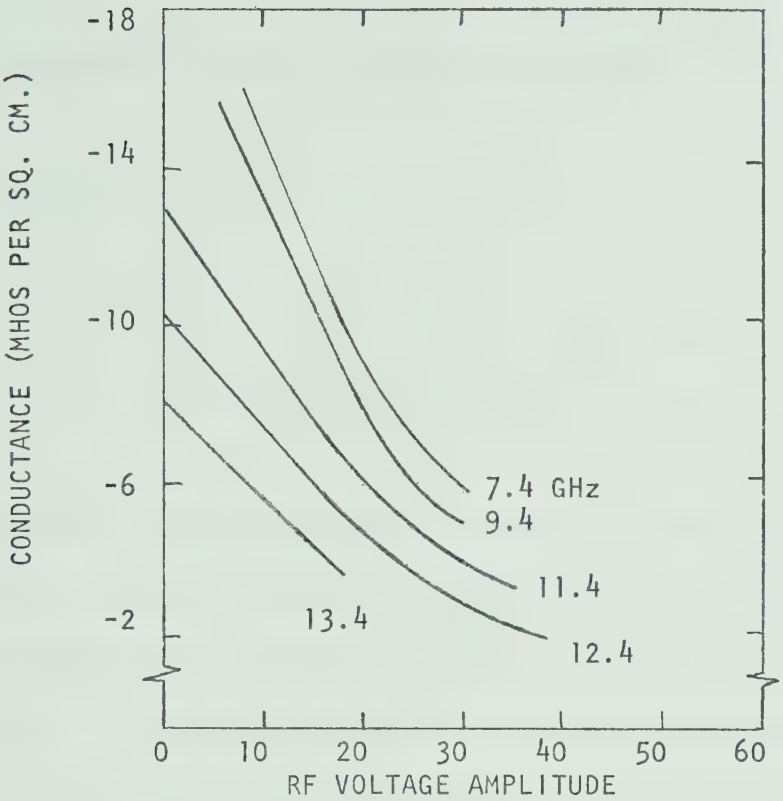

FIG. 4.2 DIODE NEGATIVE CONDUCTANCE AS A FUNCTION OF RF VOLTAGE AMPLITUDE FOR VARIOUS FIXED FREQUENCIES. CURRENT DENSITY : 200 A/CM^2.[22]

CHARACTERISTIC	VALUE (UNITS)
f : average frequency of oscillation	5.185 GHz
V_p; applied pulse voltage	5.0 V
I_p: peak bias diode current	60 mA
t_r: risetime of current pulse	10 nsec
t_d: decay time of current pulse	10 nsec
τ_p: pulse length	100 nsec
T_p: pulse period	2 µsec
V_o: preoscillation noise voltage	0.003 V
Q_L: loaded Q of circuit	51.7
P_p: peak RF power	70 mW
C_T: total capacitance of RF circuit	1.478 pF
G : total passive conductance	1.02 mmhos

TABLE 4.1 EXPERIMENTALLY MEASURED CHARACTERISTICS OF PULSE, BIAS-MODULATED IMPATT DIODE OSCILLATOR

4.15 applies, equation 4.10 may be written as follows:

$$\frac{dV}{dt} = \frac{-1}{2C} \{ G\,(1-V) + G_{ess}(I) - G_{esm}\,V\}\,V \qquad (4.16)$$

Once again, the initial condition is that the voltage at the time origin is equal to the normalized preoscillation noise voltage.

The RF voltage dependence of the electronic conductance, as given by either equations 4.11 or 4.15, is illustrated in Figure 4.3 for the build-up transient. Assuming a linear bias-current dependence, the diode small-signal conductance has also been included. Figure 4.4 illustrates the small- and large-signal conductances during the decay transient.

The object of the following analysis is to determine the build-up and decay times of the RF oscillations as a function of the loaded Q of the circuit: Q_L . First, it is determined which RF voltage dependence of the electronic conductance (i.e. equations 4.11 or 4.15 or a combination of both) best describes the experimentally measured build-up of RF oscillations. Next, a step function of the current is assumed and the build-up and decay times of the RF voltage are calculated. Finally, an optimal Q_L for the experimental RF circuit is determined and the maximum pulse repetition frequency is calculated.

Risetimes are conventionally defined as the time required

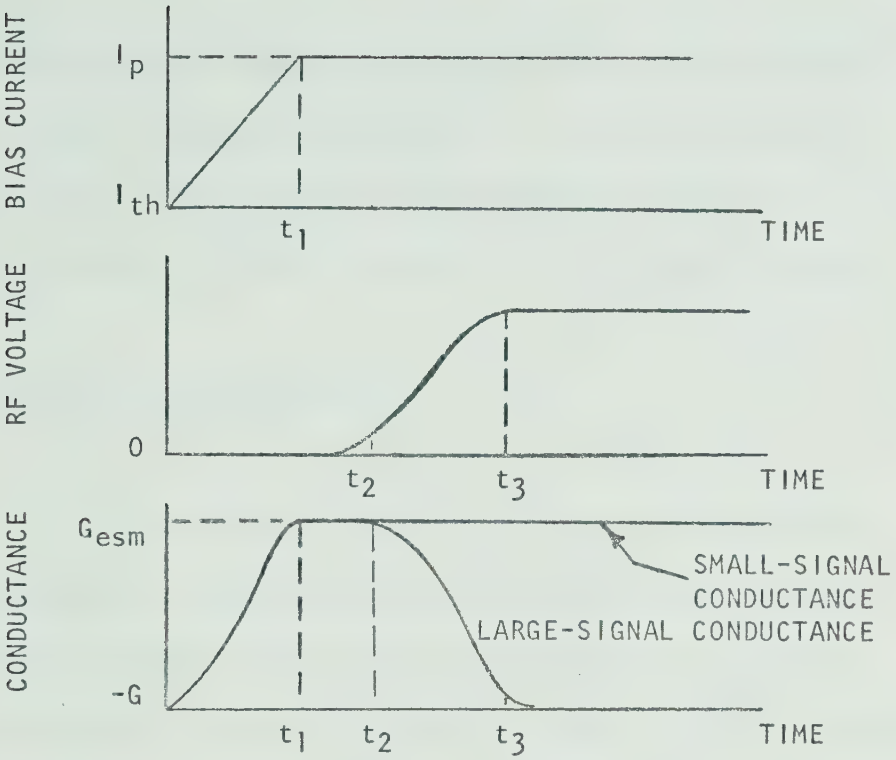

FIG. 4.3 VARIATION OF SMALL-SIGNAL AND LARGE-SIGNAL ELECTRONIC CONDUCTANCE DURING BUILD-UP OF OSCILLATION

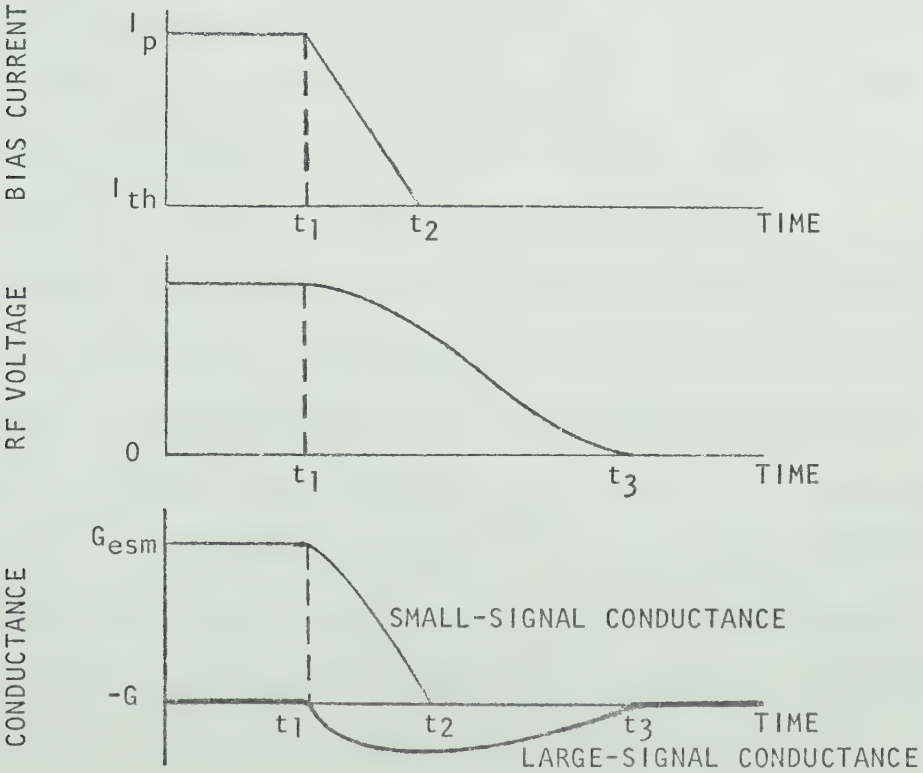

FIG. 4.4 VARIATION OF SMALL-SIGNAL AND LARGE-SIGNAL ELECTRONIC CONDUCTANCE DURING DECAY OF OSCILLATION

for the RF power to increase from 10% to 90% of its maximum value; a similar definition applies for the decay transient. The 10% and 90% points on the power waveform correspond to approximately the 31% and 95% points on the voltage waveform.

4-3 Build-Up of RF Oscillations

An IMPATT diode was biased just below the oscillation threshold and bias modulated as has been discussed in Chapter 2. The experimentally measured characteristics of the bias - modulated IMPATT oscillator are given in Table 4.1*.The evaluation of the parameters characterizing the resonator is discussed in Appendix B.

The RF pulse was fed into a detector circuit and the RF voltage amplitude was measured as a function of time during the build up of oscillation (cf. Fig. 4.5). The time origin is taken as the instant the pulse current has passed the oscillation threshold level. The maximum value of the small-signal electronic conductance, G_{esm}, can be calculated by noting that,at t=14 nsec, the current has already reached its maximum value, while the RF voltage is still very small compared to its final value. Therefore, for a short interval of time around t = 14 nsec, G_e and therefore the growth factor α are both constant. Over this short interval, the solution of equation 4.10 is simply an exponential. Therefore,

---

* Table 4.1 is located adjacent to Figure 4.2 (p. 44)

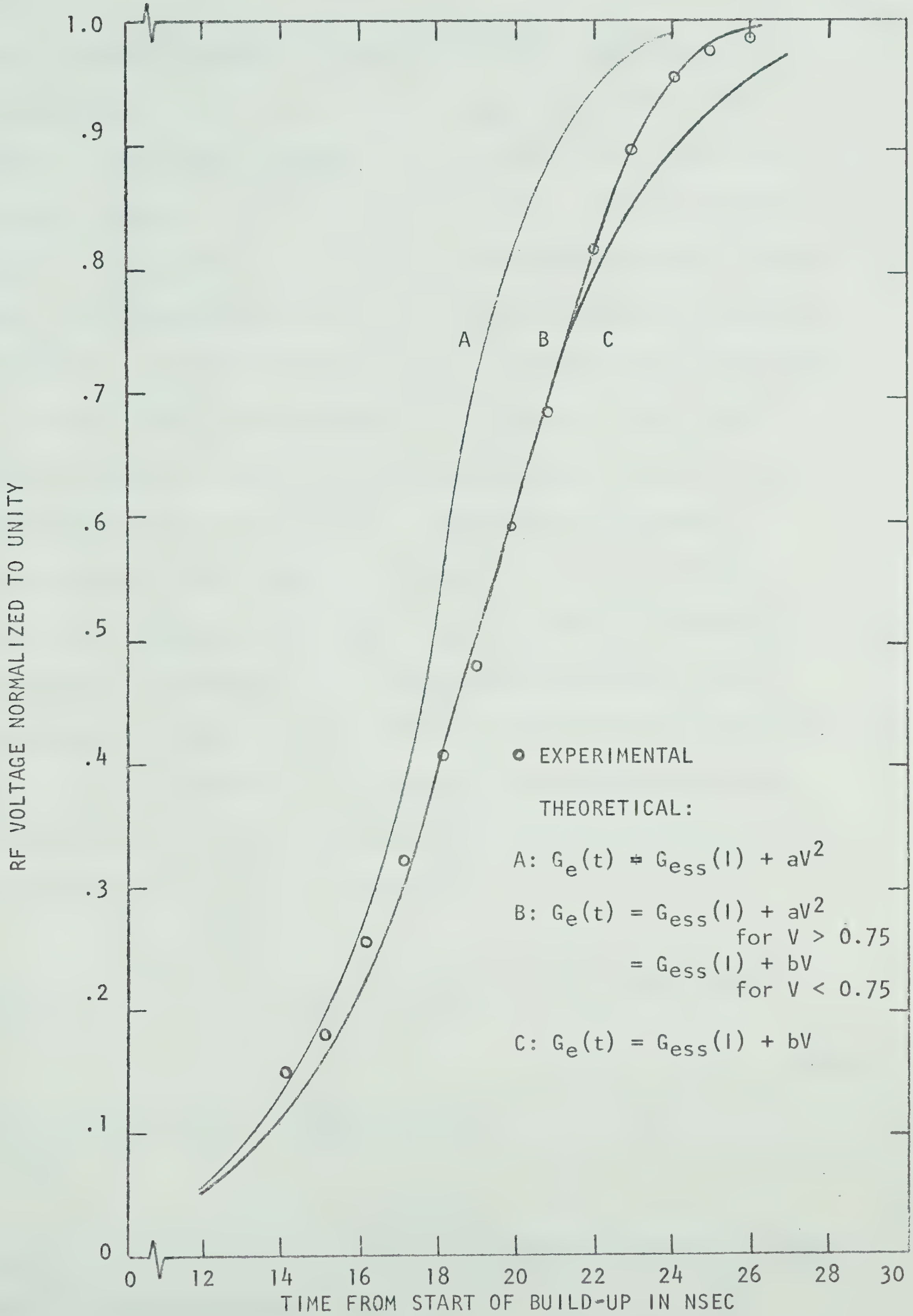

FIG. 4.5 THEORETICAL AND EXPERIMENTAL BUILD-UP OF RF VOLTAGE

noting that the voltage increases from 0.15 to .1825 during the interval from $t = 14$ to $t = 15$ nsec, G_{esm} is calculated to be equal to -1.62 mmhos. Assuming that the small-signal conductance increases linearly with the bias current, G_{ess} increases linearly from $-G$ to G_{esm} during the 10 nsec risetime of the current. Hence, under this assumption and using the resonator parameters as given in Table 4.1, equations 4.14 and 4.16 have been solved numerically; the solutions are shown graphically in Figure 4.5. The linear voltage dependence (equation 4.16) gives a better fit to the experimental results than does the linear power dependence (equation 4.14). The solution of equation 4.16 only deviates appreciably from the experimental curve for higher amplitudes. This effect corresponds to the nonlinearity appearing in the conductance-voltage plot shown in Figure 4.2. Therefore, it is assumed that a combination of equations 4.14 and 4.16 describes the behaviour of the electronic conductance as a function of the RF amplitude (cf. Fig. 4.5); that is,

$$\frac{dV}{dt} = \frac{-1}{2C} \{ G\ (1 - V) + G_{ess}(I) - G_{esm}\ V \}\ V \qquad \text{for } V < 0.75$$

$$(4.17)$$

$$\frac{dV}{dt} = \frac{-1}{2C} \{ G\ (1 - V^2) + G_{ess}(I) - G_{esm}\ V^2 \}\ V \qquad \text{for } V > 0.75$$

Equation 4.17 will be used in the calculation of the rise and decay times as a function of Q.

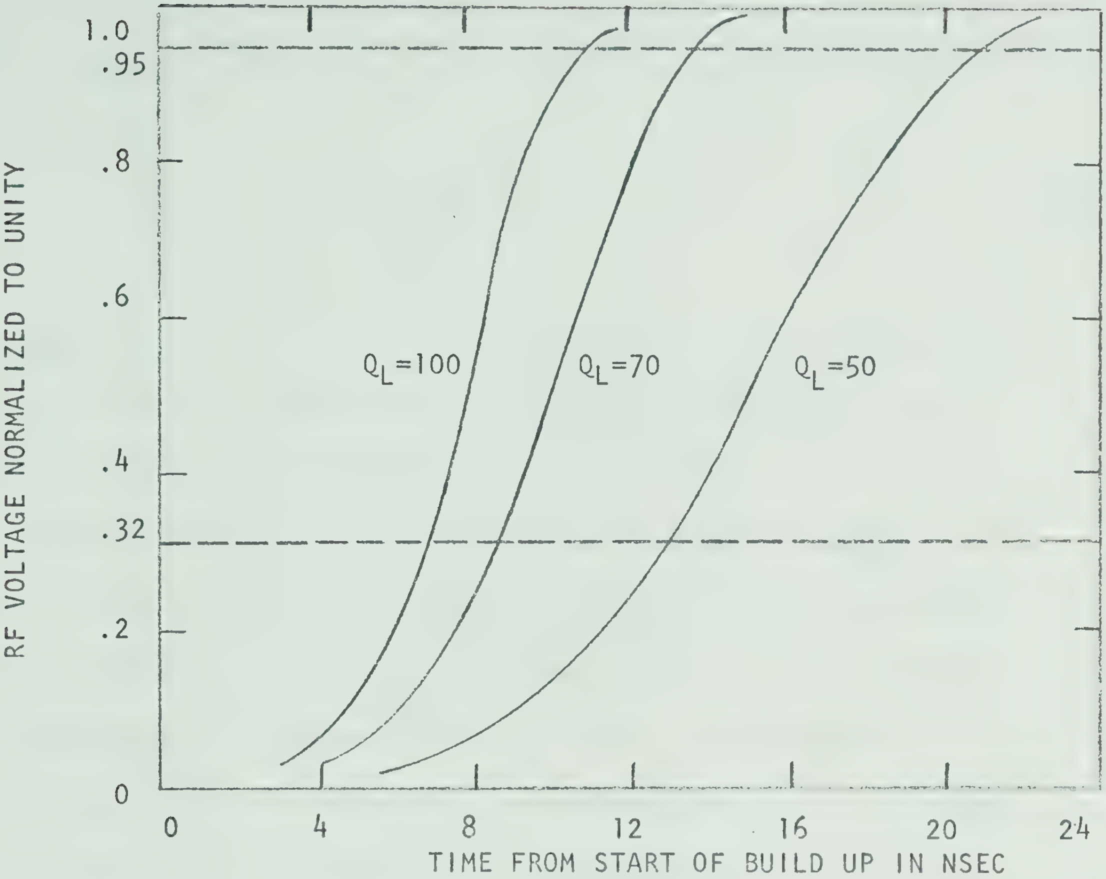

FIG. 4.6 THEORETICAL BUILD-UP OF RF VOLTAGE FOR Q_L = 100, 70 AND 50

Q_L	RISETIME IN NSEC
40	15.0
50	7.5
60	5.8
70	4.9
80	4.4
90	4.1
100	4.0
150	3.2
200	3.1
500	2.9
∞	2.7

TABLE 4.2 VARIATION OF THE RISETIME OF THE BUILD-UP OF OSCILLATIONS AS A FUNCTION OF LOADED Q

Since

$$G = \frac{2 \pi f C_T}{Q_L} \tag{4.18}$$

the positive part of the resonator conductance can be calculated as a function of Q_L. Equation 4.17 is then solved numerically, assuming a step in the current, and the envelope of the RF pulse for various values of Q_L is calculated. The results for $Q_L = 50$, 70 and 100 are shown graphically in Figure 4.6. For convenience, the calculated risetimes as a function of Q_L are given in Table 4.2. The minimum risetime attainable, using the parameters of the circuit used (cf. Table 4.1), assuming a step in the current, is 2.7 nsec for an infinite Q. The limiting factor is the build-up of oscillations in the actual resonator.

4-4 Decay of Oscillation

Under the conditions given in Table 4.1, the envelope of the decay of oscillations has been obtained experimentally; it is shown in Figure 4.7. The solutions of equations 4.14, 4.16 and 4.17 have also been included. It has been assumed that no heating occurs during the pulse; therefore, at the end of the decay of the current through the diode (i.e., after 10 nsec for the circuit used), the avalanche diode is once again biased at the threshold of oscillation. As would be expected,

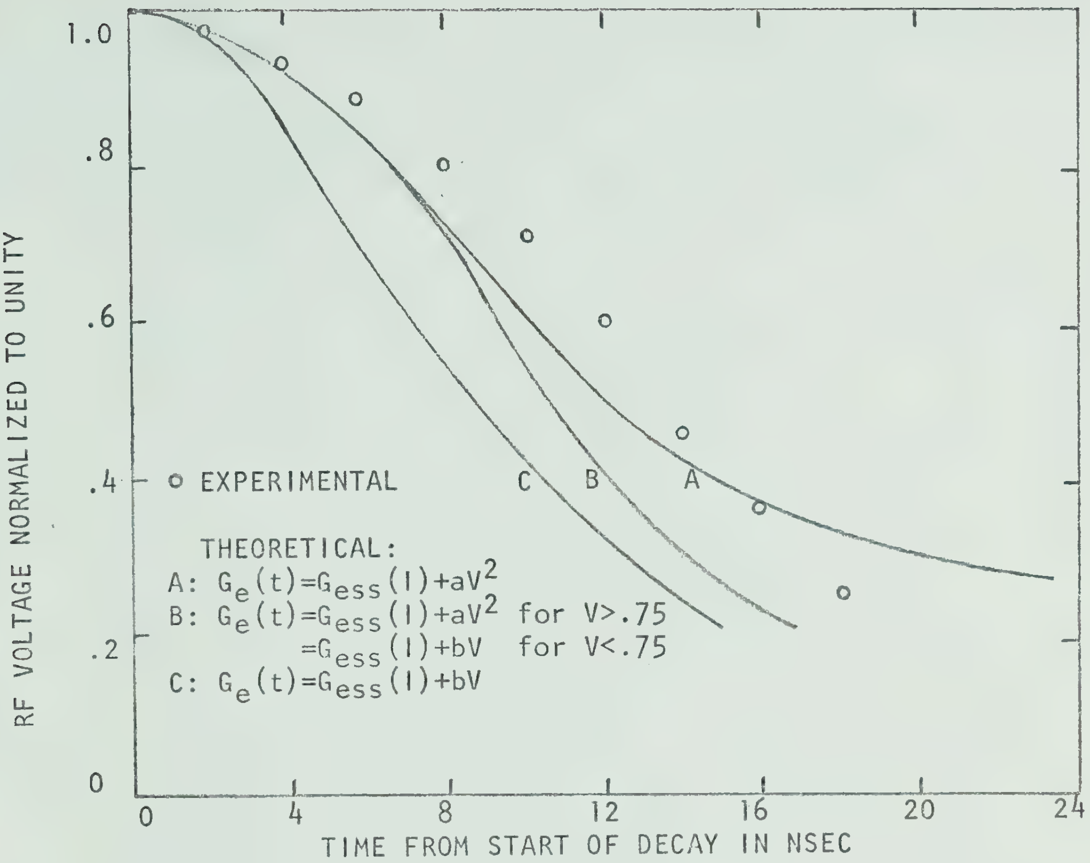

FIG. 4.7 THEORETICAL AND EXPERIMENTAL DECAY OF RF VOLTAGE

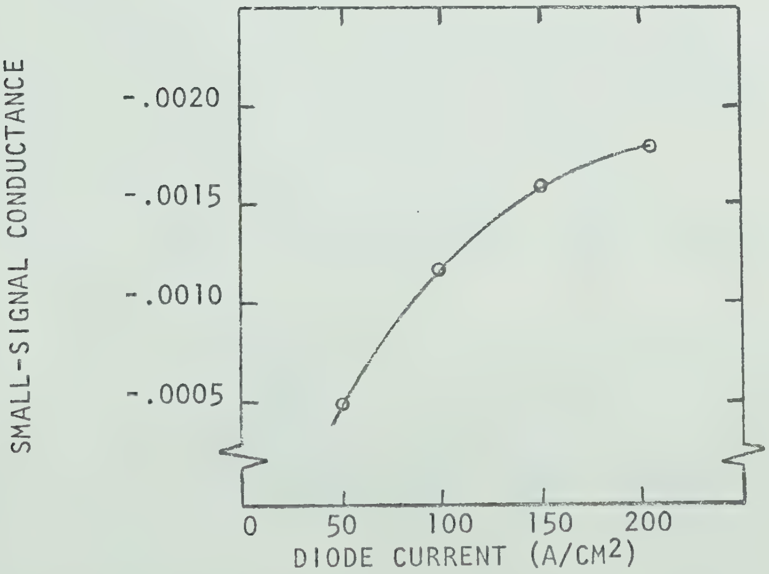

FIG. 4.8 SMALL-SIGNAL ELECTRONIC CONDUCTANCE AS A FUNCTION OF BIAS CURRENT AT 6 GHZ

the latter case gives the best fit to the experimental results. The discrepancy between the theoretical and the experimental curves can be accounted for by the following three factors:

a) As was pointed out before, equation 4.10 is least accurate near equilibrium and hence some deviation at the start of decay would be expected.

b) For high amplitudes, the slope of the experimental curve is less than that of the theoretical curve, because the largest part of any nonlinearities in the current dependence of the electronic conductance occurs for high conductance value. This is illustrated in Figure 4.8 which is taken from Scharfetter's and Gummel's[21] small signal analysis. This is of little consequence to the analysis since a step in the bias current is assumed.

c) For low amplitudes, the slope of the experimental curve is greater than that of the theoretical curve, because heating of diode has decreased the current level at the end of the current pulse,resulting in a faster decay.

For a step in the current, equation 4.17 is solved assuming, as before, no heating of the diode. The results of the calculation for Q_L = 50, 70 and 100 are shown in Figure 4.9.

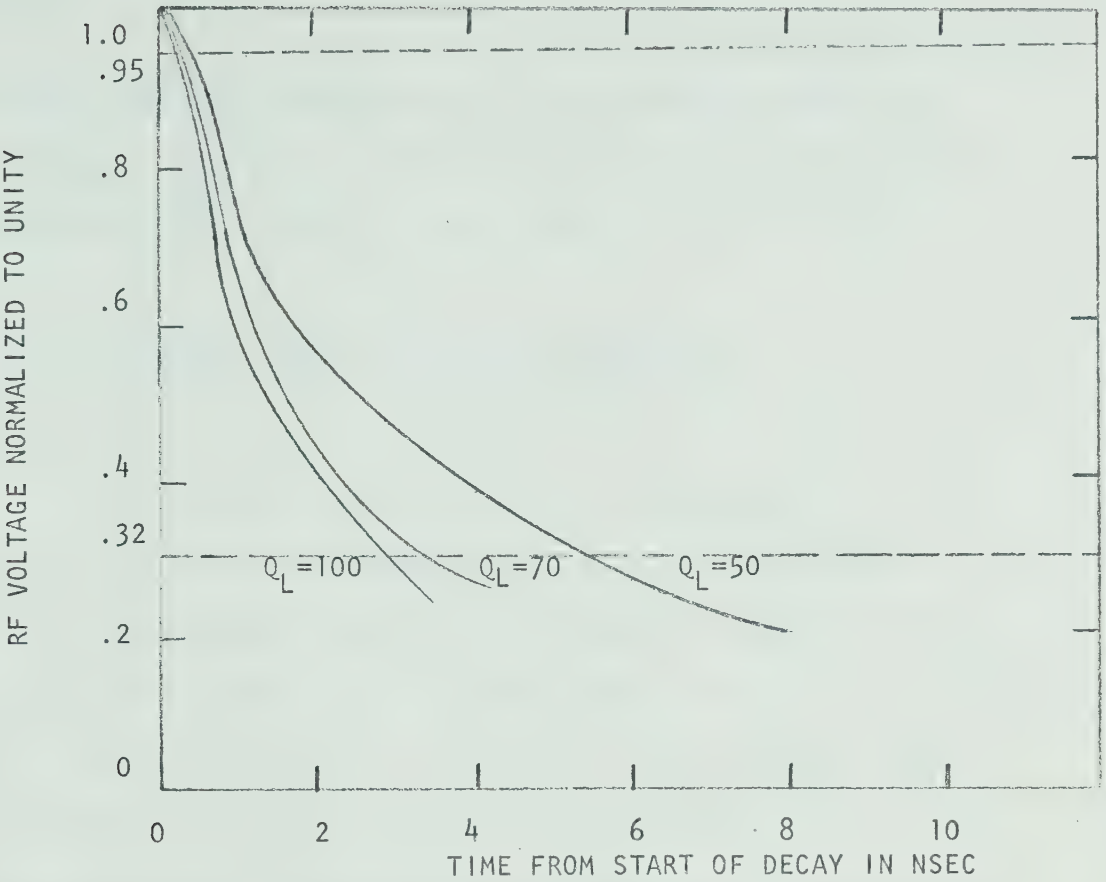

FIG. 4.9 THEORETICAL DECAY OF RF VOLTAGE FOR Q_L = 100, 70 AND 50

Q_L	DECAY IN NSEC
40	11.0
50	5.8
60	4.3
70	3.7
80	3.3
90	3.1
100	2.9
200	2.4
500	2.2
∞	2.0

TABLE 4.3 VARIATION OF THE DECAY TIME OF THE DECAY OF OSCILLATIONS AS A FUNCTION OF LOADED Q

The decay time as a function of Q_L is tabulated in Table 4.3. The minimum decay time is 2.0 nsec, the limiting factor being the decay of oscillations in the cavity.

4-5 Determination of Maximum PRF and Optimum Q

The results of the previous two sections(Tables 4.2 and 4.3) are presented graphically in Figure 4.10. The sum of the rise-and decay times is also shown as a function of Q_L. To convert this number into a minimum pulse length, it is noted that for a $\sin^2 x$ RF envelope , the sum of the transient times accounts for approximately 60% of the total pulse length. Using this approximation, the minimum pulse length is 7.8 nsec, which is only attainable for an infinite Q cavity. For Bell System's T-3 carrier equipment, this would correspond to a maximum bit rate of 64.1 Mbps compared to the 46 Mbps for which that particular system is designed.A loaded Q of about 110 is required to transmit a 46 Mbit pulse stream suitable for the T-3 system. The minimum pulse width for the experimental-circuit loaded Q of 51.7 is 13.3 nsec.

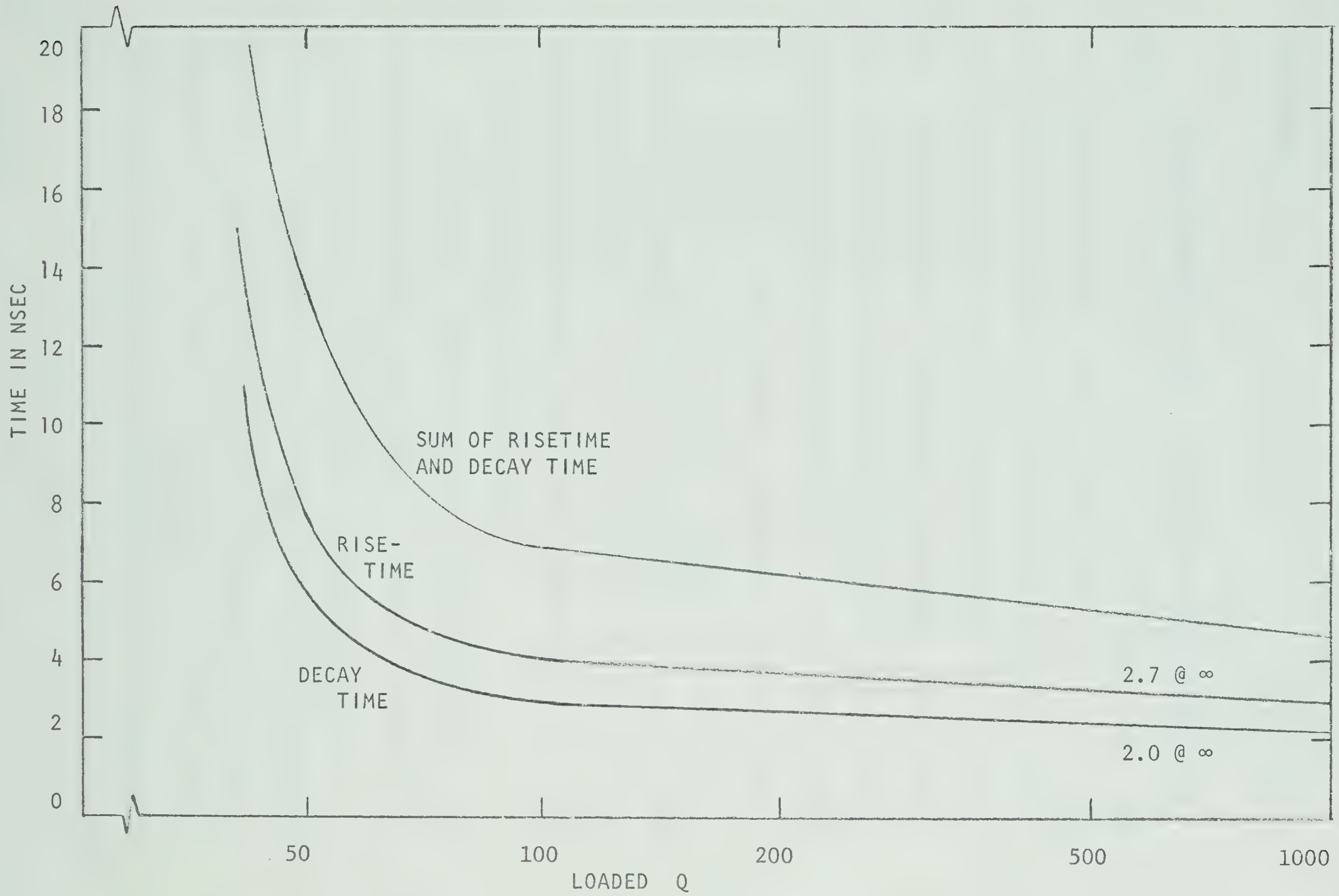

FIG. 4.10 RISE AND DECAY TIMES OF A PULSED IMPATT OSCILLATOR AS A FUNCTION OF LOADED Q

4-6 Summary

It has been found that, for the transient conditions described, the voltage dependence of the electronic conductance can be approximated by a linear function of V for low amplitudes and by a linear function of V^2 for high amplitudes. From the voltage dependence of the electronic conductance, the growth factor can be found as a function of the voltage. The growth factor is proportional to the slope of voltage at any instant. In solving the appropriate equations for a step in the current, plots of rise- and decay time as a function of Q-factor have been obtained. As would be expected, risetime decreases with increasing Q_L; however, decay time was found to decrease as well with increasing Q_L. This latter trend illustrates the effect the diode has on the cavity,since the resonator on its own would take longer to decay as its Q increased.

In conclusion, minimum rise- and decay times can be obtained by maximizing the loaded Q of a circuit. Maximizing the loaded Q of the circuit also enhances the stability of the oscillator. From Figure 4.6, it is seen that there is an appreciable delay before the output power has reached 10% of its maximum value. This delay can be decreased by increasing the Q of the circuit or, as will be seen in Chapter 6, by injecting a suitable signal into the oscillator. This delay need not affect

substantially the performance of the bias-modulated oscillator, as long as the delay is evaluated and incorporated as part of the total delay of the system.

CHAPTER V

FREQUENCY PUSHING IN BIAS-MODULATED OSCILLATORS

5-1 Introduction

The spectral distribution of the energy of the transmitted signal is an important consideration in a modulation scheme. In an ideal ASK system, the RF spectrum, centered at the carrier frequency, is identical in shape to the baseband spectrum of the modulating signal. In this case, the percentage of the power in the main lobe of the RF spectrum is the same as the percentage of the power in the main lobe of the baseband spectrum (i.e. the spectrum of the envelope). For an ideal ASK system, the RF spectrum is always symmetrical around the carrier frequency, regardless of the pulse shape.

In a digitally modulated IMPATT oscillator, the carrier frequency is not constant and an undesired FM component is present. This is due to the fact that the electronic susceptance is a function of the current through the diode, of the amplitude of RF voltage, and of the junction temperature. Hence,when the current changes, the frequency will also change. Under pulsed conditions, the shape of the current waveform is of the same nature as the shape of the applied voltage pulse, resulting

in frequency being pushed during the build-up and decay transients. The frequency also decreases during the main part of the pulse due to heating of the diode; this follows directly from the temperature dependence of breakdown voltage, as has already been discussed in Chapter 3. The feasibility of locking the oscillator frequency to an injected signal is discussed in detail in the next chapter.

5-2 Measurement of Frequency Changes During the RF Pulse

Several methods were employed to measure the instantaneous change of frequency of a pulsed IMPATT oscillator. Difficulties arose because of the small percentage change of frequency (ie. a change of a few tens of MHz for a carrier frequency of 6 GHz) to be measured. The methods tried are described below:

a) In general, only the envelope of the RF pulse is observable on a sampling oscilloscope since the oscillator commences oscillation at a slightly different phase during each applied pulse. By synchronizing the bias modulated signal to a microwave injected signal (by the use of a countdown unit), a coherent display of the RF oscillators during the RF pulse was obtained. An X-Y recorder was used to expand this display, permitting period measurements to be made. This method indicated an overall change of frequency during a 100 nsec pulse of about 50 MHz, but the

resolution was not sufficiently fine to give any usable results.

b) In this case, the output of the sampling oscilloscope was fed into a frequency selective voltmeter having a resolution of 1%. The modulated signal was triggered as before,allowing a coherent display to be obtained on the CRT. The output of the frequency selective voltmeter was fed into a peak detector and the center frequency was adjusted so as to result in a maximum reading at the detector output. The single-trigger feature of the scope was then used, resulting in a burst of approximately one hundred cycles of a varying-frequency "sine" wave. (The number of cycles was determined by the time-base setting of the oscilloscope.)Stability and reproducibility were the greatest problems in this method, though the general frequency trends of the first method were again observed.

c) A high-Q transmission cavity (TE_{111} mode) was designed and built with a 3dB bandwidth of 2 MHz (the necessary resolution). There is a definite tradeoff between the build-up time of the cavity and its Q. For a given Q, as the rate of change of frequency with time increases the response of the cavity decreases. As a result, the resolution was found to be quite inadequate for the frequency changes and pulse lengths considered. For slower rates of frequency change than encountered here, this technique should be useful.

d) By detecting the sum of the injected microwave signal and the output of the pulsed oscillator, a varying beat frequency is observable during the pulse. There are two major constraints on the injected signal: 1. the frequency of the injected signal, relative to the oscillator frequency, needs to be chosen so that a sufficient number of cycles of the beat frequency appear during the pulse, for the resolution required (typically 100MHz from the average free-running frequency of the pulsed oscillator); 2. the injected signal must be low in power level and still maintain a phase relation between the output of the oscillator and the injected signal.

In this manner, the accuracy of the frequency measurement was increased by at least two orders of magnitude over the other three methods just discussed. This method has an inherent disadvantage in that the instantaneous frequency cannot be measured under realistic locking conditions, since in this case the beat frequency would be very small. The main requirement for successful frequency measurements is that there must be a phase relation between the injected signal and the oscillator output. Figure 5.1 shows a typical pulse with a varying frequency.

One set of operating conditions was taken for illustrative purposes as being representative; these are summarized in Table 5.1. For these conditions, the results of the frequency measurement are shown graphically in Figure 5.2.

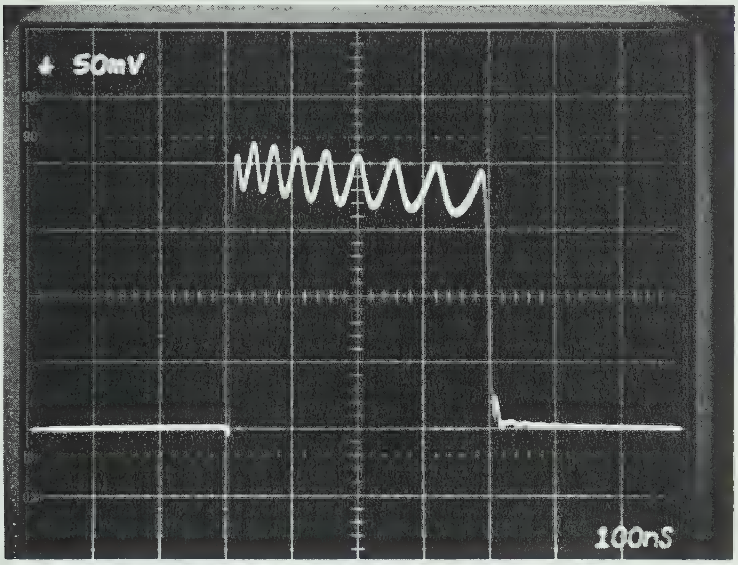

FIG. 5.1 VARYING BEAT FREQUENCY INDICATING FREQUENCY PUSHING IN BIAS-MODULATED IMPATT OSCILLATOR
frequency of injected signal= 5.8509 GHz.
injected-to-output power ratio= -14 dB.
beat frequency varies from 31 to 13 MHz.

CHARACTERISTIC	VALUE
PULSE PERIOD	1 μsec
PULSE LENGTH	100 nsec
DC BIAS CURRENT	10 mA
APPLIED VOLTAGE PULSE	5 V
PEAK POWER	80 mW
INJECTED POWER	1 mW
INJECTED FREQUENCY	5926 MHz

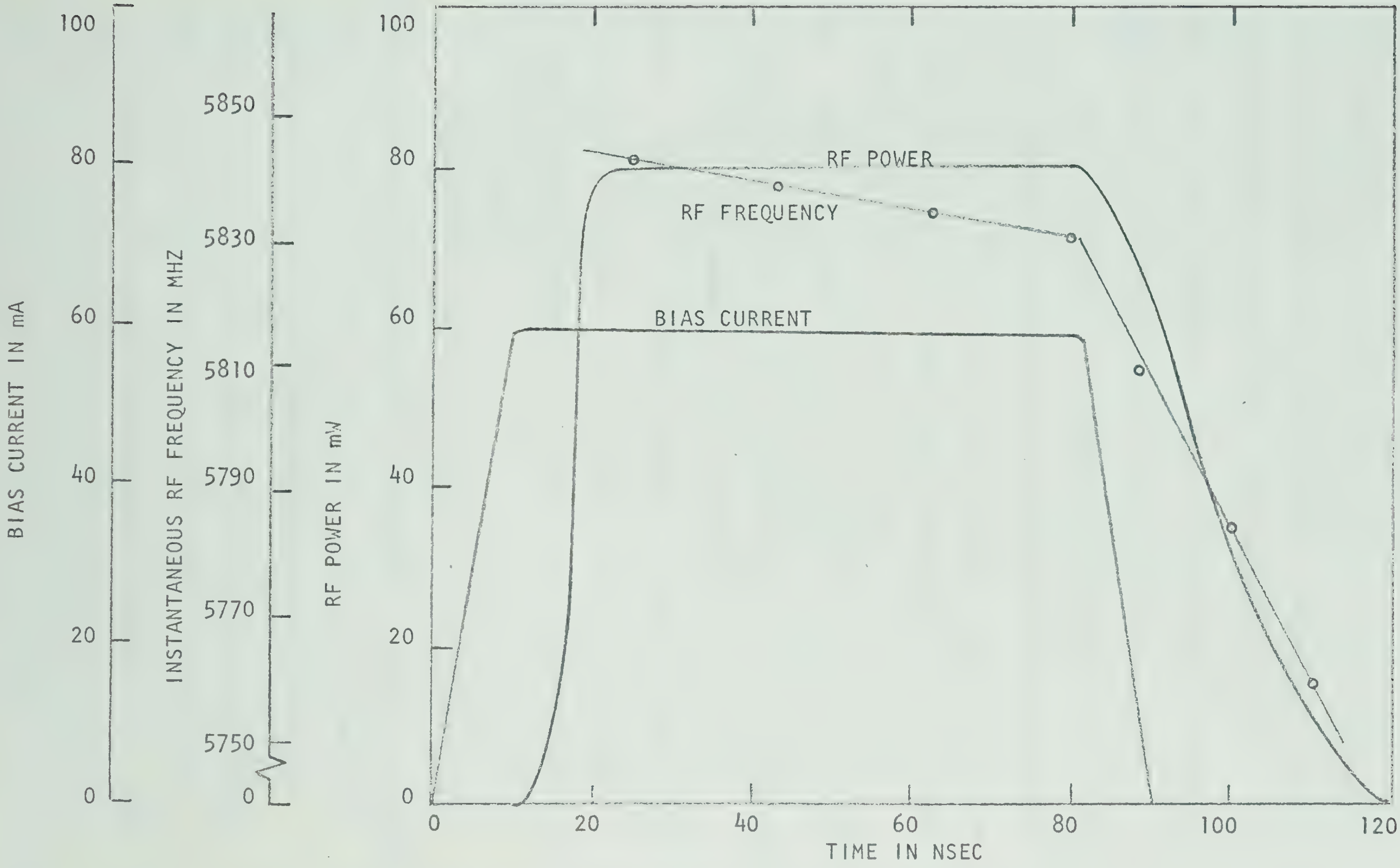

FIG. 5.2 BIAS CURRENT, OUTPUT POWER AND INSTANTANEOUS FREQUENCY FOR BIAS-MODULATED IMPATT OSCILLATOR

It is seen that a 14 MHz change was observed during the main portion of the pulse (i.e. constant power section) and a 70 MHz change during the decay transient. The build-up transient contributes very little FP since the current has reached its maximum value before any substantial power is produced.

If the off-time is increased above 600 nsec, the behaviour of the frequency is substantially unchanged since the diode has had time to cool sufficiently between pulses. Below an off-time of about 500 nsec, the average diode temperature has increased and there is a smaller temperature increase during the ON pulse. Hence the magnitude of the frequency change during the main part of the pulse becomes smaller than indicated by Figure 5.2. In fact, for a period equal to 200 nsec (for a 100 nsec pulse), there is no detectable change of frequency during the main part of the pulse. In this latter case, there is still the same frequency change (i.e. in the order of 70 MHz) during the decay transient.

Figures 5.3 show the measured effect of temperature on the frequency of a pulse. The temperature is varied by varying the duty cycle of the pulse. The dashed line for a given period represents the range of frequencies present during the main part of the pulse for that period. The y-axis represents $(f-f_c)$, where f is the instantaneous frequency during the pulse and f_c is arbitrarily set equal to the average frequency for a 50% duty cycle. It is seen that the change of frequency during the

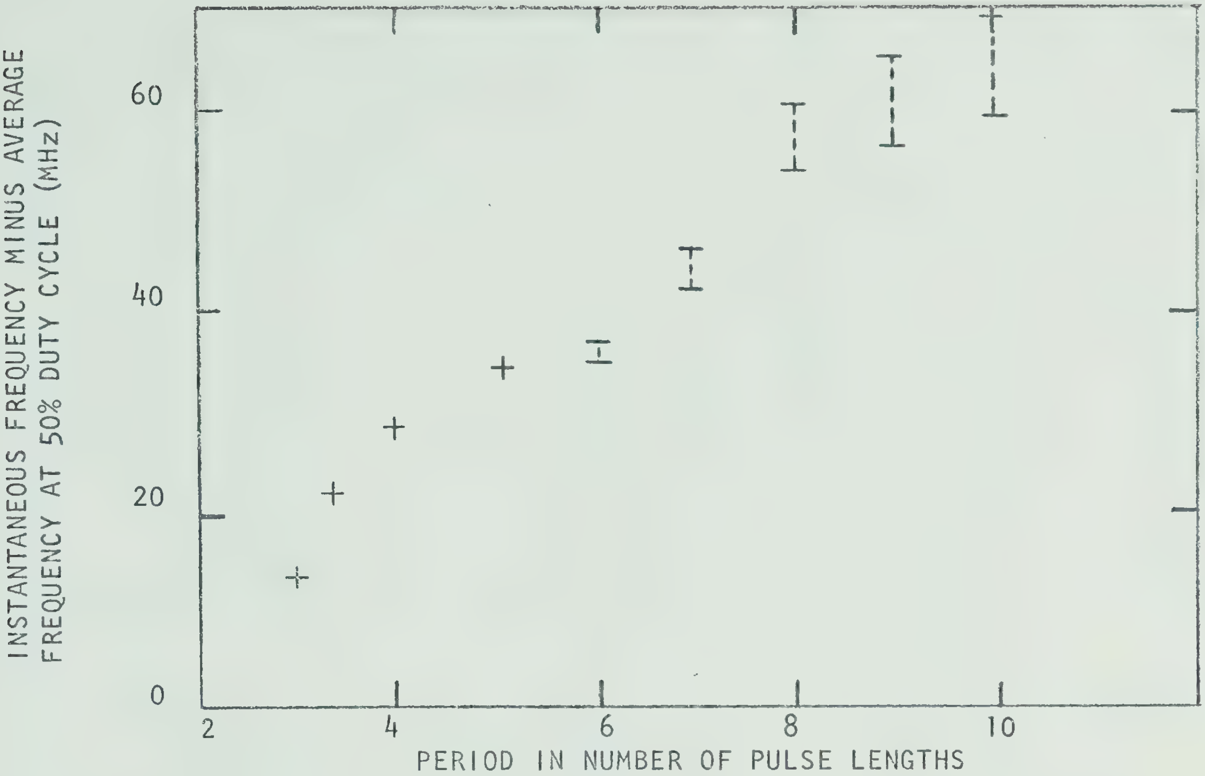

FIG. 5.3.a FREQUENCIES PRESENT DURING A 50 NSEC PULSE AS A FUNCTION OF PULSE PERIOD (i.e., 50 nsec ON time)

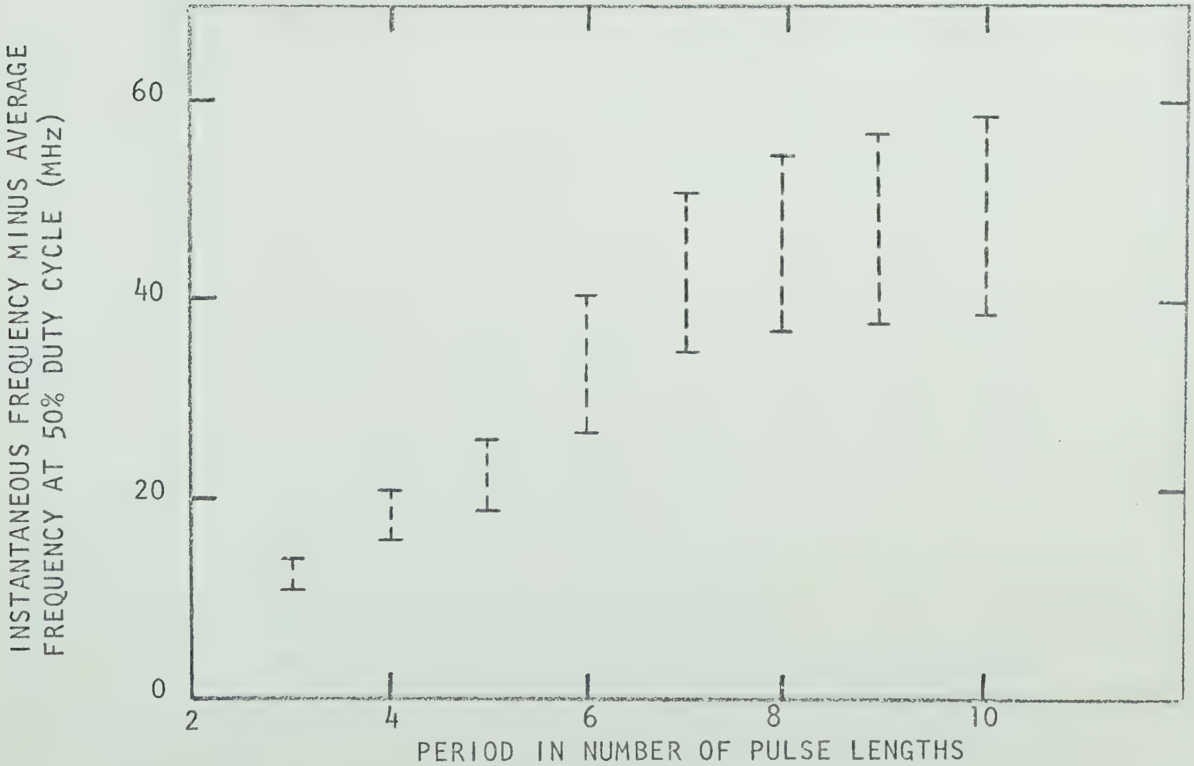

FIG. 5.3.b FREQUENCIES PRESENT DURING A 100 NSEC PULSE AS A FUNCTION OF PULSE PERIOD (i.e., 100 nsec ON time)

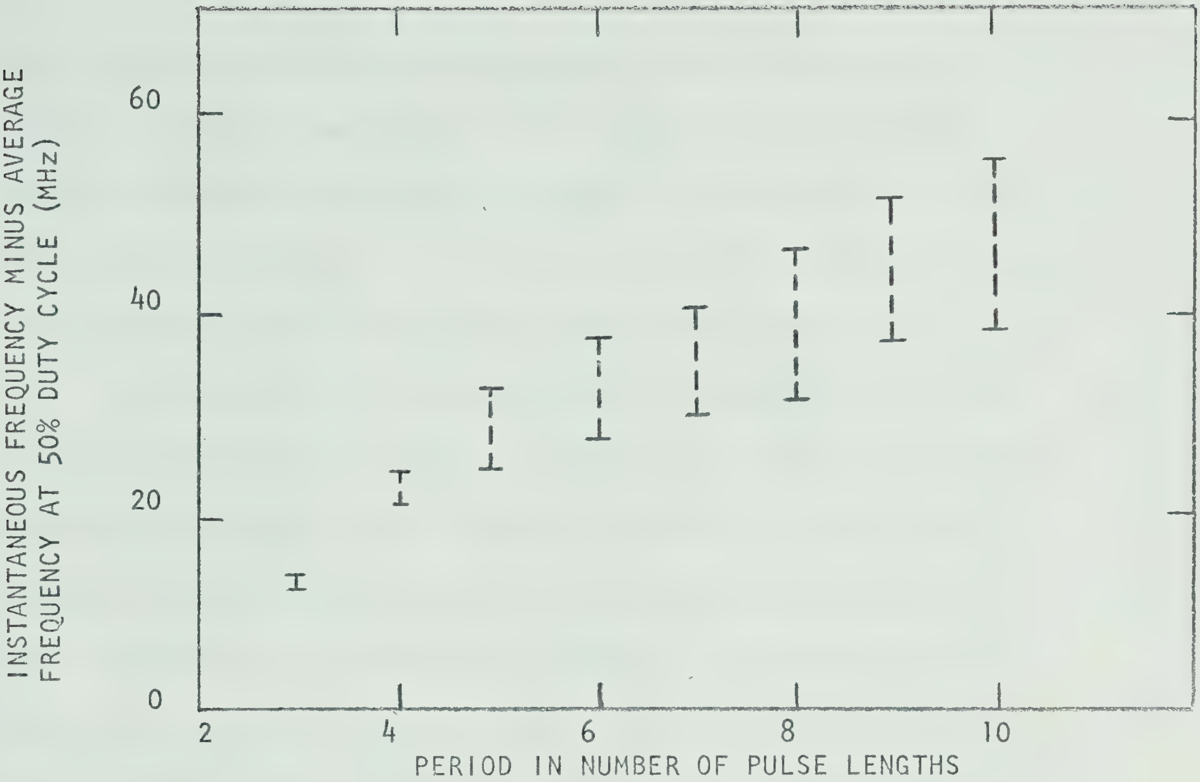

FIG. 5.3.c FREQUENCIES PRESENT DURING A 150 NSEC PULSE AS A FUNCTION OF PULSE PERIOD (i.e. 150 nsec ON time)

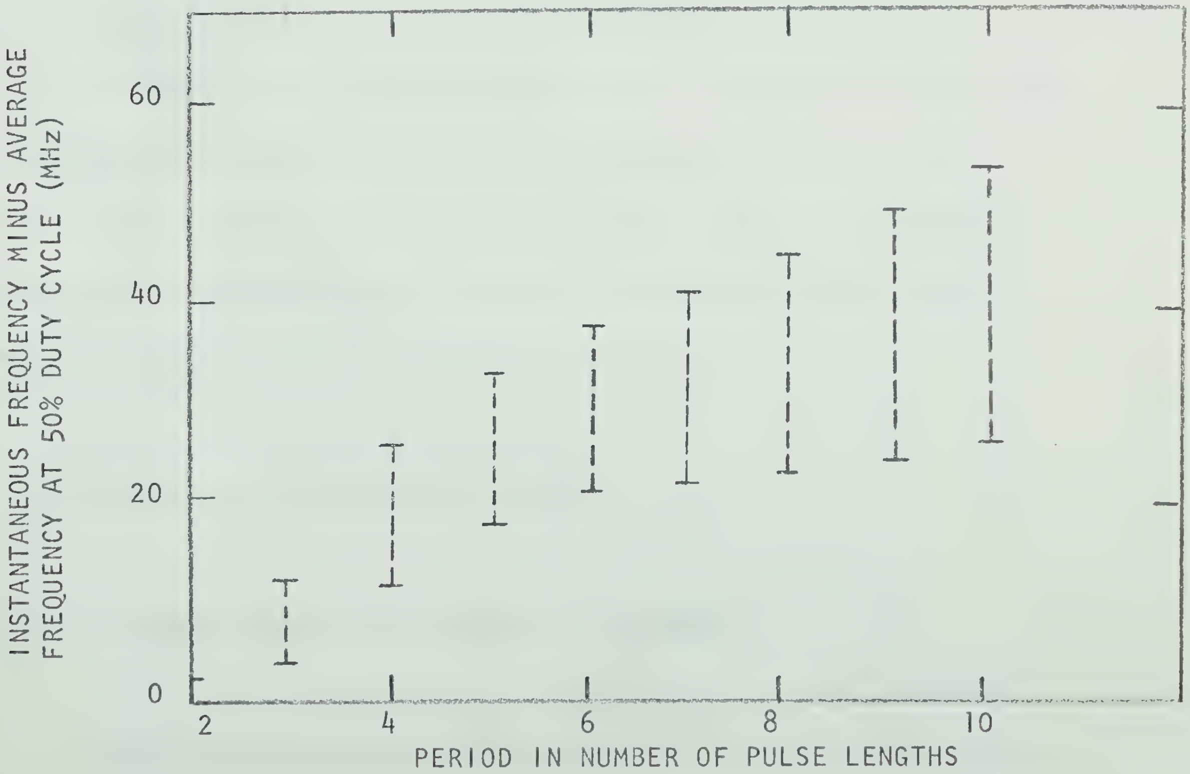

FIG. 5.3.d FREQUENCIES PRESENT DURING A 200 NSEC PULSE AS A FUNCTION OF PULSE PERIOD (i.e. 200 nsec ON time)

pulse increases as the period increases (for a given pulse length). It is also noted that the average frequency of the pulsed oscillator depends quite strongly on the length of the OFF period. In fact, for a 100 nsec pulse, the average frequency varies by 50 MHz over a duty cycle range from 10 to 50%.

The change of the average carrier frequency from pulse to pulse (in a realistic digital signal) is a drawback of bias-modulated ASK systems. This frequency change is illustrated in Figure 5.4. The top trace shows a realistic sequence of pulses without any injection; the sequence corresesponds to 0010111 for Bell's T-3 system. With injection, the last pulse shows no beat frequency while the other pulses show varying beat frequencies for various pulses.

Figure 5.3 can be realistically interpreted as being the worst case. For a practical PCM signal, the diode temperature variations would not be as extreme as indicated by the graphs for the low duty-cycle case. For high duty cycles, the graphs indicate more closely the frequency shifts encountered experimentally for a realistic sequence of pulses.

5-3 RF Spectra of Pulsed Oscillators

5-3-1 Frequency Domain Description of Signals

The purpose of the previous section was to indicate the

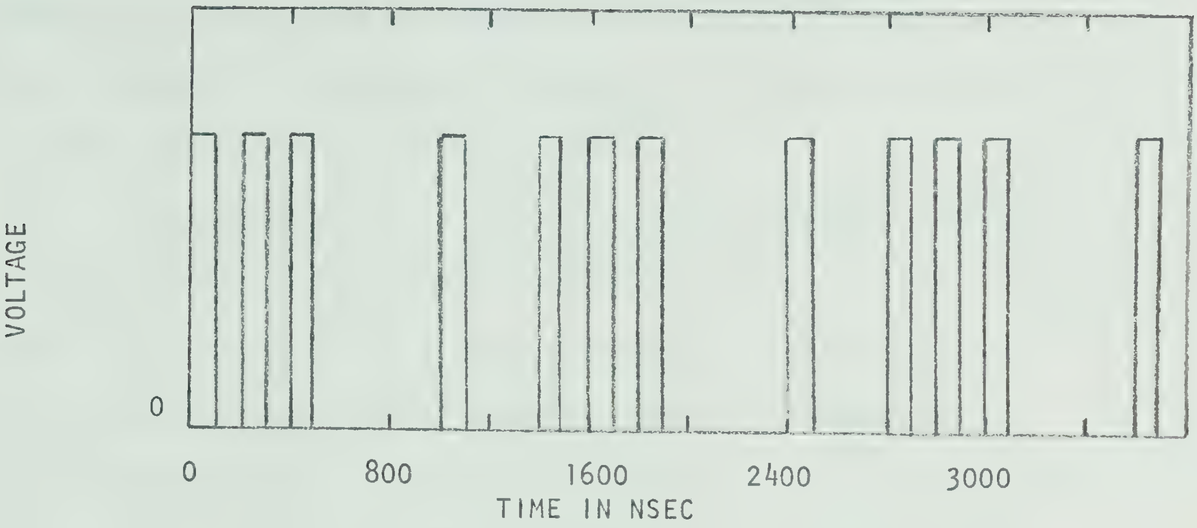

FIG. 5.4a PSEUDO-RANDOM BIT STREAM MODULATING IMPATT OSCILLATOR

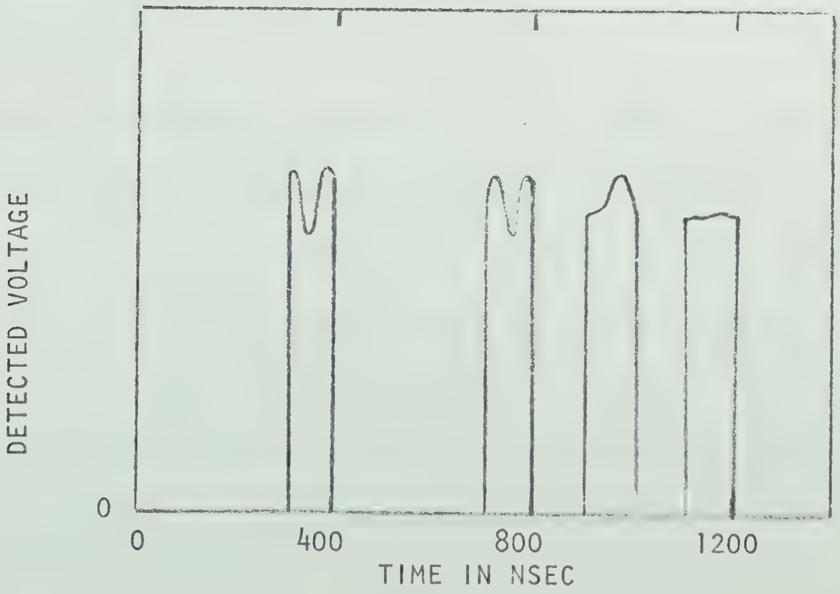

FIG. 5.4.b VARIATION OF AVERAGE FREQUENCY OF IMPATT OSCILLATOR BIAS MODULATED BY PSEUDO-RANDOM BIT STREAM (injected frequency=5.8939 GHz)

extent of frequency pushing present under pulsed conditions. These frequency changes, however, do not indicate the effect they have on the system performance of pulsed IMPATT oscillators. When dealing with communication systems, it is more common to describe signals in the frequency domain.

Spectral analysis is the study of the frequency-domain description of signals; mathematically, it is based on the Fourier Series and on the Fourier Transform. A periodic signal can be expressed as a sum of those frequency components which are harmonically related to the fundamental frequency of that signal. It is possible to show[22] that the Fourier Series for periodic waveforms may be extended to the Fourier Transform for non-periodic waveforms. The Fourier Transform of a signal, x(t), is given by:

$$X(f) = \int_{-\infty}^{\infty} x(t)\, e^{-j\omega t}\, dt \tag{5.1}$$

Because the Fourier Transform is an extension of the Fourier Series, the envelope of the spectrum of a signal which recurs periodically is identical to the envelope of that signal which occurs only once. For this reason, and rather than constraining the discussion to a particular periodicity, only Fourier Transforms of signals will be considered in the rest of this thesis.

The energy density in the frequency domain is equal to the

square of the magnitude of the Fourier Transform. Therefore, the amount of energy in a frequency band, f_1 to f_2, is given by:

$$E\Big|_{f_1 \text{ to } f_2} = \int_{f_1}^{f_2} |\, X(f) \,|^2 \, df \tag{5.2}$$

Using the above equation, the amount of energy in the bandwidth of a signal can be calculated.

Symmetry in the frequency domain is a property of all baseband signals. It is also a property of all signals that are multiplied by a constant-frequency carrier (i.e., the classical Amplitude Modulation case). It will be seen that, under certain conditions, symmetric RF spectra can result from time-varying-frequency carriers. Non-symmetric spectra, however, can arise only when varying frequency carriers are present.

5-3-2 Fourier Transforms of Variable-Frequency Pulses

The output of a pulsed oscillator may be broken up into three linear time portions (i.e., linear in frequency and amplitude): 1. build-up; 2. constant power; and 3. decay. During the transient portions, the frequency changes due to a change in the bias current and due to the inherent change in the amplitude of oscillations. During the constant power portion, the frequency changes due to a decrease of bias current caused by the heating of the diode

junction. For convenience, the model of the RF pulse is given in Figure 5.5. The limited resolution of the frequency measurement technique suggested a linear approximation for the change in frequency.

The pulse shown in Figure 5.5 can be represented mathematically as:

$$x(t) = x_1(t) + x_2(t) + x_3(t) \tag{5.3}$$

where

$x_1(t)$ is the build-up section

$x_2(t)$ is the constant power section

$x_3(t)$ is the decay section

The functional dependence of $x_2(t)$ is now determined such that it has a constant amplitude of unity, has a frequency varying linearly from f_2 to f_3 and exists only from time t_2 to t_3. It can be represented by:

$$x_2(t) = 1 \cdot \cos 2\pi\Phi(t) \tag{5.4}$$

where $\Phi(t)$ is a time-varying phase term

The instantaneous frequency is given by the time derivative of the phase term in equation 5.4 ; it varies linearly from f_2 to f_3 in time $(t_3 - t_2)$. Therefore:

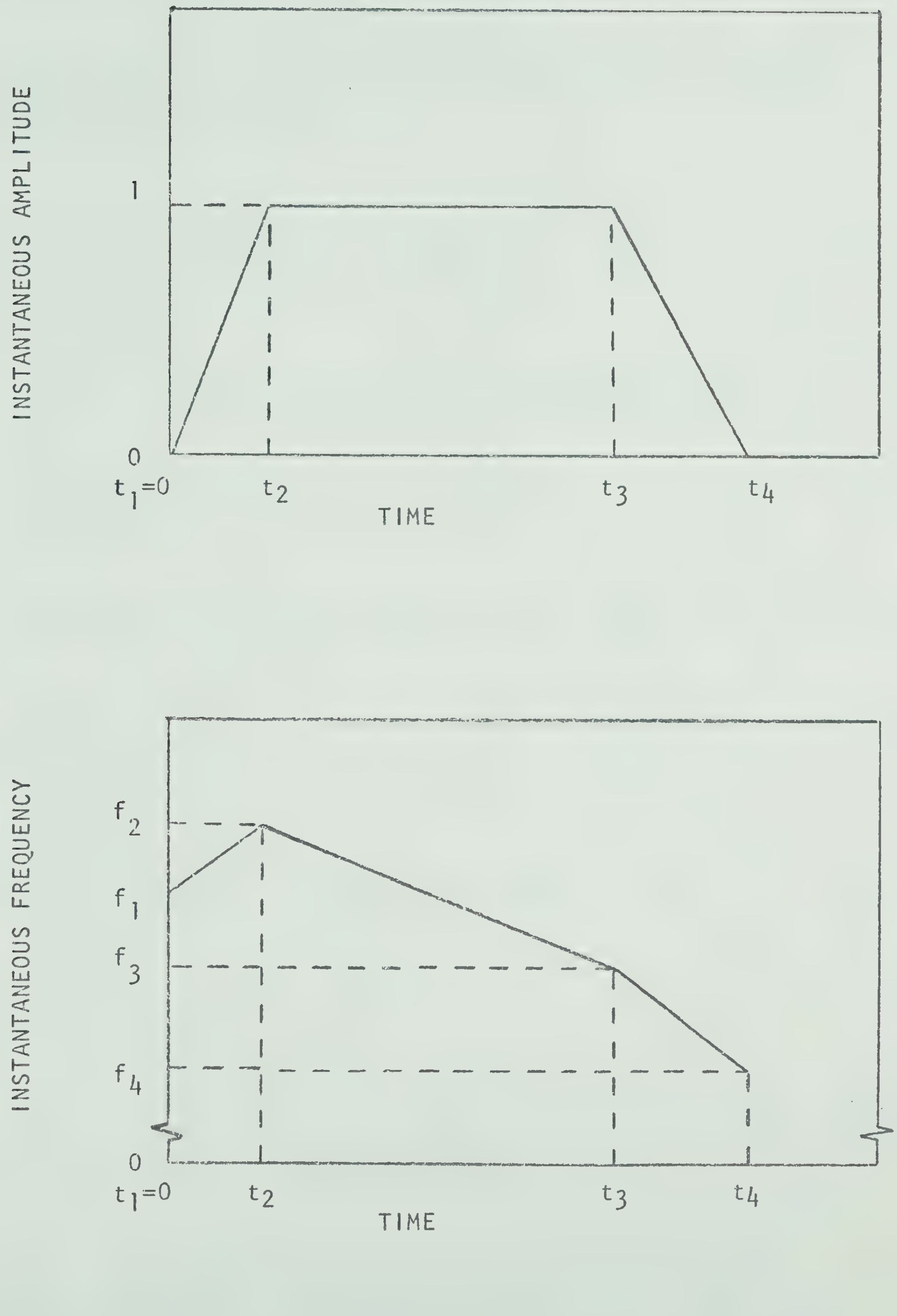

FIG. 5.5 INSTANTANEOUS AMPLITUDE (TOP) AND FREQUENCY (BOTTOM) OF THEORETICAL VARIABLE-FREQUENCY RF PULSE

$$\frac{d\Phi}{dt} = f_2 + \frac{f_3 - f_2}{t_3 - t_2} t \qquad t_2<t<t_3 \tag{5.5}$$

Integrating equation 5.5 , the following expression is obtained for the phase term in equation 5.4 :

$$\Phi(t) = f_2 t + \frac{f_3 - f_2}{2(t_3-t_2)} t^2 + \Theta_2 \tag{5.6}$$

where

Θ_2 is an arbitrary constant phase angle

Finally, $x_2(t)$ can be written as follows:

$$x_2(t) = \cos\{ 2\pi[f_2 + \frac{f_3 - f_2}{t_3 - t_2} \frac{t - t_2}{2}] (t - t_2) + 2\pi\Theta_2 \} \qquad t_2<t<t_3 \tag{5.7}$$

Likewise, $x_1(t)$ and $x_3(t)$ can be expressed as follows:

$$x_1(t) = \frac{1}{t_2} t \cos\{ 2\pi[f_1 + \frac{f_2 - f_1}{2t_2} t] t + 2\pi\theta_1 \} \qquad 0<t<t_2 \tag{5.8}$$

and

$$x_3(t) = \frac{t_4 - t}{t_4 - t_3} \cos\{ 2\pi[f_3 + \frac{f_4 - f_3}{t_4 - t_3} \frac{t - t_3}{2}] (t - t_3) + 2\pi\Theta_3 \} \qquad t_3<t<t_4 \tag{5.9}$$

The constant phase angles are chosen such that the boundary conditions are met (i.e. $x_1(t_2) = x_2(t_2)$ and $x_2(t_3) = x_3(t_3)$).

Arbitrarily setting Θ_1 equal to zero,

$$\Theta_2 = \frac{f_2 + f_1}{2} t_2 \tag{5.10}$$

and

$$\Theta_3 = \frac{f_2 + f_1}{2} t_2 + \frac{f_3 + f_2}{2} (t_3 - t_2) \tag{5.11}$$

It is shown in Appendix C that, for small changes in frequency (i.e. tens of MHz in a carrier of 6 GHz),

$$\int_{-\infty}^{\infty} \cos 2\pi\Phi(t)\, e^{-j\omega t}\, dt = \frac{1}{2} \int_{-\infty}^{\infty} e^{j2\pi[\Phi(t) - ft]}\, dt \tag{5.12}$$

Therefore, the Fourier Transform of x(t) may be written as follows:

$$\begin{aligned} X(f) &= \int_0^{t_2} x_1(t)\, e^{-j\omega t}\, dt + \int_{t_2}^{t_3} x_2(t)\, e^{-j\omega t}\, dt + \int_{t_3}^{t_4} x_3(t)\, e^{-j\omega t} dt \\ &= \int_0^{t_2} \frac{t}{2t_2} \exp j\{2\pi[f_1 + \frac{f_2 - f_1}{2t_2} t]\, t - 2\pi f t\}\, dt \\ &\quad + \int_{t_2}^{t_3} \frac{1}{2} \exp j\{2\pi[f_2 + \frac{f_3 - f_2}{t_3 - t_2} \frac{t - t_2}{2}]\, (t - t_2) + 2\pi\Theta_2 - 2\pi f t\}\, dt \\ &\quad + \int_{t_3}^{t_4} \frac{1}{2} \frac{t_4 - t}{t_4 - t_3} \exp j\{2\pi[f_3 + \frac{f_4 - f_3}{t_4 - t_3} \frac{t - t_3}{2}]\, (t - t_3) \\ &\qquad + 2\pi\Theta_3 - 2\pi f t\}\, dt \end{aligned} \tag{5.13}$$

A computer program that calculates the magnitude of the Fourier Transform given in equation 5.13 is described in Appendix C.

As an illustration of the effect of a variable frequency carrier on the spectrum of a pulse, an idealized square wave is considered. The amplitude of the pulse is taken as unity while the frequency is taken as varying linearly from $f_1 = 6.007$ to $f_2 = 5.993$ GHz during a 100 nsec pulse (Fig. 5.6). The resulting spectra are given in Figure 5.7. The baseband spectrum has a bandwidth of 10 MHz and 92% of the signal energy is in this bandwidth. Due to frequency pushing of the carrier, the signal energy has been redistributed symmetrically in the RF spectrum resulting in only 85.5% of the energy in the 20 MHz bandwidth of the RF signal. In this case and in all of the following cases, the RF spectrum bandwidth is defined as 2 times the baseband bandwidth. It is also noted that the "0" frequency point on the graph corresponds to the center of the main lobe (6.000GHz) for RF spectra and that the graph is normalized to 1.

Next, the baseband and RF spectra corresponding to the frequency measurements given in Figure 5.2 (and repeated in Table 5.2 in terms of the four pivot points of the general pulse of Figure 5.5) are calculated. In Figure 5.8, the computed

TABLE 5.2 EXPERIMENTAL DATA IN TERMS OF PIVOT POINTS OF GENERAL PULSE

CHARACTERISTIC	PIVOT #1	PIVOT #2	PIVOT #3	PIVOT #4
TIME (nsec)	0	10	80	120
AMPLITUDE	0	1	1	0
FREQUENCY (MHz)	5844	5844	5830	5760

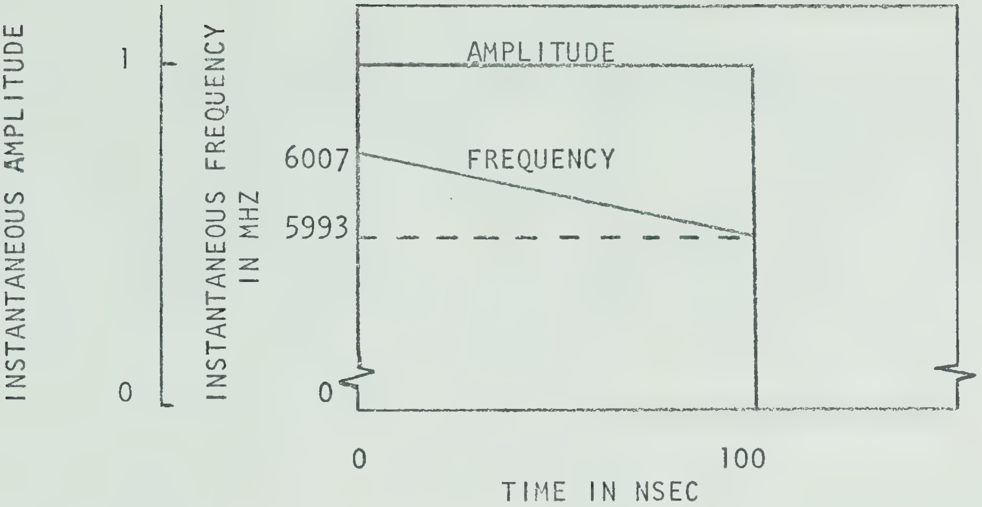

FIG.5.6 INSTANTANEOUS AMPLITUDE AND FREQUENCY OF SQUARE PULSE ILLUSTRATING THE EFFECT OF LINEAR CHANGE IN FREQUENCY

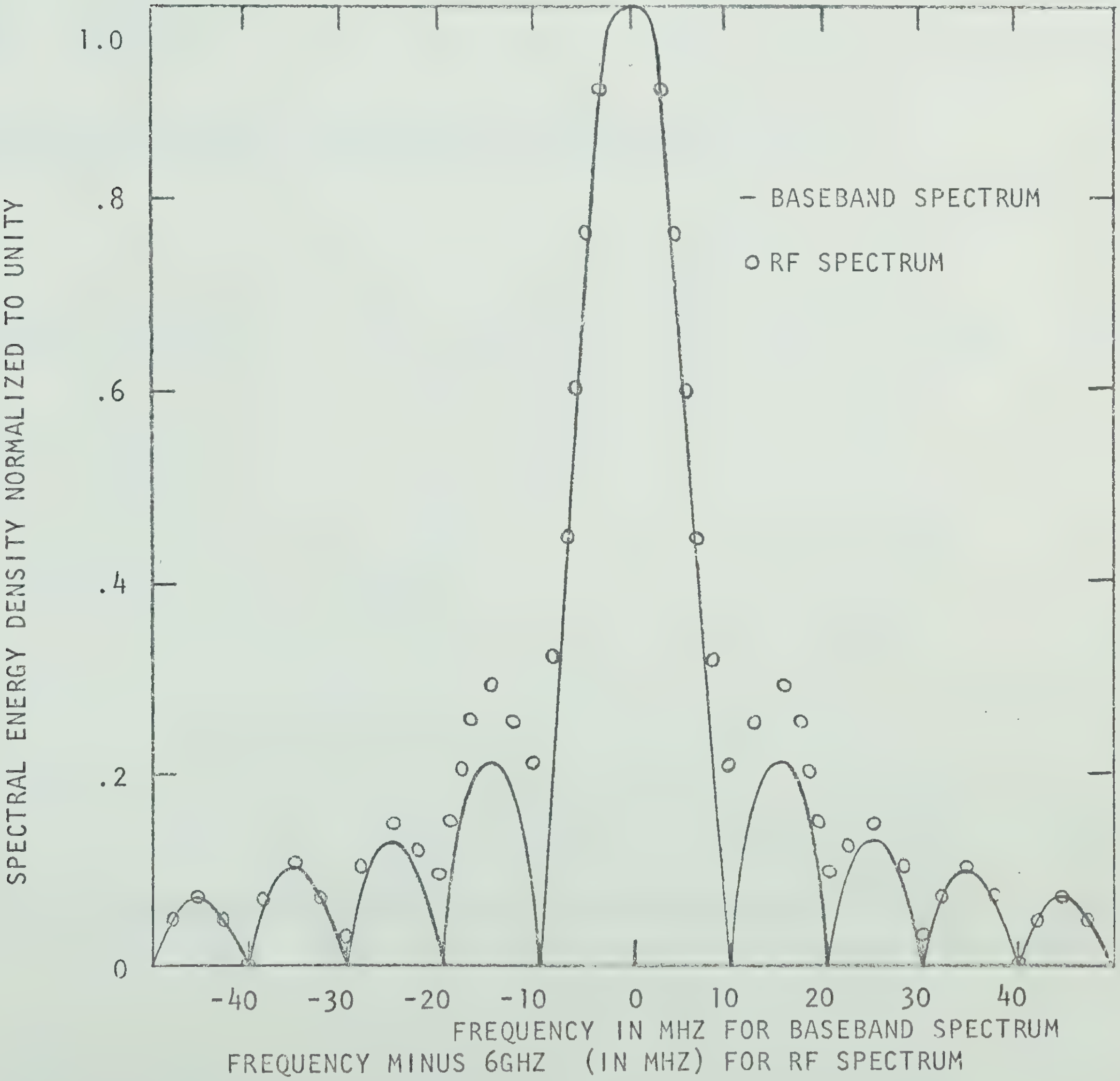

FIG. 5.7 BASEBAND AND RF SPECTRA SQUARE PULSE WITH LINEAR CHANGE IN FREQUENCY (CF. FIG. 5.6)

and measured RF spectra are plotted. In Figure 5.9 , the baseband spectra are compared. The amount of energy in the bandwidth of the baseband signal accounts for 96% of the total signal energy. On the other hand, the RF spectrum is quite non-symmetric, with about 80% of its energy in its bandwidth. As can be seen, there is a redistribution of energy into the frequencies below the center of the main lobe. This extra energy in the lower frequencies would result in considerable power being wasted in adjacent communication bands.

5-4 AM-FM Tradeoff in Bias-Modulated IMPATT Oscillators

The tradeoff between the amount of AM and the amount of frequency pushing has been illustrated in the previous section. In the case of a constant carrier and a square wave envelope, it was found that 92% of the power was in the main lobe of both the RF and the baseband spectra. A pure AM system results. By rounding off the pulse somewhat (10 nsec rise time and 40 nsec decay time), the power in the main lobe of the baseband signal has increased to 96% (i.e. the AM component) while the RF signal (i.e. with FP) has only 80% of its power in its bandwidth. Thus there is a tradeoff between the AM and FP components in the signal. In other words, there is an optimum decay time

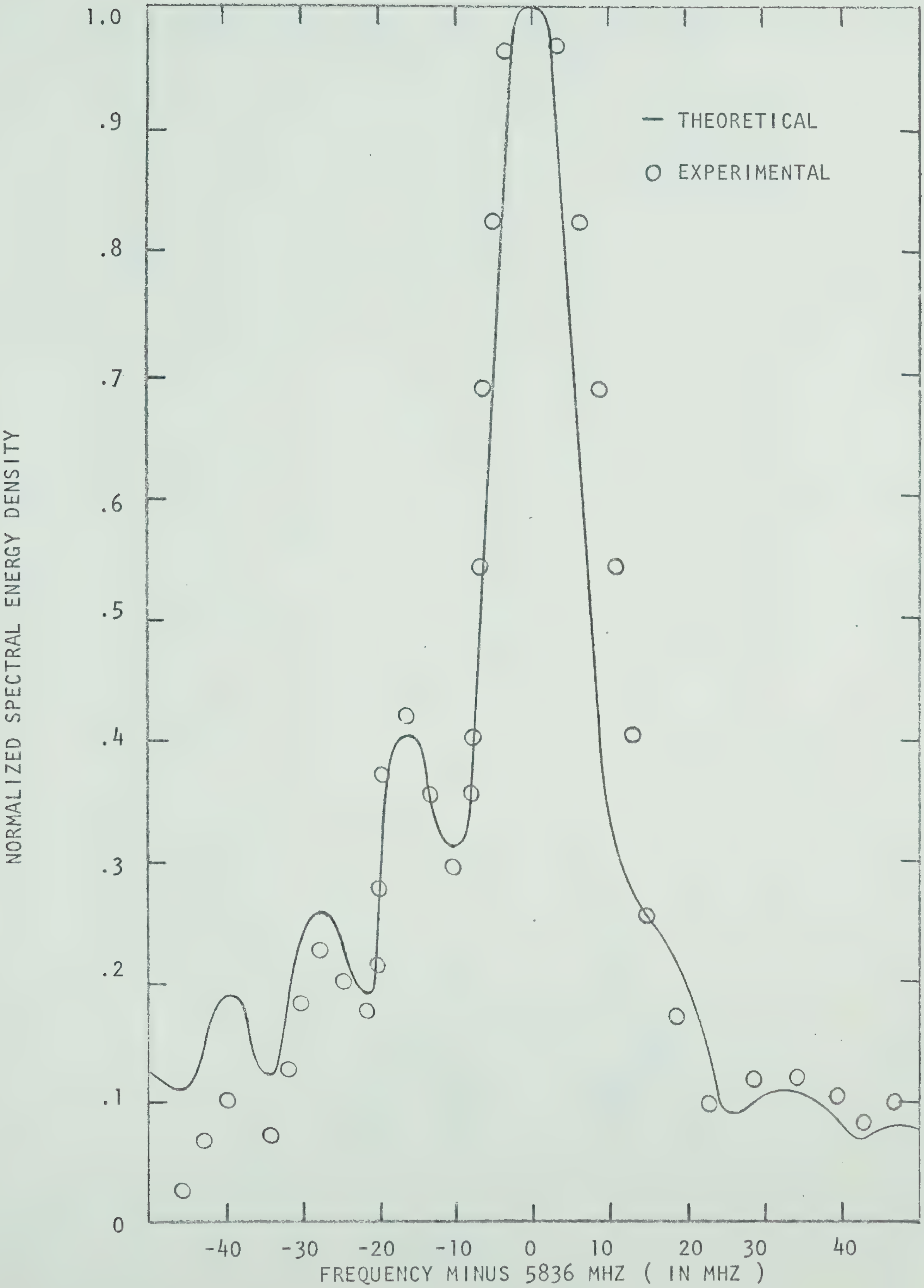

FIG. 5.8 THEORETICAL AND MEASURED RF SPECTRA OF OUTPUT OF BIAS-MODULATED IMPATT OSCILLATOR

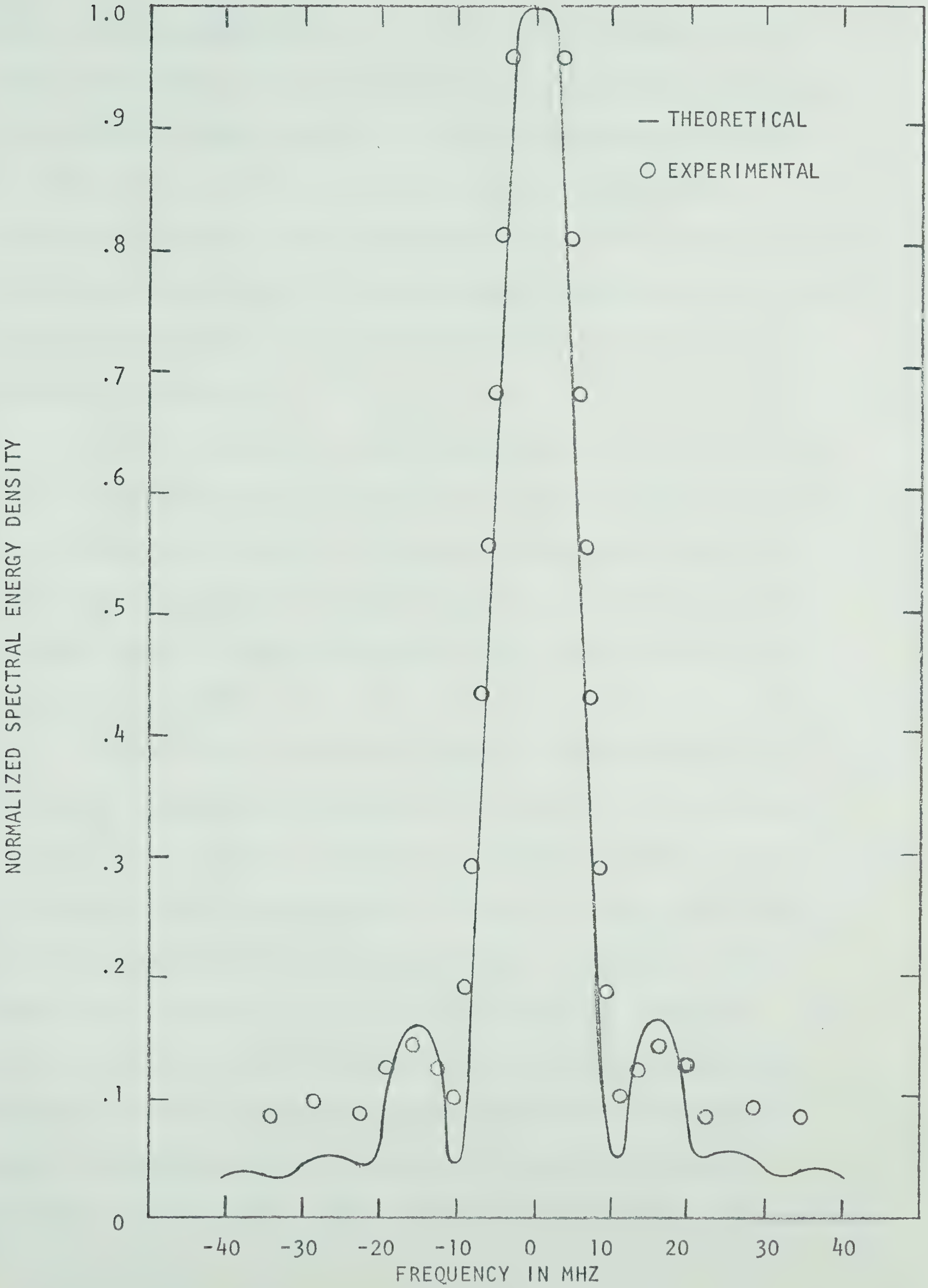

FIG. 5.9 THEORETICAL AND MEASURED BASEBAND SPECTRA OF DETECTED OUTPUT OF BIAS-MODULATED IMPATT OSCILLATOR

which puts the maximum amount of power in the bandwidth of the signal. The build-up time of the RF pulse is not readily controllable since the bias current has reached its maximum value before any substantial power is produced; the build-up is primarily determined by the RF voltage dependence of the electronic conductance. The decay process, however, is controlled by the decay of the diode bias current, as well as by the RF voltage dependence of the electronic conductance.

It will be seen that the optimum decay time is a function of the change of frequency during the main part of the pulse (i.e. the constant power section). As has been seen, this change is a function of the junction temperature, which in turn depends on the pulse width, on the pulse amplitude and on the actual pulse sequence transmitted.

A plot of the percentage of power in the bandwidth of a signal as a function of the decay time of the RF pulse is given in Figure 5.10. The pulse length is approximately 100 nsec and the build-up time of the RF pulse is fixed at 10 nsec. The curve labelled "baseband" shows the upper limit of the power in the bandwidth of a signal due to the envelope of that signal; a shorter decay time results in less power in the main lobe of the baseband spectrum. The family of curves labelled "RF spectra" shows the variation of the percentage of power in the signal bandwidth with decay time, as a function of the frequency change, ΔF,

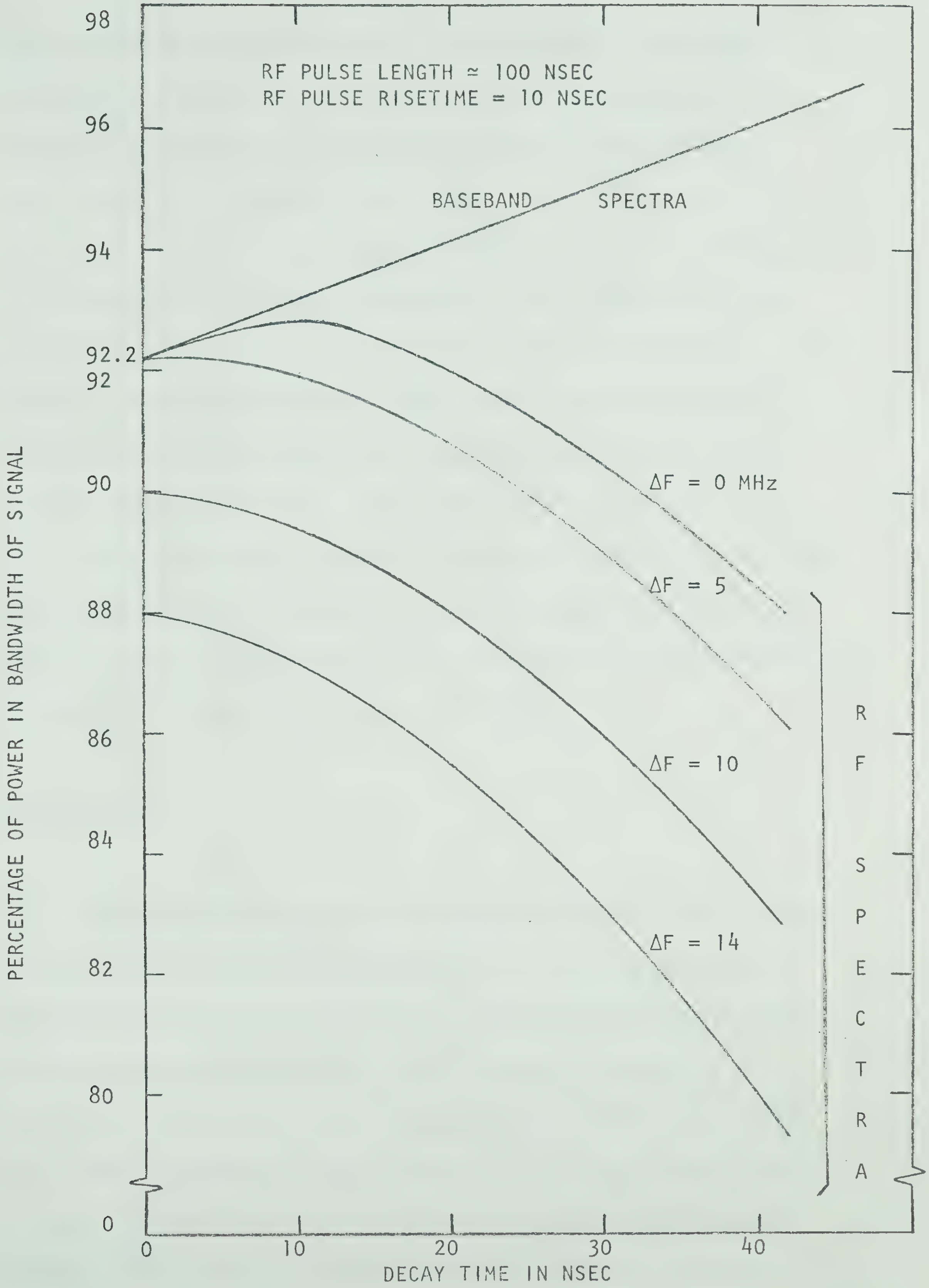

FIG. 5.10 TRADEOFF BETWEEN AM AND FM COMPONENTS IN PULSED AVALANCHE OSCILLATORS

during the main part of the pulse. For ΔF greater than 5 MHz, decreasing the decay time increases the amount of power in the bandwidth of the signal. For these cases, the optimum decay time is zero. For ΔF smaller than 5 MHz, the optimum decay time ranges between 0 and 10 nsec depending on the actual change in frequency; for no frequency pushing, the optimum decay time is 10 nsec. For ΔF less than 5 MHz, the difference between choosing a decay time at the optimum point or at some other point between 0 and 10 nsec is, at most, a one percent change in the percentage of power in the signal bandwidth.

In conclusion, little can be gained by optimizing the decay time in any practical system: the shortest possible decay time should be used. The possibility of locking the carrier by injecting an appropriate signal is discussed in Chapter 6.

5-5 Summary

Frequency pushing in bias-modulated IMPATT oscillators has been discussed. Four different methods of measuring the change of frequency during an RF pulse have been presented. The required resolution was attained using a beat frequency technique. In this way, the accuracy of the frequency measurement was increased by at least two orders of magnitude over the other three methods. A change of frequency of up to 25 MHz was measured during the constant power section of the RF pulse. In addition,a 70 MHz

change was observed during the decay transient; frequency pushing during the build-up transient had a negligible effect on the RF spectra, because of the low RF power level during the build-up of the current pulse.

A computer program was developed to Fourier Transform an arbitrary variable-frequency pulse. The AM - FM tradeoff in bias-modulated IMPATT oscillators has been discussed. It was found that the decay time, which maximizes the amount of power in the signal bandwidth, is a function of the frequency change during the main portion of the pulse. However, little is gained by optimizing the decay time and the shortest practical decay time should be used.

CHAPTER VI

INJECTION OF PULSED IMPATT OSCILLATORS

6-1 Introduction

It is a common practice in communication systems to stabilize an oscillator by phase locking it to a stable low-power cw signal. Locking theory was first explained adequately by Adler[23] in his paper published in 1946. His work was confined to cw operation, though, as will be seen, it has applications in "pulsed operation". Taking into account the discussion of the previous chapter, "pulsed operation" refers to a pulsed oscillator with a significant amount of undesired frequency modulation.

In Section 6-2, the frequency-domain effects of injection of a cw signal into a "pulsed" avalanche diode oscillator are considered. It will be seen that the rate of change of the frequency is an important factor in injection locking of "pulsed" oscillators: as the rate of change of frequency increases, progressively more power is required for frequency locking. In fact, the minimum injected power required for frequency locking of a "pulsed" oscillator is a non-linear function of the average rate of change of frequency. This section concludes with a discussion of the effects of low-power injection on the coherence of successive pulses.

In section 6.3, the time-domain effects of injection are considered. It will be seen that there is a minimum injected power level above which the leading-edge jitter of the pulse is reduced. As the injected power is increased, the amount of time required for the RF oscillations to build up to their final value is decreased.

6-2 Frequency-Domain Effects of Injection

The locking bandwidth describes over what range the main oscillator will follow the frequency of an injected signal. Under steady-state conditions, Adler's equation relates the half locking bandwidth to the injected-to-output power ratio and to the parameters of the circuit; that is[23]:

$$BW = \frac{f_o}{Q_L}\sqrt{\frac{P_{INJ}}{P_O}} \tag{6.1}$$

where

P_{INJ}/P_O is the injected-to-output power ratio

f_o is the free-running oscillator frequency

Q_L is the loaded Q of the circuit

BW is the locking bandwidth

Equation 6.1 is illustrated in Figure 6.1 for $Q_L = 52.9$ and for a center frequency of 5.8634 GHz; the slope of the line is 20 dB

per decade.

An experiment was conducted to study the injection-locking properties of "pulsed" IMPATT oscillators. In order to reduce the effects of the transient sections of the RF pulse, a 500 nsec pulse was chosen. The change of frequency during the main part of the pulse was varied by increasing or decreasing the OFF time between pulses (cf. Fig. 5.3). The instantaneous frequency during the pulse was measured using the beat frequency technique described in Chapter 5. The limited resolution of this method forced a linearity assumption for the frequency as a function of time during the duration of the pulse. Therefore, the average rate of change of frequency, $\Delta F/\Delta t$, was calculated by dividing the total frequency change by the length of the pulse.

The results of measuring the locking bandwidth as a function of the injected-to-output power ratio for various values of average rate of change of frequency are presented graphically in Figure 6.1. The locking bandwidth is the frequency variation of the injected signal over which a zero beat frequency appears during the pulse. Figure 6.2 illustrates the effects of reducing the injected power on the amount of frequency locking. In the top curve, the frequency of the pulsed oscillator is completely locked to the frequency of the injected signal. As the injected power is decreased, the extent of frequency locking is progressively decreased, until no substantial locking occurs,

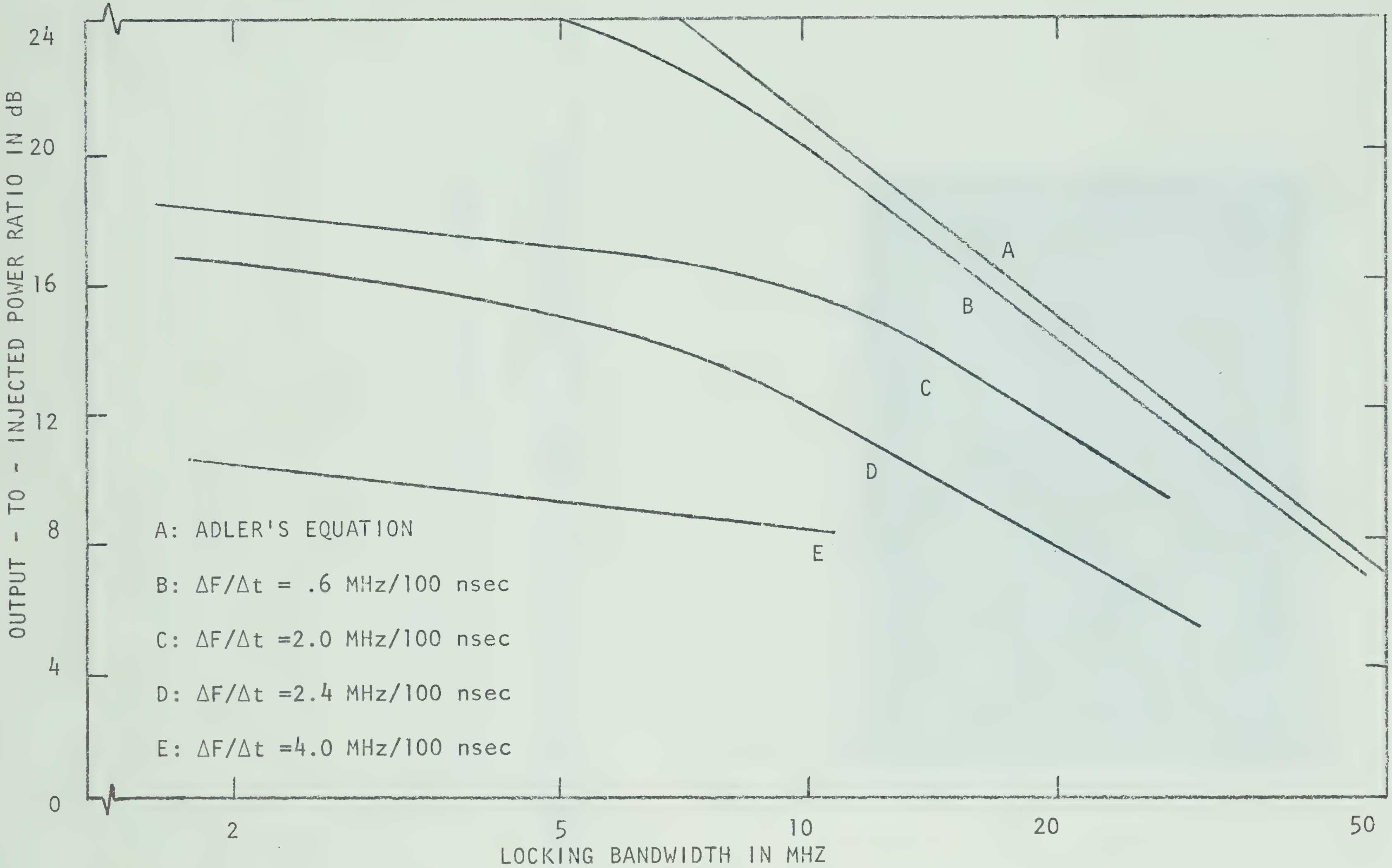

FIG. 6.1 INJECTION-LOCKING CHARACTERISTICS OF BIAS-MODULATED OSCILLATORS

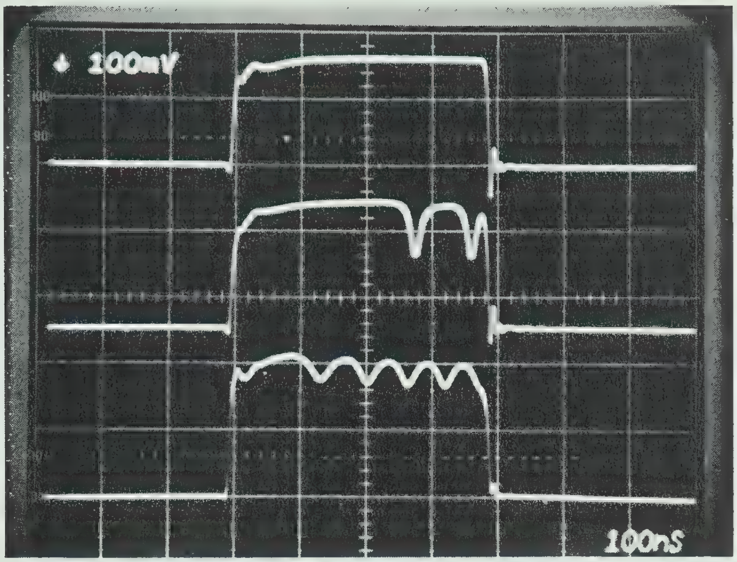

FIG. 6.2 EFFECTS OF DECREASING OUTPUT-TO-INJECTED POWER RATIO ON THE AMOUNT OF FREQUENCY LOCKING IN A PULSED IMPATT DIODE OSCILLATOR.

output-to-injected power ratio: top: 9.0 dB
middle: 11.5 dB
bottom: 17.5 dB

as is shown in the bottom curve.

For an average rate of change of frequency of .6 MHz per 100 nsec, approximately .4 dB more power is required for a given locking bandwidth than for Adler's steady-state case. In agreement with the work of Udelson and Hines[24], the results for small average rates of change of frequency strongly resemble those predicted by Adler (i.e., they exhibit 20 dB per decade slopes and comparable intercepts). However, as the rate of frequency change increases, a non-linearity appears in the injection-locking curves. In addition, the slope of the linear section becomes progressively less similar to that predicted by Adler's injection theory. These deviations from steady-state injection theory are largely due to the actual frequencies present in the output of a pulsed oscillator. For example, assuming a 3 MHz change in frequency during a very long pulse (i.e., a small rate of change of frequency), a 10 MHz locking bandwidth implies an effective locking bandwidth of 13 MHz. As the rate of change of frequency increases, it has a larger effect on the injection-locking characteristic of a pulsed IMPATT oscillator. In fact, the minimum amount of injected power required for frequency locking is a non-linear function of the rate of change of frequency. An experimentally obtained plot of the minimum injected-to-output power ratio required for frequency locking, as a function of the average rate of change of frequency, is shown in Figure 6.3.

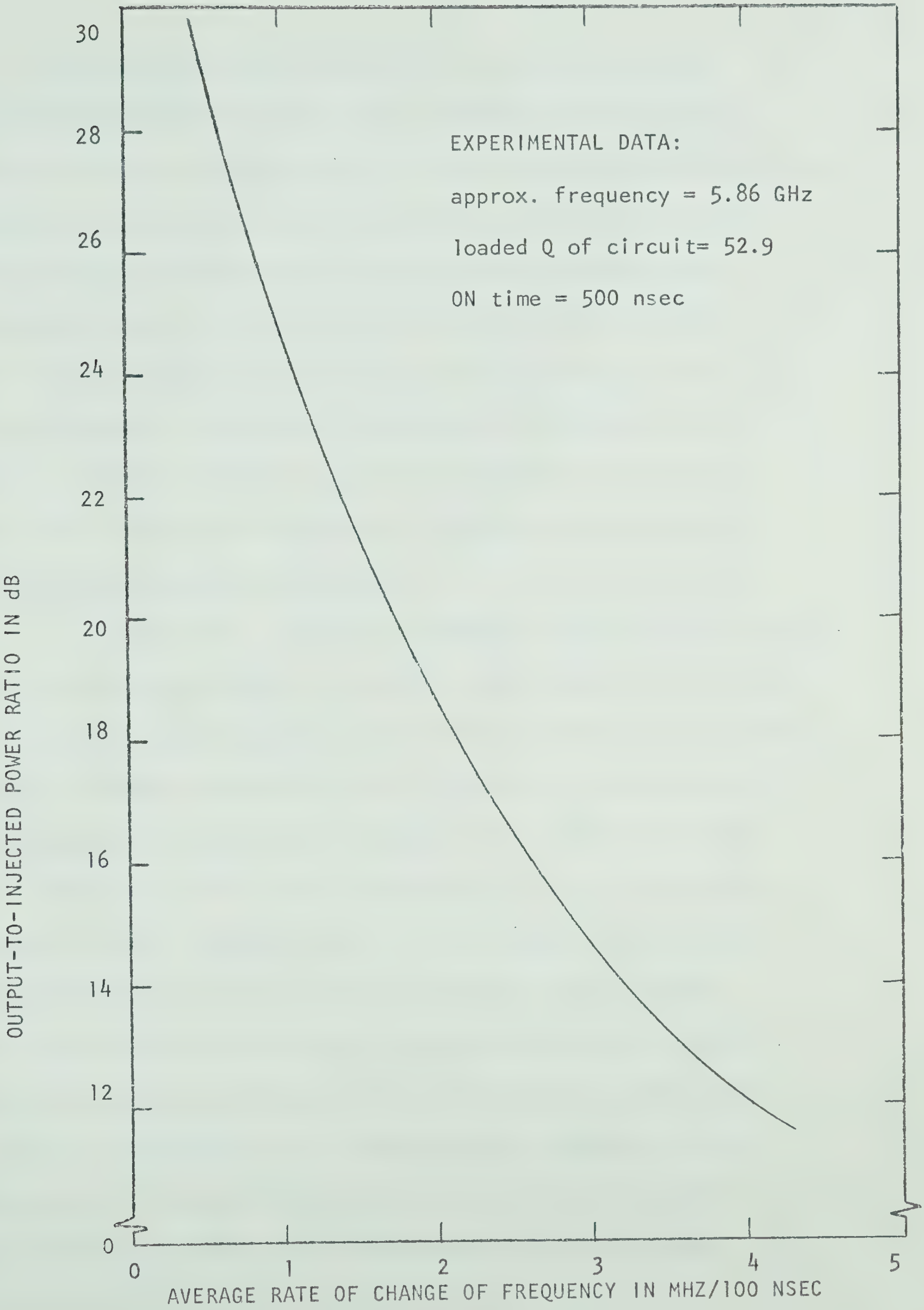

FIG. 6.3 VARIATION OF MINIMUM OUTPUT-TO-INJECTED POWER RATIO REQUIRED FOR FREQUENCY LOCKING AS A FUNCTION OF AVERAGE RATE OF CHANGE OF FREQUENCY

As has been noted in Section 5-2, the frequency of the 100 nsec pulse (10% duty cycle) changed by 14 MHz during the main part of the pulse and by 70 MHz during the transients.High relative injected powers are required to lock the frequency during the main part of such a pulse. Stabilization of the frequency during the entire pulse (including transients) is virtually impossible (cf. Fig. 6.3) since the rate of change of the frequency during the transients is in the order of a couple of hundred MHz/100 nsec. Any discussion of locking during the transients is complicated by the fact that both the amplitude and frequency are varying.

In section 2-1, a coherent display of the RF oscillations was obtained by injecting a low power signal into the main oscillator and by triggering the applied voltage pulse by the injected signal (through a countdown unit). In this way, the pulse, RF oscillations and the injected signal are all related in phase. Thus, there is pulse-to-pulse coherence as long as the injected signal is above a certain level. At this level, the oscillator momentarily locks onto the injected signal. Because of the high rate of change of frequency, as soon as the oscillations start, the locked condition is lost. Nevertheless, phase coherence has been established. For this case, the injected power is just above the preoscillation noise level and so, just when the oscillations start, the injected and oscillator powers

are equal. Locking is immediately lost due to the combined effects of the change in frequency and of the increase in amplitude. The minimum injected power required for phase coherence is not a function of the peak power of the oscillator. An experimentally obtained plot of the minimum injected power as a function of the difference between the injected frequency and the free-running frequency of the pulsed oscillator is shown in Figure 6.4. Therefore, the preoscillation noise level of the oscillator tested is approximately -34 dBm.

As the injected power is increased above the noise level, a progressively greater time portion of the RF pulse is locked to the frequency of the injected signal. As has been seen, a significant amount of locking occurs only for very high relative injected powers.

6-3 Time-Domain Effects of Injection

As was pointed out in Section 6-2, pulse-to-pulse coherence can be obtained by injecting a signal greater in power than the preoscillation noise level (i.e., the mean value of the noise power before oscillations start). In this case, instantaneous frequency locking occurs at the beginning of each pulse. Injecting such a signal also has effects in the time domain: namely, reduction of the leading-edge jitter of the RF pulse and of the time required for the RF oscillations to build-up to their steady-state value. Without injection, the build-up of oscillations starts at the pre-

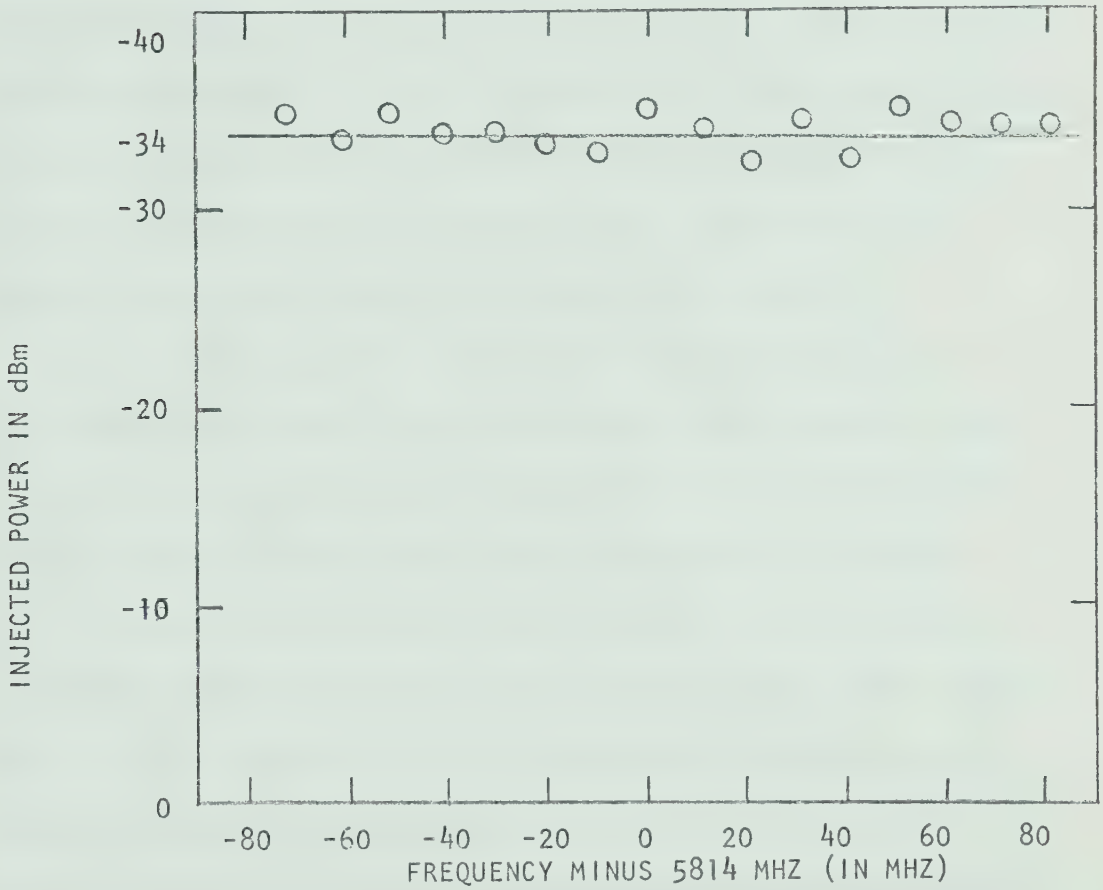

FIG. 6.4 MINIMUM INJECTED POWER REQUIRED FOR PHASE COHERENCE AS A FUNCTION OF FREQUENCY

oscillation noise level. As the amplitude of the noise is a random process with a certain mean and variance, each RF pulse starts at a slightly different amplitude introducing jitter into the leading edge of the pulse. By injecting a signal of power greater than the preoscillation noise level, the randomness of the starting amplitude is largely eliminated. Consequently, the leading-edge jitter of the pulse is greatly reduced. This time-domain effect is to be distinguished from pulse-to-pulse coherence which is a frequency-domain effect, wherein, phase coherence exists between the RF oscillations from one pulse to another.

By increasing the level of the injected signal, the RF amplitude at the onset of oscillations is also increased. Consequently, the amount of time required for the RF oscillations to reach their steady-state value is decreased. The amount of this decrease as a function of the injected power was evaluated as follows. The IMPATT diode was arbitrarily biased above breakdown, but not necessarily at the oscillation-threshold level. Without injection, the RF power had reached 10% of its final value in 20 nsec, as measured from the 10% point on the current pulse. As the injected power was increased, this delay between the power and current pulses decreased. A plot of the measured delay as a function of the injected power (in dB above the noise level) is shown in Figure 6.5. Results are shown for three different injection frequencies, covering a range of 50 MHz on both sides of the average frequency of the pulsed oscillator. Figure 6.5

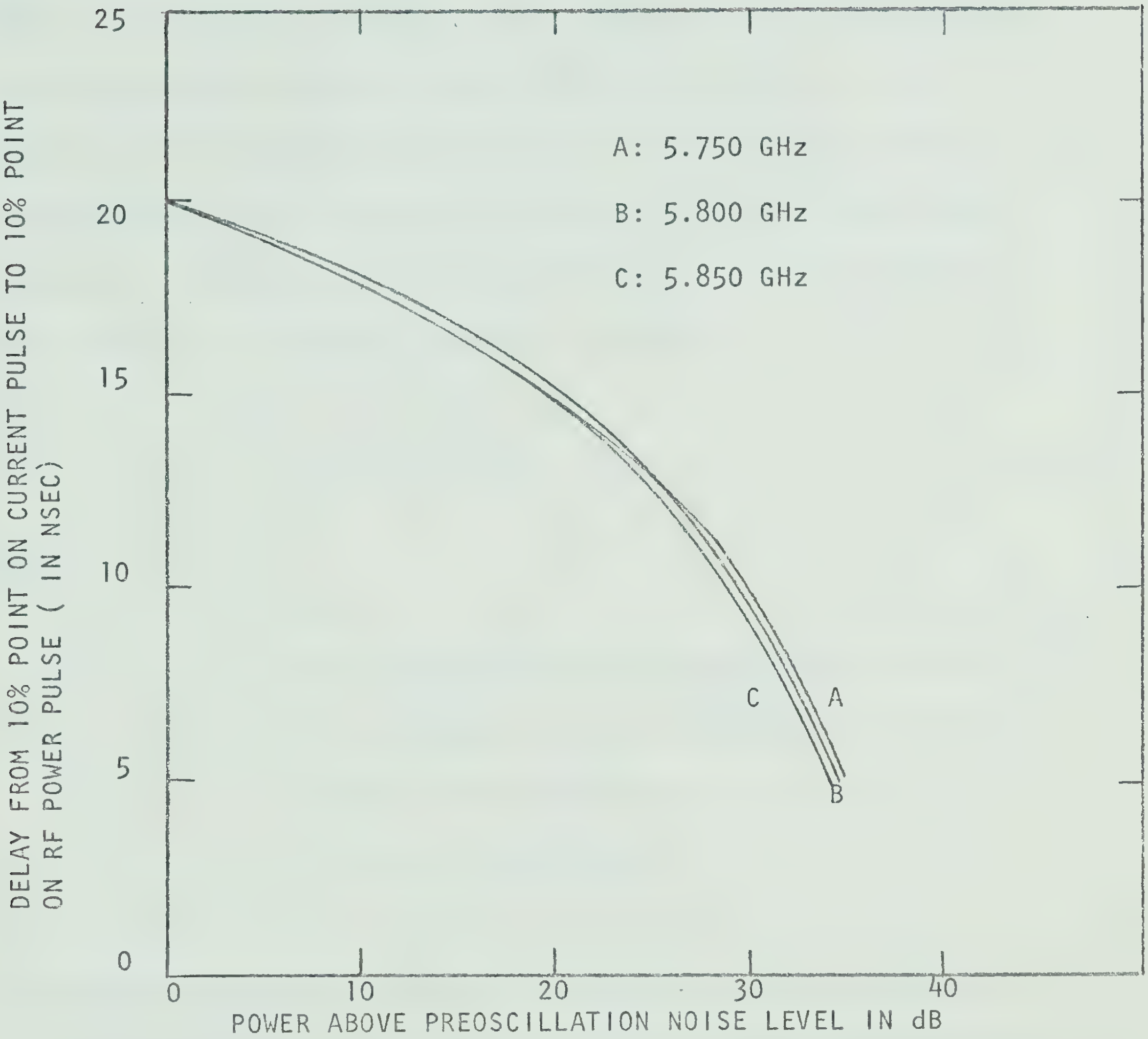

FIG. 6.5 DELAY IN BUILD-UP OF RF POWER AS A FUNCTION OF INJECTED POWER

shows that, for low injected powers, the delay varied almost linearly with the power in dB. From the curve relating the amount of delay as a function of the injected power, information can be obtained on the build up of RF oscillations: in the absence of an injected signal, the oscillations start at the preoscillation noise level; after 5 nsec, the power level has increased by 20 dB and so on. From Chapter 4, for low voltages, the voltage as a function of time is given by:

$$V = V_o e^{\alpha(I)t} \tag{6.2}$$

where

V_o is the initial voltage of some section in which α may be considered constant

$\alpha(I)$ is the growth factor

I is the bias current

If the bias current is constant, the growth factor is constant as well,resulting in a linear function of the delay as a function of power in dB. However, the bias current is changing during part of the build-up and so a non-linear curve is to be expected. The main result is that injection can be used to significantly reduce the time required for the RF oscillations to build up from the noise level to their steady-state value.

6-4 Summary

The injection properties of pulsed avalanche oscillators have been discussed. It has been found that pulse-to-pulse coherence and reduction of leading-edge jitter can be attained by injecting a signal greater in power than the preoscillation noise level. Increasing the injected power above the noise level can substantially decrease the build-up time of the RF oscillations. Therefore, injecting a low power signal (e.g. 20 dB below the main oscillator power) into a pulsed oscillator can greatly improve the performance of an ASK system.

In Chapter 5, it was found that a large amount of frequency pushing is present in a pulsed avalanche diode oscillator. At that time, it was suggested that frequency locking might prove useful in reducing the amount of undesired frequency modulation in the output of a pulsed avalanche oscillator. Further investigation has shown that excessively high powers are required to lock the frequency during the entire RF pulse. It has also been found that the rate of change of frequency is an important parameter in the injection locking properties of pulsed IMPATT oscillators.

CHAPTER VII

SUMMARY AND CONCLUSION

A systematic study of the properties of bias modulation of IMPATT diode oscillators has been carried out. The results obtained indicate that bias-modulated avalanche diode oscillators can be used as a practical means of Amplitude Shift Keying a binary signal. In theory, such a modulation scheme exhibits error performance comparable to, or better than, most other modulation systems. There are also definite cost advantages in using bias-modulated oscillators, due to simpler hardware requirements. The following conclusions can be drawn from the study of bias-modulated avalanche oscillators:

1. From an analysis of the experimental bias circuit, the minimum rise- and decay times of the bias current can be calculated. Thus, the minimum pulse length, that the bias circuit used in this work can handle, has been established at 25 nsec; this specifies the maximum bit rate for the experimental bias circuit.This rate can be increased by further eliminating the parasitics in the bias circuit.

2. From an analysis of the RF circuit, the effects of the external circuit on the performance of a bias-modulated oscillator can be evaluated. It was found that the minimum rise- and

decay times of the RF oscillations can be obtained by maximizing the loaded Q of the circuit. Thus, the minimum pulse length that the experimental RF circuit can handle has been found to be 7.8 nsec.

3. The static temperature characteristics of avalanche diodes can be determined experimentally. It was found that, due to the temperature dependence of the diode breakdown voltage, the DC bias current varies with time. As a result, the bias level should be chosen so that the bias current never exceeds the oscillation threshold level during an OFF pulse.

4. The major effect of the change in the bias current, because of the heating and cooling of the diode, was found to be due to the current dependence of the diode electronic susceptance. As the susceptance changes, frequency pushing of the bias-modulated oscillator occurs. Two related effects were observed: (a). because of the diode-temperature variations, the average frequency of oscillation was noted to vary by as much as 65 MHz from one pulse to another; (b). the frequency during the main portion of an RF pulse was also noted to change by as much as 20 MHz for a 100 nsec pulse. In addition, during the rise- and decay times of the applied current pulse, the frequency changed

by as much as 100 MHz during this transient period. This latter effect did not vary appreciably from pulse to pulse.

5. The RF spectra of pulsed oscillators were found to be somewhat "puffed up" and non-symmetrical. Consequently, because of the variation of frequency during the RF pulse, the power has been noted to be redistributed in the RF spectrum. In fact, as little as 80% of the total power was measured in the bandwidth of the RF signal, compared to over 95% of the total power in the bandwidth of the baseband signal. As a result, a large portion of the signal power is lost from the bandwidth of the signal.

6. The tradeoff between the AM and FM components present at the output of the pulsed oscillator was investigated. The existence of a tradeoff arises from the fact that short rise- and decay times minimize the effect of the FM components, but, on the other hand, reduce the amount of power in the bandwidth of the baseband signal. It was found that, in most cases considered, the FM components override the AM components, and hence the shortest transients are most desirable.

7. In order to reduce or even eliminate the undesired FM components in the output of bias-modulated avalanche diode

oscillators, a thorough study of the possibilities of injection locking pulse IMPATT oscillators was conducted. It was found that the amount of power required for locking the majority of the RF pulse is a non-linear function of the rate of change of frequency with time. Relatively high locking powers are required to lock the frequency of the entire RF pulse, including transients, because of the very high rates of change of frequency during the transient times. Injection at reasonable levels is only useful for locking pulse oscillators with slow rates of frequency change. Therefore, injection locking is of limited use in substantially reducing FM noise in the output of bias-modulated IMPATT oscillators.

8. Injection of a low power signal (i.e. greater in power than the preoscillation noise level) does have beneficial effects on the system performance of a bias-modulated oscillator. Such an injection results in phase-to-phase coherence between pulses and largely eliminates leading-edge jitter in the RF pulse. It was found that increasing the level of the injected signal leads to a faster build-up of oscillation.

The variation of the diode temperature limits the usefulness of the bias-modulation concept. Injection locking is limited in its use in substantial reduction of frequency

pushing in the output of pulsed avalanche oscillators. Pulse shaping techniques can further reduce the effects of frequency pushing. A controlled variation in the junction temperature is seen to be a possible improvement in the problem.

Figure 7.1 shows a schematic of a possible system incorporating pulse shaping and injection locking. An IMPATT oscillator is pulsed continuously at the system bit rate. The PIN Line Modulator is synchronously modulated by the binary PCM baseband signal. In this way, the temperature of the diode is kept within a fixed known limit. Biasing is no problem for periodically pulsed oscillators. Frequency deviations are kept to a minimum by the small variations in the junction temperature, as well as by the injected signal. Frequency pushing can be minimized by proper pulse shaping. The injected signal also results in pulse-to-pulse coherence, minimal leading-edge jitter and faster build-up times. The error performance of such a system must be thoroughly evaluated both theoretically and experimentally. The research work reported in this thesis should facilitate any further exploratory work into ASK systems.

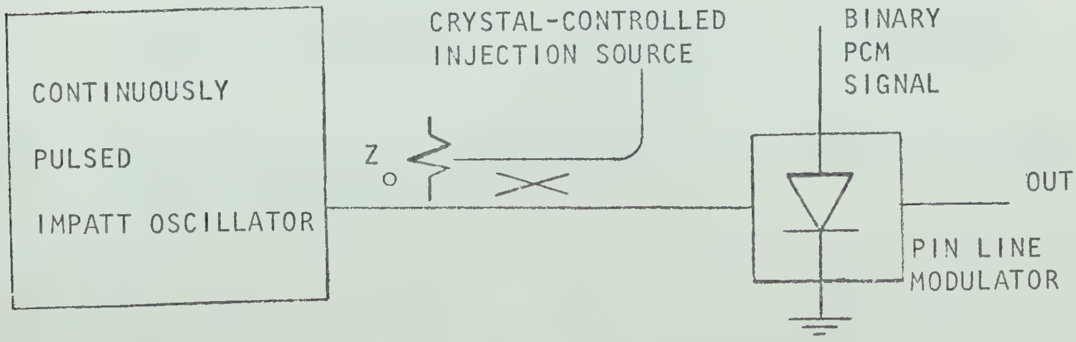

FIG. 7.1 PROPOSED BIAS-MODULATED OSCILLATOR WITH PIN LINE MODULATOR

REFERENCES

1. A.B. Carlson, Communication Systems: An Introduction to Signals and Noise in Electrical Communication, New York, McGraw-Hill, 1968, pp.379-394.

2. B. Glance, " Power Spectra of Multilevel Digital Phase Modulated Signals", Bell System Tech. J., vol. 50, November 1971, pp.2857-2878.

3. A.B. Carlson, Communication Systems: An Introduction to Signals and Noise in Electrical Communication, New York, McGraw-Hill, 1968, p.386.

4. S. Nakamura and Y. Inoue," Digital 4-Phase Modulation Using Diode Switches in 2GHz Band", Electronics and Communications in Japan, vol.50, June 1967, pp.120-127.

5. M. Hines," Limitations in Phase Shifting Using Semiconductor Diodes", Proc. IEEE, vol. 52, June 1964, pp.697-708.

6. K. Kurokawa, B. Owen, W.J. Clemetson, N.D. Kenyon and W.O. Schlosser," An Experimental Millimeter-wave Path Length Modulator", Bell System Tech. J., vol. 50, November 1971, pp.2917-2946.

7. Hewlett Packard Technical Staff, PIN Diode as a Microwave Modulator, H.P. Application Note #58, August 1967.

8. G.I. Haddad, Avalanche Transit-Time Devices, Dedham, Mass., Artech House, 1972.

9. R.P. Tetarenko, private communication.

10. Hewlett Packard Specification Sheet for HP 5082-0437 IMPATT Diodes.

11. K. Kurokawa," Some Basic Characteristics of Broadband Negative Resistance Oscillator Circuits", Bell Systems Tech. J., vol. 48, July-August 1969, pp.1937-1956.

12. Lenkurt Electric Technical Staff," Pulse Code Modulation", Lenkurt Modulator, March 1968.

13. M. Gupta and R. Lomax," A Self consistent Large Signal Analysis of a Read-type IMPATT Diode Oscillator", *IEEE Trans. on Electron Devices,* vol. ED-18, August 1971, pp.544-550.

14. R. Whinnery and H.Jamieson," Coaxial Line Discontinuities", *Proc. IRE*, vol. 32, November 1944, pp.695-709.

15. R. Haitz, H. Stover and N. Tolar," A Method for Heat Flow Resistance Measurements in Avalanche Diodes", *IEEE Trans. on Electron Devices*, vol. ED-16, May 1969, pp.438-444.

16. J. Nigrin," Double Pulse Measurements of Avalanching p-n Junction Submicrosecond Transient Thermal Response", *The Review of Scientific Instruments*, vol. 43, February 1972, pp.264-268.

17. H.A. Watson, *Microwave Semiconductor Devices and Their Circuit Applications*, New York, McGraw-Hill, 1969, pp.290-295.

18. J. Nigrin," Double Pulse Measurements of Avalanching p-n Junction Submicrosecond Transient Thermal Response", *The Review of Scientific Instruments*, vol. 43, February 1972, pp.264-268.

19. N.B. Kramer,"Characterization and Modeling of IMPATT Oscillators", *IEEE Trans. on Electron Devices*, vol. ED-15, November 1968, pp.838-846.

20. D.L. Scharfetter and H.K. Gummel," Large-Signal Analysis of a Silicon Read Diode Oscillator", *IEEE Trans. on Electron Devices*, vol. ED-16, January 1969 pp.64-77, [Fig. 4].

21. H.K. Gummel and D.L. Scharfetter," Avalanche Region of IMPATT Diodes", *Bell System Tech. J.*, vol. 45, July 1966, pp.1797-1837, [Fig. 14].

22. A.B. Carlson, *Communication Systems: An Introduction to Signals and Noise in Electrical Communication*, New York, McGraw-Hill, 1968, pp. 27 - 28.

23. R. Adler, " A Study of Locking Phenomena in Oscillators", *Proc. IRE*, vol. 34, June 1946, p.351

24. R.E. Hines and B.J. Udelson, " Effects of a CW Injected Signal on a Pulsed Avalanche Oscillator", *Proc. IEEE*, vol. 57, November 1969, (Letter), pp. 2091-2092.

25. E.L. Ginzton, *Microwave Measurements*, New York, McGraw-Hill, 1957, pp. 406-417.

26. Ibid. p. 415

Appendix A

ANALYSIS OF THE BIAS CIRCUIT

The circuit shown in Figure A.1 is analyzed for a unit step input voltage. Assuming that the DC blocking capacitor is of negligible value (i.e. $C_T = 0$), the total impedance as seen from the switch is given by the following expression:

$$Z(s) = R_s + \frac{(R_D + sL)/sC_H}{R_D + sL + 1/sC_H} \tag{A.1}$$

The current through R_s due to a unit step input voltage is given by:

$$I(s) = \frac{V(s)}{Z(s)} = \frac{1}{s}\,\frac{1}{Z(s)} \tag{A.2}$$

$$= \frac{1}{s}\,\frac{1 + sR_DC_H + s^2LC_H}{(R_D + R_s) + s(R_D + R_sC_H + L) + s^2(R_sLC_H)} \tag{A.3}$$

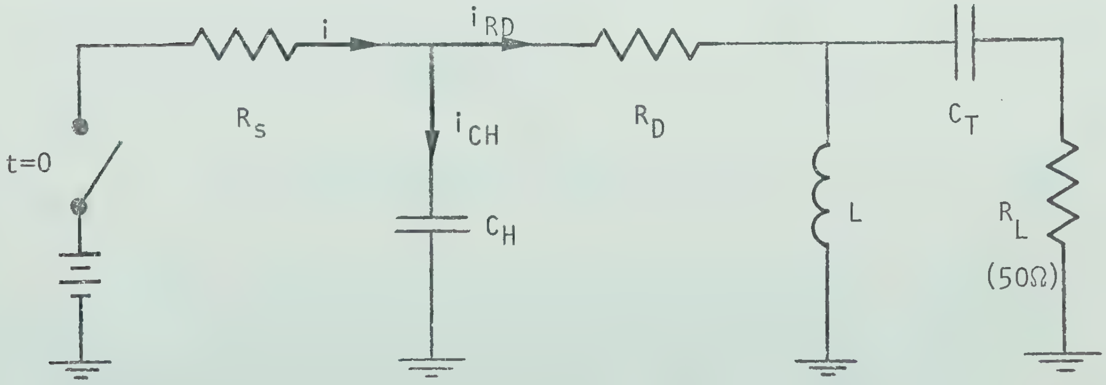

where: $R_s = 50\Omega$, $R_D = 150\Omega$, $C_H = 100\text{pF}$, $L = 180\text{nH}$, $C_T = 12\text{pF}$

FIG. A.1 EQUIVALENT CIRCUIT OF BIAS CIRCUIT

Putting in the appropriate values for the constants and taking the inverse LaPlace Transform of equation A.3, the current through R_s in the time domain is obtained:

$$i(t) = 5 + 16.38 \; e^{-.3055t} - 1.38 \; e^{-.7278t} \qquad (A.4)$$

where t is in nsec

i is in mA

The current through R_D is given by:

$$i_{RD}(t) = i(t) - i_{CH}(t) \qquad (A.5)$$

where

$$i_{CH}(t) = C_H \frac{d}{dt}(1 - i(t)R_s) \qquad (A.6)$$

The expression for $i_{RD}(t)$ is now obtained by substituting equations A.4 and A.6 into A.5 :

$$i_{RD}(t) = i(t) + R_s C_H \frac{d}{dt} i(t) \qquad (A.7)$$

$$= 5 - 8.64 \; e^{-.3055t} + 3.64 \; e^{-.7278t} \qquad (A.8)$$

Equation A.8 is the required result and is tabulated in Table A.1. The risetime of the current through R_D is seen to be 8.2 nsec.

TIME IN NSEC	CURRENT THROUGH R_D IN mA
0.0	0.000
1.0	0.392
1.1	0.500
2.0	1.159
3.0	1.955
4.0	2.652
5.0	3.220
6.0	3.664
7.0	4.004
8.0	4.261
9.0	4.453
9.3	4.500
10.0	4.595
11.0	4.701
12.0	4.780
15.0	4.912
20.0	4.981
∞	5.000

TABLE A.1 CURRENT THROUGH R_D IN RESPONSE TO A UNIT STEP INPUT VOLTAGE

Appendix B

EVALUATION OF RESONATOR PARAMETERS

The double-slug cavity described in Chapter 2 has been evaluated at a frequency of 5.688 GHz. This frequency corresponded to the center frequency of the resonator with the IMPATT diode biased just below the breakdown voltage. Under these conditions, the resonator can be modelled as a parallel R-L-C circuit, as seen from the position of the detuned short. (cf. Fig. B.1)

The capacitance of the diode was measured as a function of the reverse-bias voltage. The diode package capacitance (C_p) was also measured by inserting an open-circuited package at the terminals of the Boonton 71A L-C meter. C_p was found to be 0.2 pF.

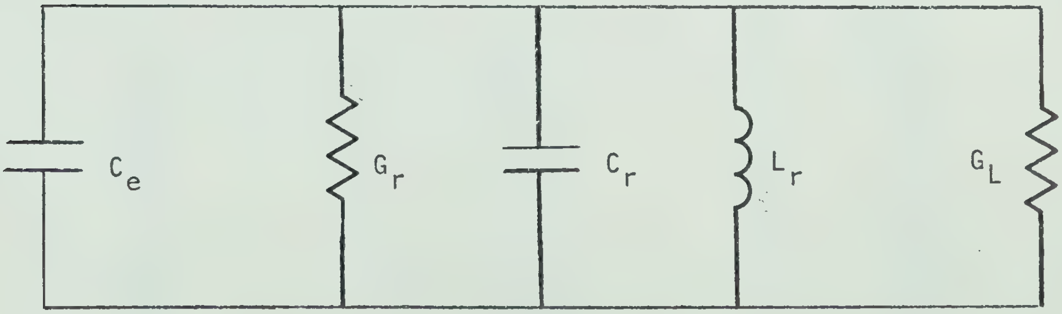

where

C_e is the depletion layer capacitance
G_r is the resonator losses including the parasitic conductances of the IMPATT diode
C_r is the resonator capacitance (C_p included)
L_r is the resonator inductance including coupling
G_L is the transformed load conductance

FIG. B.1 EQUIVALENT RESONATOR CIRCUIT

The center frequency of the resonator was also measured as a function of the reverse-bias voltage across the diode. The frequency was determined by noting that the reflected power was a minimum at the resonant frequency. In order to increase the sensitivity of the measurement, the signal generator, which fed a signal into the resonator, was modulated with a 1000 Hz square wave and the detected power was read on a tuned voltmeter. The results of the capacitance and frequency measurements are tabulated in Table B.1.

From this data, the total capacitance of the resonator (i.e. $C_T = C_r + C_e$) can be calculated by noting the change in the resonator frequency due to a change in the total resonator

TABLE B.1 DIODE CAPACITANCE AND RESONATOR FREQUENCY AS A FUNCTION OF REVERSE DIODE VOLTAGE

REVERSE-BIAS VOLTAGE (V)	DIODE CAPACITANCE (pF)	FREQUENCY (GHz)
0	3.040	5.158
10	1.153	5.235
20	0.881	5.322
30	0.758	5.392
40	0.685	5.444
50	0.633	5.502
60	0.594	5.543
70	0.567	5.588
80	0.544	5.622
90	0.525	5.657
92	0.5215	5.664
94	0.518	5.670
96	0.5145	5.6755
98	0.511	5.682
100	0.508	5.688

capacitance. For a parallel R-L-C circuit, the resonant frequency is given by:

$$f_o = \frac{1}{2\pi} \frac{1}{\sqrt{L_r C_T}} \tag{B.1}$$

Solving for C_T and differentiating with respect to the frequency, the following expression for the total capacitance of the cavity is obtained:

$$C_T = \frac{-f_o}{2} \frac{dC}{df} \simeq \frac{-f_c}{2} \frac{\Delta C}{\Delta f} \tag{B.2}$$

In the derivation of equation B.2, it has implicitly been assumed that the inductance of the resonator is constant over a small change in frequency. From Table B.1, it is seen that,for a change in bias voltage from 96 to 100 V, the total capacitance of the circuit changes by 0.0065 pF resulting in a change of frequency of 12.5 MHz in a center frequency of 5.682 GHz. Substituting these values into equation B.2, the total capacitance is calculated to be:

$$C_T = 1.478 \text{ pF} \tag{B.3}$$

Using equation B.1 and the appropriate values for C_T and f_o, the value of the resonator inductance is solved for. Therefore:

$$L_r = 0.533 \text{ nH} \tag{B.4}$$

The position of the detuned short was found by using the procedure outlined in Ginzton[25]. It was determined that the cavity was undercoupled because the position of the detuned short corresponded to a voltage maximum when the cavity was tuned to resonance. Since the impedance as seen from a voltage maximum is purely resistive and is given by the product of the characteristic impedance of the circuit and the measured VSWR, the coupling coefficient, β, is equal to the inverse of the VSWR. In this case, the coupling coefficientwas found to be 0.474. Had the detuned short position corresponded to a voltage minimum, the cavity would have been overcoupled and the coupling coefficient would have equalled the measured VSWR. With the diode reverse-biased by a voltage of 100 V, β was determined; this condition corresponded to a center frequency of 5.688 GHz. Figure B.2 graphically shows the experimental variation of the VSWR as a function of the frequency. To find the loaded and unloaded Q's (i.e. Q_L and Q_o respectively), it is necessary to identify the values of the VSWR which correspond to the half-power points. The half-power points are given analytically by[26]:

for Q_o,

$$\text{VSWR}\Big|_{\text{half-power points}} = \frac{2 + \beta^2 + \sqrt{(4+\beta^4)}}{2\beta} = 4.47 \qquad \text{(B.5)}$$

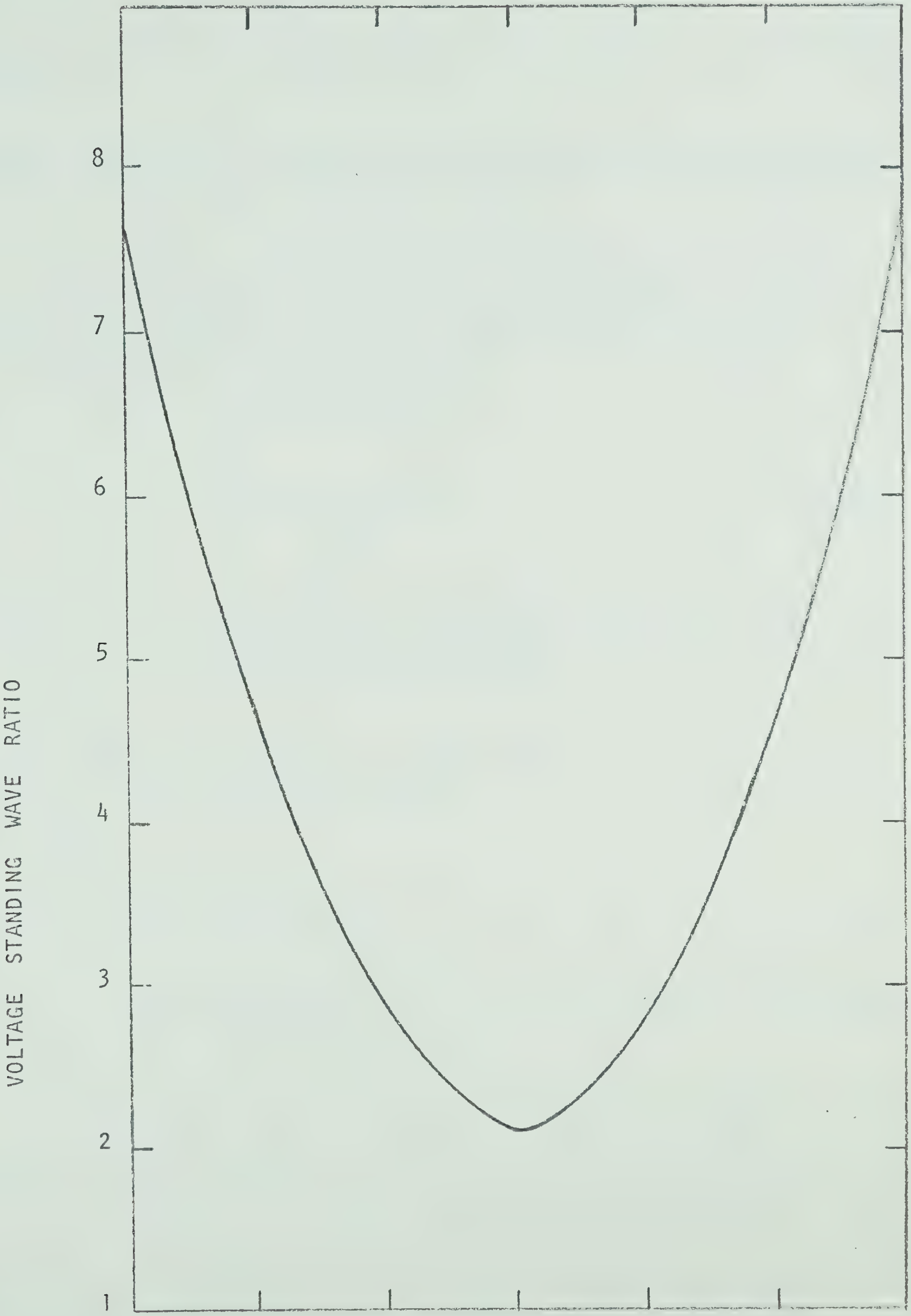

FIG. B.2 EXPERIMENTAL VARIATION OF VOLTAGE STANDING WAVE RATIO AT THE OUTPUT OF THE RESONATOR AS A FUNCTION OF FREQUENCY

for Q_L,

$$\text{VSWR}\Big|_{\text{half-power points}} = \frac{1 + \beta + \beta^2 + (1 + \beta)\sqrt{(1 + \beta^2)}}{\beta} = 7.03 \quad \text{(B.6)}$$

The values of the loaded and unloaded Q's are found by noting the frequencies at which the half-power VSWR's occur (cf. Fig. B.2) and by using the following expression:

$$Q = \frac{f_o}{f_U - f_L} \quad \text{(B.7)}$$

where f_U and f_L are the upper and lower half-power frequencies respectively.

In this fashion, it is found that the loaded and unloaded Q's are given by:

$$Q_L = 51.7 \quad \text{(B.8)}$$

$$Q_o = 82.5 \quad \text{(B.9)}$$

Having determined the loaded and unloaded Q's, and the lumped-constant inductance and capacitance of the cavity (cf. equations B.8,B.9,B.4 and B.3), the resonator conductance, G_r, and the load conductance as seen by the resonator, G_L, can be calculated from the following two expressions:

$$G_r = \frac{2\pi f C_T}{Q_o} \tag{B.10}$$

and

$$G_L = \frac{2\pi f C_T}{Q_L} \tag{B.11}$$

In this way, it has been found that:

$$G_r = 0.639 \text{ mmhos} \tag{B.12}$$

$$G_L = 0.381 \text{ mmhos} \tag{B.13}$$

The resonator conductance can be related to an equivalent series resistance, R_s, by the following equation:

$$R_s = \frac{1}{G_r Q_o^2} = 0.232\ \Omega \tag{B.14}$$

In conclusion, the resonator has been characterised at a center frequency of 5.682 GHz in terms of an equivalent R-L-C circuit. The IMPATT diode has been included as a depletion layer capacitance and a parasitic conductance.

Appendix C

FOURIER TRANSFORM OF VARIABLE-FREQUENCY PULSE

The general pulse to be transformed is shown in Figure C.1. There are three sections, all linear with time in frequency and amplitude. This pulse can be represented mathematically as:

$$x(t) = x_1(t) + x_2(t) + x_3(t) \qquad \text{(C.1)}$$

where:

$$x_1(t) = \frac{A_2}{t_2} t \cos\left\{2\pi\left[f_1 + \frac{f_2 - f_1}{t_2}\,\frac{t}{2}\right] t\right\} \qquad 0<t<t_2 \qquad \text{(C.2)}$$

$$x_2(t) = \left[A_2 + \frac{A_3 - A_2}{t_3 - t_2}(t - t_2)\right] \cos\left\{2\pi\left[f_2 + \frac{f_3 - f_2}{t_3 - t_2}\,\frac{t - t_2}{2}\right](t - t_2) + \pi(f_2 + f_1)t_2\right\} \qquad t_2<t<t_3 \qquad \text{(C.3)}$$

$$x_3(t) = \left[A_3 + \frac{A_4 - A_3}{t_4 - t_3}(t - t_3)\right] \cos\left\{2\pi\left[f_3 + \frac{f_4 - f_3}{t_4 - t_3}\,\frac{t - t_3}{2}\right](t - t_3) + \pi(f_2 + f_1)t_2 + \pi(f_3 + f_2)(t_3 - t_2)\right\} \qquad t_3<t<t_4 \qquad \text{(C.4)}$$

The Fourier Transform of a function y(t) is defined as follows:

$$Y(f) = \int_{-\infty}^{\infty} y(t)\, e^{-j\omega t}\, dt \qquad \text{(C.5)}$$

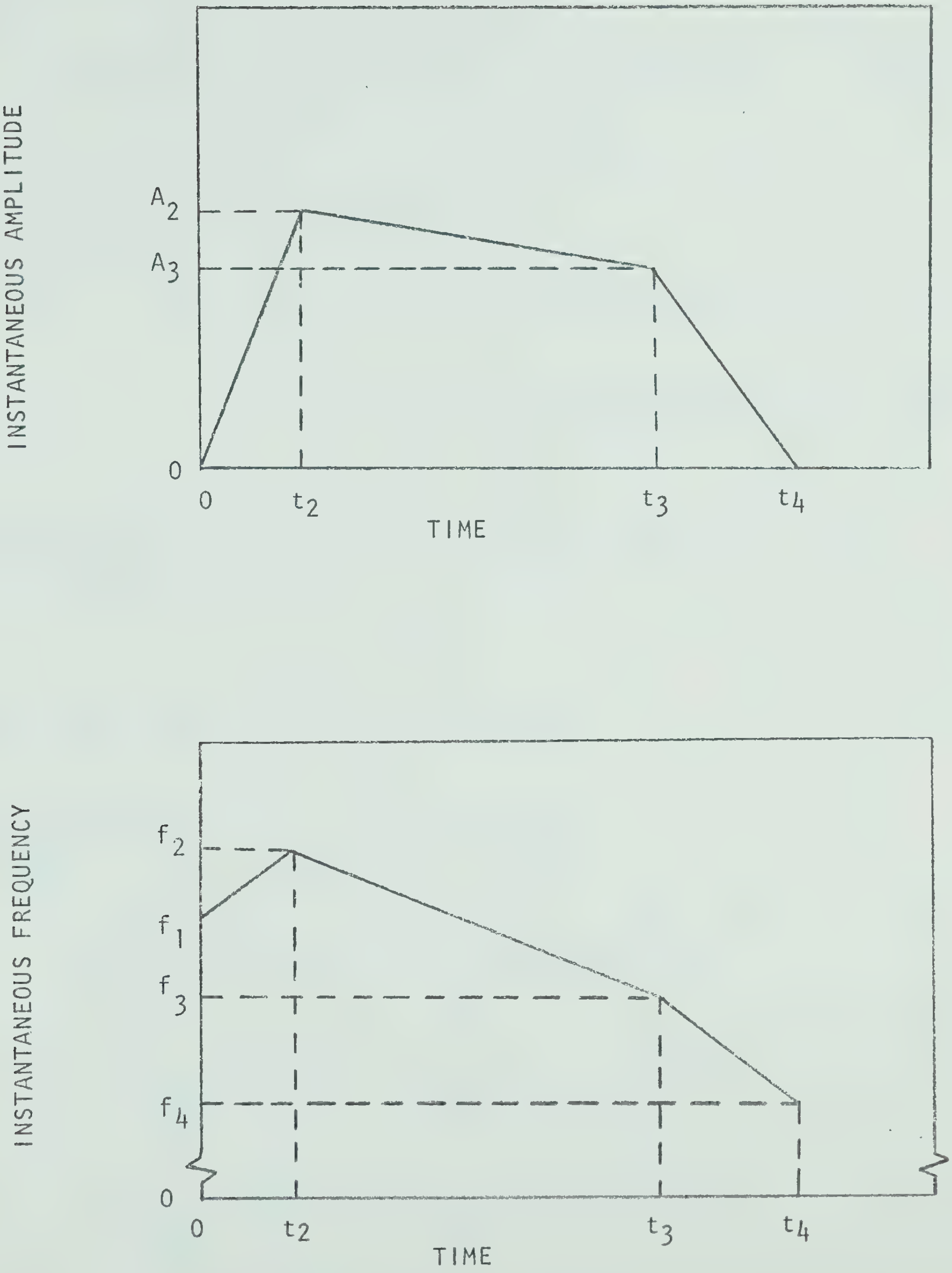

FIG. C.1 INSTANTANEOUS AMPLITUDE (TOP) AND FREQUENCY (BOTTOM) OF THEORETICAL VARIABLE-FREQUENCY PULSE

Equation C.5 can also be written as follows:

$$Y(f) = \int_{-\infty}^{\infty} y(t)\cos 2\pi ft\, dt - j\int_{-\infty}^{\infty} y(t)\sin 2\pi ft\, dt \qquad (C.6)$$

Using the two trigonometric identities:

$$\cos\alpha \cos\beta = 0.5\cos(\alpha - \beta) + 0.5\cos(\alpha + \beta) \qquad (C.7)$$

$$\sin\alpha \cos\beta = 0.5\sin(\alpha - \beta) + 0.5\sin(\alpha + \beta) \qquad (C.8)$$

it can be seen that for the first section of the general pulse shown in Figure C.1:

$$\int_0^{t_2} x_1(t)\cos 2\pi ft\, dt - j\int_0^{t_2} x_1(t)\sin 2\pi ft\, dt \qquad (C.9)$$

$$= \int_0^{t_2} \frac{tA_2}{2t_2}\cos\{2\pi[f_1 t + \frac{f_2 - f_1}{2t_2} t^2 - ft]\}\, dt$$

$$- j\int_0^{t_2} \frac{tA_2}{2t_2}\sin\{2\pi[f_1 t + \frac{f_2 - f_1}{2t_2} t^2 - ft]\}\, dt$$

$$+ \int_0^{t_2} \frac{tA_2}{2t_2}\cos\{2\pi[f_1 t + \frac{f_2 - f_1}{2t_2} t^2 + ft]\}\, dt$$

$$- j\int_0^{t_2} \frac{tA_2}{2t_2}\sin\{2\pi[f_1 t + \frac{f_2 - f_1}{2t_2} t^2 + ft]\}\, dt \qquad (C.10)$$

Since the region of interest for the frequency f is a couple of hundred MHz on each side of f_1 and since f_1 is in the order of

6000 MHz, the last two integrals in equation C.10 can be neglected. Therefore, equation C.10 can be rewritten:

$$\int_0^{t_2} x_1(t)\cos 2\pi ft\,dt - j\int_0^{t_2} x_1(t)\sin 2\pi ft\,dt$$

$$= \int_0^{t_2} \frac{tA_2}{2t_2}\exp-\{2\pi[f_1 + \frac{f_2 - f_1}{2t_2}t^2 - ft]\}\;dt \qquad (C.11)$$

A similar analysis can be done for sections #2 and #3 (i.e. $x_2(t)$ and $x_3(t)$).

The Fourier Transform of the pulse given in Figure C.1 can therefore be written as follows:

$$\begin{aligned}X(f) = {} & \int_0^{t_2} \frac{A_2 t}{2t_2}\exp-\{2\pi[f_1 + \frac{f_2 - f_1}{2t_2}t^2 - ft]\}\;dt \\ & + \int_{t_2}^{t_3} [A_2 + \frac{A_3 - A_2}{t_3 - t_2}(t - t_2)]\exp-\{2\pi[f_2 + \frac{f_3 - f_2}{t_3 - t_2}\frac{t - t_2}{2}] \\ & \qquad (t - t_2) + \pi(f_2 + f_1)t_2\} \\ & + \int_{t_3}^{t_4} [A_3 + \frac{A_4 - A_3}{t_4 - t_3}(t - t_3)]\exp-\{2\pi[f_3 + \frac{f_4 - f_3}{t_4 - t_3}\frac{t - t_3}{2}] \\ & \qquad (t - t_3) + \pi(f_2 + f_1)t_2 + \pi(f_3 + f_2)(t_3 - t_2)\}\end{aligned} \qquad (C.12)$$

The squared magnitude of the Fourier Transform can be obtained by

summing the squares of the real and imaginery parts of equation C.12.

The integrations in equation C.12 were performed numerically using Simpson's integration formula; that is,

$$\int_a^b f(x)\,dx = h/3\ [f_o + 4f_1 + 2f_2 \ldots\ldots + f_n] \qquad \text{(C.13)}$$

where

n is an even integer equal to the number of strips in interval a to b,

h is the width of each strip,

f_n is the value of f(x) at the end of the n^{th} strip,

In fact,a second order polynomial is passed through three points of the function and the integration is done over two strips at a time.

A flow chart of the computer program used to calculate the magnitude of the Fourier Transform of a variable-frequency pulse is given in Figure C.2. The only data required is the amplitude, frequency and time of the four pivot points as defined in Figure C.1 as well as the number of strips required for each section.

The computer printout includes the input data, the magnitude of X(f), the magnitude of X(f) normalized to unity,

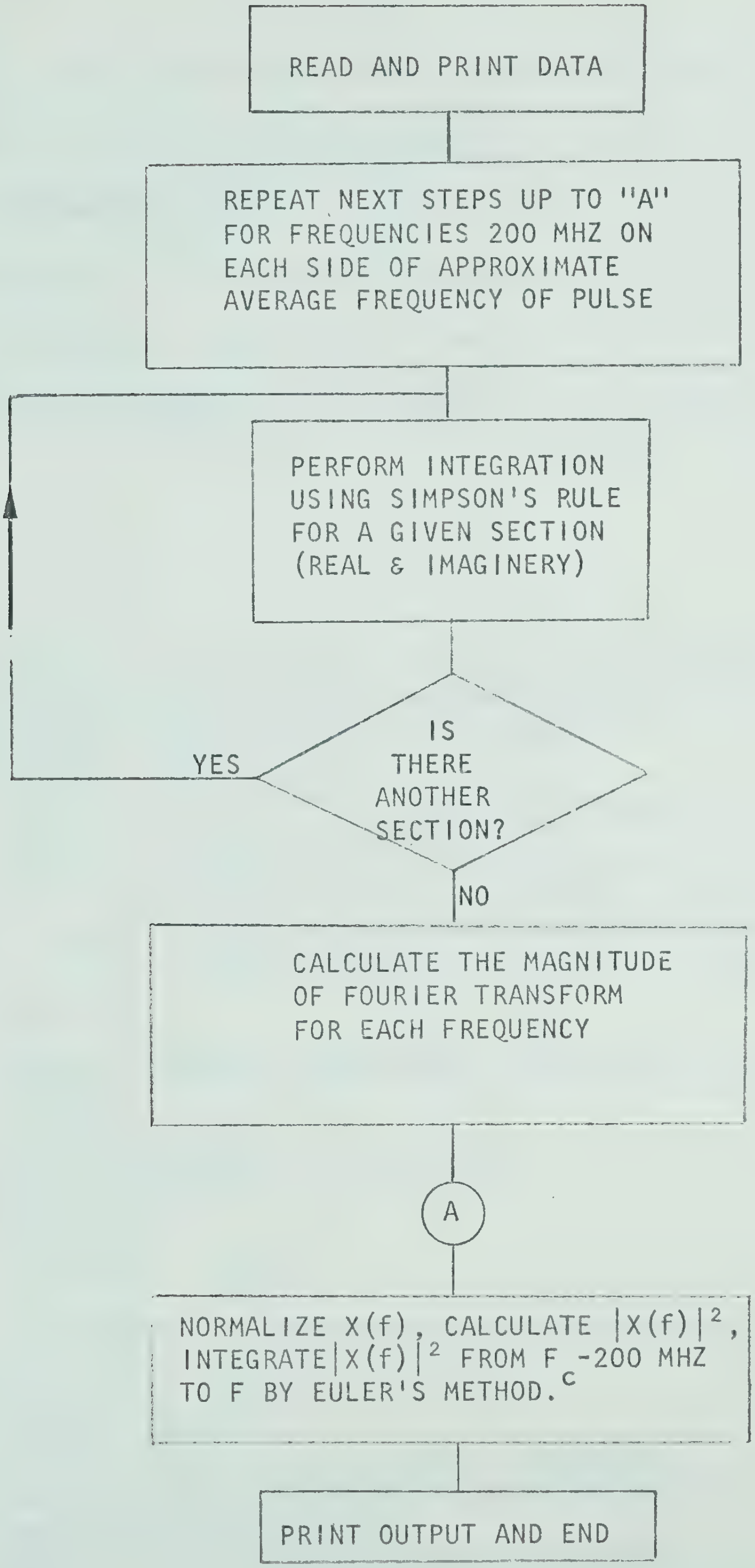

FIG. C.2 FLOW CHART OF PROGRAM TO CALCULATE FOURIER TRANSFORM OF VARIABLE-FREQUENCY PULSE

the square of the magnitude of X(f) normalized to unity and the integration of virtually all the power below a certain frequency "f". This latter term makes it possible to calculate the percentage of the total power in any band of frequencies (e.g. in the main lobe). The computer program was written in FORTRAN IV and was run on an IBM 360 computer. The listing of the program follows in full:

```
C     PROGRAM TO CALCULATE THE MAGNITUDE OF THE FOURIER TRANSFORM
C     OF A PULSE WITH VARIABLE FREQUENCY AND AMPLITUDE.
C     SIMPSON'S INTEGRATION FORMULA IS USED
C     THERE ARE THREE SECTIONS
C     SECTION 1 - TIME T1 TO T2, LINEAR AMPLITUDE A1 TO A2,
C                 LINEAR FREQUENCY F1 TO F2
C     SECTION 2 - TIME T2 TO T3, LINEAR AMPLITUDE A2 TO A3,
C                 LINEAR FREQUENCY F2 TO F3
C     SECTION 3 - TIME T3 TO T4, LINEAR AMPLITUDE A3 TO A4,
C                 LINEAR FREQUENCY F3 TO F4
C     T1=A1=A4=0
C
      DIMENSION SUM(400), SNORM(400), PNORM(400), PSUM(400)
      INTEGER F
      REAL LAST1, LAST2
C     NDATA IS THE NUMBER OF DATA SETS
      READ 60, NDATA
   60 FORMAT(I2)
      DO 99 NRUN = 1,NDATA
C
C     N1,N2 &N3 ARE THE NUMBER OF STEPS IN SECTIONS 1,2 & 3
      READ 10, N1, N2, N3
   10 FORMAT(3I3)
      PRINT 15, N1,N2,N3
   15 FORMAT('1','N1=  ',I3,6X,'N2=  ',I3,6X,'N3=  ',I3)
      READ 20, A1,A2,A3,A4,F1,F2,F3,F4,T1,T2,T3,T4
   20 FORMAT(4F3.2,4F3.0,4F3.0)
      PRINT 30, A1,F1,T1,A2,F2,T2,A3,F3,T3,A4,F4,T4
   30 FORMAT(' ','A1=  ',F4.2,5X,'F1=  ',F4.0,5X,'T1=  ',F4.0,/,'A2=
     C ',F4.2,5X,'F2=  ',F4.0,5X,'T2=  ',F4.0,/,'A3=  ',F4.2,5X,'F3=
     C ',F4.0,5X,'T3=  ',F4.0,/,'A4=  ',F4.2,5X,'F4=  ',F4.0,5X,'T4=
     C ',F4.0)
      C=2.*3.14159*.001
```

```
C
      DO 88 F=1,400
C
C     REAL PART OF INTEGRAL FOR SECTION 1
      DA1=(A2-A1)/(T2-T1)
      DF1=(F2-F1)/T2*.5
      EVEN1=0
      ODD1=0
      FIRST1=A1
      LAST1=A2*COS(C*(F2+F1)*T2/2-C*F*T2)
      DO 11 I=2,N1,2
      T=(T2-T1)*(I-1)/N1+T1
      EVEN1=EVEN1+4*(A1+DA1*T)*COS(C*(F1+DF1*T)*T-C*F*T*)
   11 CONTINUE
      DO 22 I=3,N1,2
      T=(T2-T1)*(I-1)/N1+T1
      ODD1=ODD1+2*(A1+DA1*T)*COS(C*(F1+DF1*T)*T-C*F*T)
   22 CONTINUE
      SUM1=(T2-T1)/(N1*3)*(FIRST1+LAST1+EVEN1+ODD1)
C
C     COMPLEX PART OF INTEGRAL FOR SECTION 1
      CEVN1=0
      COD1=0
      CFIRS1=0
      CLAS1=A2*SIN(C*(F2+F1)*T2/2-C*F*T2)
      DO 111 I=2,N1,2
      T=(T2-T1)*(I-1)/N1+T1
      CEVN1=CEVN1+4*(A1+DA1*T)*SIN(C*(F1+DF1*T)*T-C*F*T)
  111 CONTINUE
      DO 222 I=3,N1,2
      T=(T2-T1)*(I-1)/N1+T1
      COD1=COD1+2*(A1+DA1*T)*SIN(C*(F1+DF1*T)*T-C*F*T)
  222 CONTINUE
      CSM1=(T2-T1)/(N1*3)*(CFIRS1+CLAS1+COD1+CEVN1)
      CSM2=0
      SUM2=0
      CSM3=0
      SUM3=0
      IF(N2.EQ.0)GO TO 77
C
C     REAL PART OF INTEGRAL FOR SECTION 2
      EVEN2=0
      ODD2=0
      DA2=(A3-A2)/(T3-T2)
      DF2=(F3-F2)/(T3-T2)*.5
      FAIS=C*(F2+F1)*T2/2
      FIRST2=A2*COS(FAIS-C*F*T2)
      LAST2=A3*COS(C*(F3+F2)*(T3-T2)/2-C*F*T3+FAIS)
```

```
      DO 33 I=2,N2,2
      T=(T3-T2)*(I-1)/N2+T2
      EVEN2=EVEN2+4*(A2+DA2*(T-T2))*COS(C*(F2+DF2*(T-T2))*(T-T2)-
     CC*F*T*+FAIS)
   33 CONTINUE
      DO 44 I=3,N2,2
      T=(T3-T2)*(I-1)/N2+T2
      ODD2=ODD2+2*(A2+DA2*(T-T2))*COS(C*(F2+DF2*(T-T2))*(T-T2)-C*F*T
     C+FAIS)
   44 CONTINUE
      SUM2=(T3-T2)/(N2*3)*(FIRST2+LAST2+EVEN2+ODD2)
C
C     COMPLEX PART OF INTEGRAL FOR SECTION 2
      CEVN2=0
      COD2=0
      CFIRS2=A2*SIN(FAIS-C*F*T2)
      CLAS2=A3*SIN(C*(F3+F2)*(T3-T2)/2-C*F*T3+FAIS)
      DO 333 I=2,N2,2
      T=(T3-T2)*(I-1)/N2+T2
      CEVN2=CEVN2+4*(A2+DA2*(T-T2))*SIN(C*(F2+DF2*(T-T2))*(T-T2)-C*F
     C*T+FAIS
  333 CONTINUE
      DO 444 I=3,N2,2
      T=(T3-T2)*(I-1)/N2+T2
      COD2=COD2+2*(A2+DA2*(T-T2))*SIN(C*(F2+DF2*(T-T2))*(T-T2)-C*F*T
     C+FAIS)
  444 CONTINUE
      CSM2=(T3-T2)/(N2*3)*(CFIRS2+CLAS2+CEVN2+COD2)
      IF(N3.EQ.0)GO TO 77
C
C     REAL PART OF INTEGRAL FOR SECTION 3
      EVEN3=0
      ODD3=0
      DA3=(A4-A3)/(T4-T3)
      DF3=(F4-F3)/(T4-T3)*.5
      FAIS=C*(F2+F1)*T2/2+C*(F3+F2)*(T3-T2)/2
      FIRST3=A3*COS(FAIS-C*F*T3)
      LAST3=A4*COS(C*(F4+F3)*(T4-T3)/2-C*F*T4+FAIS)
      DO 55 I=2,N3,2
      T=(T4-T3)*(I-1)/N3+T3
      EVEN3=EVEN3+4*(A3+DA3*(T-T3))*COS(C*(F3+DF3*(T-T3))*(T-T3)-C*
     CF*T+FAIS)
   55 CONTINUE
      DO 66 I=3,N3,2
      T=(T4-T3)*(I-1)/N3+T3
      ODD3=ODD3+2*(A3+DA3*(T-T3))*COS(C*(F3+DF3*(T-T3))*(T-T3)-C*F*T
     C+FAIS)
   66 CONTINUE
      SUM3=(T4-T3)/(N3*3)*(FIRST3+LAST3+EVEN3+ODD3)
C
```

```
C     COMPLEX PART OF INTEGRAL FOR SECTION 3
      CEVN3=0
      COD3=0
      CFIRS3=A3*SIN(FAIS-C*F*T3)
      CLAS3=A4*SIN(C*(F4+F3)*(T4-T3)/2-C*F*T4+FAIS)
      DO 555 I=2,N3,2
      T=(T4-T3)*(I-1)/N3+T3
      CEVN3=CEVN3+4*(A3+DA3*(T-T3))*SIN(C*(F3+DF3*(T-T3))*(T-T3)-C*
     CF*T+FAIS)
  555 CONTINUE
      DO 666 I=3,N3,2
      T=(T4-T3)*(I-1)/N3+T3
      COD3=COD3+2*(A3+DA3*(T-T3))*SIN(C*(F3+DF3*(T-T3))*(T-T3)-C*F*T
     C+FAIS)
  666 CONTINUE
      CSM3=(T4-T3)/(N3*3)*(CFIRS3+CLAS3+CEVN3+COD3)
C
   77 CONTINUE
      SUM(F)=SQRT((SUM1+SUM2+SUM3)**2+(CSM1+CSM2+CSM3)**2)
   88 CONTINUE
C
      SMAX=0
      DO 1 J=1,400
      IF(ABS(SUM(J))-SMAX)2,2,3
    3 SMAX=ABS(SUM(J))
    2 CONTINUE
    1 CONTINUE
C
      PRINT 40
   40 FORMAT(' ','     F IN MHZ             VOLT           NORM.VOLT.
     CNORM. POWER    SUMOF NORM. POWER FROM F=0 TO F')
      DO 4 K=1,400
      SNORM(K)=SUM(K)/SMAX
      PNORM(K)=SNORM(K)**2
    4 CONTINUE
      PSUM(1)=0
      DO 5 J=2,400
      PSUM(J)=PSUM(J-1)+(PNORM(J)+PNORM(J-1))
    5 CONTINUE
      DO 6 M=1,400
      PRINT 50,M,SUM(M),SNORM(M),PNORM(M),PSUM(M)
   50 FORMAT(' ',6X,I3,6X,F10.6,9X,F10.8,8X,F10.8,10X,F10.5)
    6 CONTINUE
   99 CONTINUE
      STOP
      END
```